Molecular mechanisms involved in midbrain dopaminergic neuron migration during murine development

Dissertation

zur

Erlangung des Doktorgrades (Dr. rer. nat.)

der

Mathematisch-Naturwissenschaftlichen Fakultät

der

Rheinischen Friedrich-Wilhelms-Universität Bonn

vorgelegt von

Gabriela Oana Bodea, geb. Dragomir

aus Pucioasa, Rumänien

Bonn, 2014

Angefertigt mit Genehmigung der Mathematisch-Naturwissenschaftlichen Fakultät der Rheinischen Friedrich-Wilhelms-Universität Bonn

1. Gutachter: PD Dr. Sandra Blaess

2. Gutachter: Prof. Dr. Michael Hoch

Tag der Promotion: 7. April 2014

Erscheinungsjahr: 2014

"Every man can, if he so desires, become the sculptor of his own brain"

Santiago Ramon y Cajal

TABLE OF CONTENTS

ABBREVIATIONS

6B4 PG	6B4 proteoglycan-phosphacan
A(8...10)	Area (8...10)
AKT	Protein kinase B
ANOVA	Analysis of variance
AP	Alkaline phosphatase
AP	Anteroposterior
ApoER2	Apolipoprotein E receptor 2
bp	Base pair
BrdU	Bromodeoxyuridine
BRN3A	Brain specific homeobox / POU domain protein 3A
BSA	Bovine serum albumine
Calb	Calbindin
Calbindin	Ca^{2+} binding protein
cAMP	Cyxclic adenosine monophosphate
cAMP	Cyclic adenosine monophosphate
CDK5	Cyclin-dependent kinase 5
cDNA	Complementary DNA
CNS	Central nervous system
Cre	Causes Recombination
CreER	Cre estrogen receptor fusion protein
CRK	Proto-oncogene c-crk
Cx	Cortex
CXCL12	Chemokine (C-X-C motif) Ligand 12
CXCR4	Chemokine (C-X-C motif) Receptor 4
CXCR7	Chemokine (C-X-C motif) Receptor 7
DAB1	Disabled-1
DAPI	4'-6-Diamidino-2-phenylindole
DAT	Dopamine transporter
DCC	Deleted in colorectal carcinoma
DCX	Doublecortin
DMEM	Dulbecco's Modified Eagle Medium
DMSO	Dimethylsulfoxide
DNA	Deoxyribonucleic acid
DNAse	desoxyribonuclease
dNTP	deoxynucleotidetriphosphate
DV	dorsoventral
E	Embryonic day
ECM	Extracellular matrix
EN1/2	Engrailed 1 and 2
ENA/VASP	Vasodilator-stimulated phosphoprotein
EphBs	Ephrin receptor tyrosine kinases
ER	Rstrogen receptor ligand-binding domain
EtBr	Ethidium bromide
EYFP	Enhanced yellow fluorescent protein
F1	Filial generation 1
Fb	Forebrain
FGF8	Fibroblast growth factor 8
FOXA2	Forkhead box protein A2
GBX2	Gastrulation Brain homeobox 2
GFP	Green fluorescent protein
GIFM	Genetic inducible fate mapping
GIRK2	G-protein regulated inward rectifier potassium channel-2
GnRH	gonadotropin-releasing hormone neurons
GPCR	G-protein coupled receptor
Hb	Hindbrain
HSP90	Heat shock protein
Ig	Immunoglobulin

ISH	In situ hybridization
KO	Knockout
L1	Cell adhesion molecule L1
LB	Luria Bertani Medium
LMX1a/b	LIM homeobox transcription factor 1 α and β
Lox P	Locus of x over P1
LSD	Fisher's least significant difference
Mb	Midbrain
MbDA	Midbrain dopaminergic neurons
MHB	Mid-hindbrain boundary
mRNA	Messenger RNA
MSX1	Msh homeobox 1
mVTA	Medial ventral tegmental area
n	Refraction index
N	Number of animals
N-Cad	N-cadherin
N-CAM	Polysialylated neural cell adhesion molecule
NCAM-H	Highly polysialylated neuronal cell adeshion molecule
NgCAM	Neuron-glia cell adhesion molecule
NGN2	Neurogenin 2
NICD	Notch internal cytoplasmatic domain
NKX2.2	NK2 homebox 2
NKX6.1	NK6 homeobox protein1
NURR1	Nuclear receptor subfamily 4, group A, member 2
OD	Optical density
OTX2	Orthodenticle homeobox 2
P (..)	Postnatal day
PAR3/PAR6	Partitioning defective 3 homolog/Partitioning defective 6 homolog
PBS	Phosphate buffered saline
PCR	Polymerase chain reaction
PFA	Paraformaldehyde
PI3K	Phosphatidylinositol- 3-kinase
PITX3	Paired-like homeodomain transcription factor 3
PKA	Protein kinase A
PKC	Protein kinase C
PLC-β	Phospholipase C-β
PTCH1	Patched-1
RAP1	Ras-proximate-1 or Ras-related protein-1
RN	Red nucleus
RNA	Ribonucleic acid
RNAse	Ribonuclease
rpm	Rounds per minute
RRF	Retrorubral field
SEM	Standard error of the mean
SFK	Src-tyrosine kinase family/Fyn-kinase
SHH	Sonic hedgehog
SIM1	Single-minded homolog 1
SMO	Smoothened
SN	Substantia nigra
STK11	Serine/Threonine kinase 11
TH	Tyrosine hydroxylase
TM	4-hydroxy-tamoxifen
Tris	Tris(hydroxymethyl)aminomethane
TSLIM	Thin-sheet laser imaging microscope
VLDLR	Very low density lipoprotein receptor
VMAT	Vesicular monoamine transporter 2
VTA	Ventral tegmental area
VZ	Ventricular zone
WNT1	Wingless-related MMTV integration site 111

2

SUMMARY

Midbrain dopaminergic (MbDA) neurons are located in the ventral tegmental area (VTA) and the substantia nigra (SN) and are involved in many brain functions including motor control, reward associated behavior and modulation of emotions. This thesis dissects the migratory routes and the molecular mechanisms underlying the migration of the subsets of MbDA neurons that form the SN and the VTA. Previous attempts to study the migration of MbDA neurons were hampered by the lack of markers for migrating SN and VTA neurons and the lack of a system to monitor their migration in real time. In this study, different MbDA progenitor populations, which give rise to either SN or medial VTA (mVTA) were heritably labeled using a genetic inducible fate mapping method and the changing position of their descendants was assesed at several stages during their migration phase. To monitor migrating MbDA neurons in real time, an organotypic slice culture system of the developing midbrain was established. In this culture system the migratory behaviour of distinct MbDN populations was characterized by time-lapse imaging of fluorescently labeled fate-mapped SN or mVTA neurons. Furthermore, to assess leading edge orientation, the morphology of MbDA neurons was characterized at several developmental stages by three dimensional imaging of whole brains.

The results of this study reveal two distinct modes of MbDA migration: MbDA neurons destined for the SN migrate first radially from their progenitor domain to the forming mantle layer and subsequently switch to tangential migration to reach their final position in the lateral midbrain. In contrast, neurons destined to the mVTA mainly undergo radial migration. The data further show that components of the Reelin signaling pathway are specifically expressed in a lateral MbDA subpopulation during embryonic development. CXCR4, a chemokine receptor, is expressed in medially located MbDA neurons and its ligand, CXCL12, is expressed in the meninges surrounding the midbrain. Time-lapse imaging of migrating MbDA neurons in presence of Reelin blocking antibody and analysis of mice in which Reelin signaling was inactivated demonstrate that Reelin signaling regulates the speed and trajectory of tangentially migrating MbDA neurons and the formation of the SN. In contrast, inactivation of CXCR4/CXCL12 signaling leads to accumulation of MbDA neurons in dorsal aspects of the MbDA neuronal field suggesting that CXCR4/CXCL12 signaling might modulate the radial migration of MbDA neurons.

This study provides a detailed characterization of the distinct migratory pathways taken by MbDA neurons destined for the SN or the mVTA and provides insight into the molecular mechanisms that control different modes of MbDA neuronal migration. These mechanistic insights might serve as a model that can be applied to understand the formation of other nuclei in the ventral brain, where the migration processes are less well understood than in the layered structures of the dorsal brain. Moreover, the results of this study might contribute to improving the *in vitro* production of MbDA neurons from induced pluripotent or embryonic stem cells by providing markers to identify different subtypes of MbDA neurons during their generation.

ZUSAMMENFASSUNG

Dopaminerge Mittelhirn-Neurone (MbDA Neurone) befinden sich im ventralen tegmentalen Areal (VTA) und der Substantia nigra (SN) und modulieren willkürliche Bewegungen, Belohnungsverhalten und Emotionen. Die vorliegende Doktorarbeit analysiert die Migrationswege und die molekularen Mechanismen, die für die Migration der Subpopulation von MbDA Neuronen wichtig sind, die sich zu der SN und dem VTA entwickeln. Bisherige Versuche, die Migration von MbDA Subpopulationen im Detail zu untersuchen, waren nur wenig erfolgreich, da weder Marker für migrierende SN und VTA Neurone noch ein experimentelles System für die Echtzeit-Beobachtung der MbDA Neurone etabliert waren.

In der vorliegenden Studie wurden verschiedene MbDA Vorläuferpopulationen, die sich entweder zu MbDA Neuronen in der SN oder dem mittleren Teil des VTA entwickeln, mit Hilfe einer genetischen Methode zu verschiedenen Entwicklungszeitpunkten markiert. Zunächst wurden über mehrer Entwicklungsstadien die sich verändernden Positionen der so markierten MbDA Neurone bestimmt, um einen Einblick in ihre Migrationswege zu gewinnen. Um migrierende MbDA Neuronen direkt beobachten zu können, wurden organotypische Schnittkulturen des embryonalen Mittelhirns etabliert. In diesem Kultursystem wurde das Migrationsverhalten von fluoreszenzmarkierten SN oder VTA Neuronen mit Zeitraffer-Mikroskopie untersucht. Um die Orientierung der migrierenden Neurone zu analysieren, wurde die Morphologie von MbDA Neuronen zu mehreren Entwicklungsstadien durch dreidimensionale Bildgebung charakterisiert.

Die Ergebnisse dieser Studie zeigen, dass unterschiedliche MbDA Subpopulationen unterschiedliche Migrationsverhalten aufweisen: MbDA Neurone, die sich zur SN entwickeln, wandern zuerst radial von ihrer Vorläuferdomäne in die Mantelschicht. Anschließend migrieren sie tangential, um ihre endgültige Position im lateralen Mittelhirn zu erreichen. Dagegen wandern MbDA Neurone, die sich zum mittleren Teil des VTA entwickeln, hauptsächlich radial. Die vorliegenden Daten zeigen weiter, dass während der Embryonalentwicklung Komponenten des Reelin Signalwegs spezifisch in einer lateral gelegenen MbDA Population exprimiert sind. Hingegen ist CXCR4, ein Chemokinrezeptor, nur in medial gelegenen MbDA Neuronen exprimiert. Der CXCR4 Ligand CXCL12 wird in der Pia mater exprimiert, die das Mittelhirn umschliesst. Zeitraffer-Mikroskopie von migrierenden MbDA Neuronen in Gegenwart eines Reelin-inhibierenden Anitkörpers und die Analyse von Mäusen, in denen der Reelin-Signalweg inaktiviert wurde, zeigen, dass das Reelin-Signal die Geschwindigkeit und Bewegungsbahn tangential wandernder MbDA Neuronen und die Bildung der SN reguliert. Im Gegensatz dazu führt die Inaktivierung des CXCL12/CXCR4 Signalwegs zu einer Ansammlung von MbDA Neuronen im dorsalen Bereich des VTA. Diese Ergebnisse deuten darauf hin, dass der CXCR4/CXCL12 Signalweg die radiale Wanderung der MbDA Neuronen moduliert.

4

Diese Studie charakterisiert die Migrationswege der MbDA Neurone, die sich zur SN oder dem mittleren Teil des VTA entwickeln und gibt Einblicke in die molekularen Mechanismen, die verschiedene Arten der MbDA Migration kontrollieren. Diese mechanistischen Erkenntnisse könnten als Modell dienen, um die Entstehung anderer, in Kernen organisierter ventraler Gehirnbereiche besser zu verstehen, da bisher Migrationsprozesse in ventralen Gehirnbereichen weit weniger gut verstanden werden als im dorsalen Gehirn, wo Neurone in Zellschichten organisiert sind. Schließlich könnten die Ergebnisse dieser Studie möglicherweise dazu beitragen, die *in vitro* Erzeugung von MbDA Neuronen aus induzierten pluripotenten oder embryonalen Stammzellen zu verbessern, da mit Hilfe der hier identifizierten Markern verschiedene Unterarten von MbDA Neuronen schon während ihrer Entstehung identifiziert werden könnten.

1. INTRODUCTION

The mammalian brain is a precisely organized and complex structure that controls various functions of the body. The mammalian brain arises from a simple neuroepithelial structure and its complexity is established through the coordinated generation and organization of a vast diversity of neural cell types. A key feature in the organization of neural cells is that the cells are located in a specific structure or region of the nervous system, within highly organized cell cluster and laminae. To reach their specific position in the brain, neurons often have to undergo long distance migration from their place of origin. Arriving at the correct final position is necessary for the neurons to establish proper neural network, which are essential for accomplishing complex brain functions.

Neuronal migration in the mammalian brain is achieved through very elaborate patterns of cell movements. Defects in neuronal migration in humans are implicated in epilepsy, mental retardation and severe learning disabilities (Gleeson and Walsh, 2000). Migratory behavior and underlying molecular mechanisms have been extensively studied in the dorsal brain, in particular in the cerebral and cerebellar cortex, where neurons undergo radial and/or tangential migration to organize themselves into neuronal layers (Figure 1A). Neurons in ventral brain areas, including midbrain dopaminergic (MbDA) neurons, are rarely organized into layers but are arranged into a complex array of neuronal clusters, also called nuclei (Figure 1B). MbDA nuclei are involved in many brain functions, such as motor integration, cognition, emotive and reward behaviors. Dysfunctions in MbDA system have been linked with many neurological and psychiatric disorders, including Parkinson's disease, depression and schizophrenia. Due to their clinical importance, MbDA neurons have been the subject of extensive investigations. However, very little is known about the migration events and the molecular mechanism that guide neurons to form these neuronal clusters.

1.1 Midbrain dopaminergic neuron diversity in the mammalian brain

In the central nervous system (CNS), dopaminergic neurons are localized in the olfactory bulb, the hypothalamus and the mesencephalon (midbrain). MbDA neurons are located in the ventral midbrain and are the main source of dopamine neurotransmitter in the mammalian CNS. The development of various histology methods and tracing studies enabled the anatomical mapping of the MbDA system. Based on their anatomical position, MbDA neurons are organized into three major nuclei: the lateral substantia nigra pars compacta (SN, A9), the medialy ventral tegmental area (VTA, A10), and the retrorubral field (RRF, A8) in the posterolateral midbrain (Dahlstrom and Fuxe, 1964). These nuclei have distinct projections and functions, which are not yet fully understood.
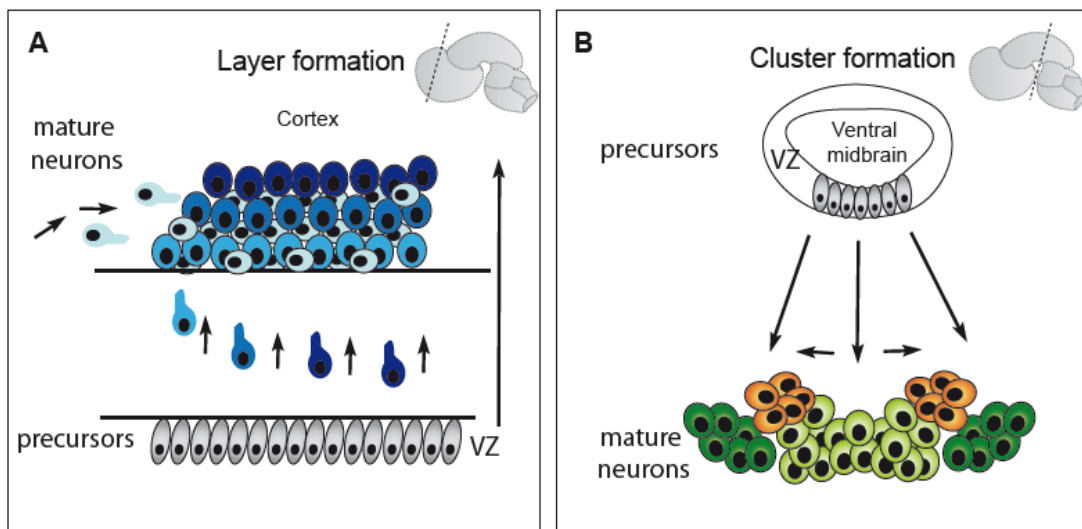
Figure 1. Neuronal migration in dorsal brain areas (A) results in formation of neuronal layers, whereas in (B) ventral brain areas neurons migrate and form clusters or nuclei. VZ: ventricular zone

The MbDA neurons project to striatal (caudate and putamen nucleus), limbic (nucleus accumbens, amygdala, olfactory tubercle, septum) and cortical areas (prefrontal cortex, cingulate cortex, perirhinal cortex) (Bentivoglio and Morelli, 2005; Bjorklund and Dunnett, 2007). SN and VTA neurons project to distinct areas, but some of their projections are partially overlapping. Most SN neurons project to the dorsal-lateral striatum (putamen and caudate nucleus) and form the mesostriatal pathway (Figure 2). The SN neurons of the mesostriatal pathway are involved in regulation of motor control and their degeneration results in the major symptoms of Parkinson's disease. Some SN neurons also innervate cortical and limbic areas (Figure 2). The VTA projection pattern is more complicated. Thus, the posteromedial VTA projects to ventromedial striatum (medial olfactory tubercle, medial nucleus accumbens shell); most of the anteromedial VTA, lateral VTA and lateralposterior RRF project to ventrolateral striatum (nucleus accumbens core, lateral shell and lateral tubercle) and the medial posterior VTA projects to ventrolateral striatum (nucleus accumbens shell and core), medial prefrontal cortex and basolateral amygdala (Bentivoglio and Morelli, 2005; Ikemoto, 2007; Lammel et al., 2008; Lammel et al., 2011; Lammel et al., 2012; Sillitoe and Vogel, 2008; Van den Heuvel and Pasterkamp, 2008). The VTA neurons form the mesocorticolimbic system and are involved in regulation of emotions and reward-associated behavior. Defects in dopaminergic transmission within the mesocorticolimbic system have been associated with drug addiction, depression, attention deficit hyperactivity disorder and schizophrenia (Chenu et al., 2009; Dailly et al., 2004; Sulzer, 2007; Winterer and Weinberger, 2004; Wise, 2009). RRF neurons play a role in modulating the nigrostriatal and mesolimbic pathways (Deutch et al., 1988).
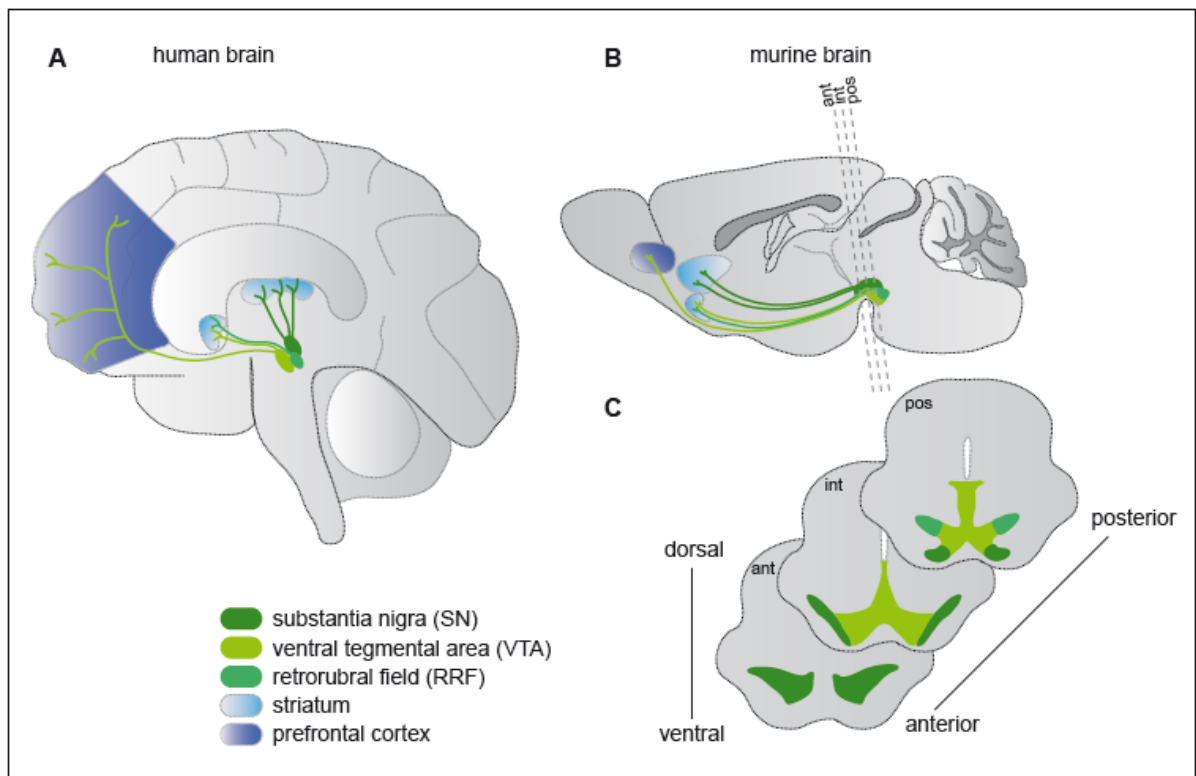
Figure 2. Midbrain dopaminergic (MbDA) system. (A,B) Anatomical localization of MbDA neurons in different nuclei and their axonal projections target areas in the human (A) and murine (B) forebrain (sagittal view). (C) Coronal view, level of sections indicated in B, ant: anterior, int: intermediate, pos: posterior

In addition to anatomical classification into SN, VTA and RRF and functional characterization based on their different projection pattern, MbDA neurons were further distinguished based on their electrophysiological and molecular properties. By combining retrograde tracing with brain slice electrophysiological recording, Lammel and colleagues (2008), revealed different firing properties for MbDA neurons projecting to striatal and limbic areas versus cortical areas. Moreover, this study revealed that a part of the VTA neurons were missing some of the electrophysiological properties, thought before to be specific for MbDA neurons.

Transcriptome and marker analyses that have been done in MbDA, SN and VTA subpopulations in the adult brain, found several receptors, transcription factors and channels to be differentially expressed (Barrett et al., 2001; Greene et al., 2005; Simunovic et al., 2008; Zhou et al., 2011). For example only SN neurons and few nearby VTA neurons express GIRK2 (G-protein regulated inward rectifier potassium channel-2) (Reyes et al., 2012; Schein et al., 1998), whereas most of MbDA neurons of the VTA express Calbindin (Ca^{2+} binding protein) (Alfahel-Kakunda and Silverman, 1997; Pan and Ryan, 2012; Rogers, 1992). It is not well understood yet how these molecular and electrophysiological differences contribute to the functional diversity of MbDA neurons.

Moreover, while described anatomical, functional, physiological and molecular diversity of MbDA neurons has been established, it remains unclear when and how this diversity is

generated during development. A comprehensive understanding of the genetic cues and extrinsic signals controlling the fate choice of precursor cells into specific MbDA neurons is required.

1.2 Development of MbDA neurons

MbDA neurons develop in a complex and continuous multi step process. MbDA neuron development starts with midbrain regionalization and cell fate specification, followed by differentiation and migration. Later events include growth of axonal processes and synapse formation (Figure 3). Various signaling molecules, transcription factors and cell receptor molecules tightly control MbDA development.
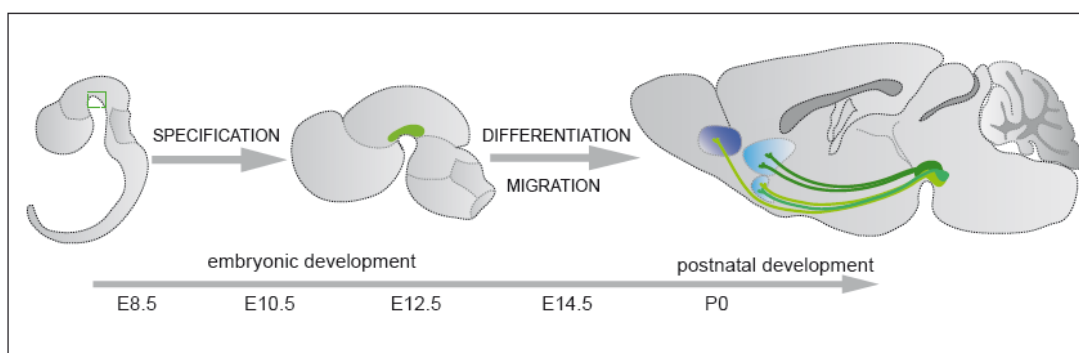
Figure 3. Timeline of MbDA neuron development. Progenitors in the ventral midbrain are specified to MbDA fate between embryonic day (E) 8.5 and E11.5. They differentiate, migrate and form projections between E11.5 and E14.5. Subsequently, MbDA neurons establish synaptic contacts with neurons in their forebrain target areas, creating a complex and functional circuitry after P0.

1.2.1 Regional specification of MbDA progenitors

MbDA progenitors are specified along the dorsoventral (DV) and anteroposterior (AP) axes of ventral tube at the intersection of two signals: SHH (Sonic hedgehog) expressed along the ventral neural tube and FGF8 (Fibroblast Growth Factor 8) locally secreted at MHB (mid-hindbrain boundary) and anterior hindbrain (Hb) (Ye et al., 1998)(Figure 4 A). SHH and FGF8 function as organizers, secreted signaling molecules that can induce and pattern a neighboring tissue. While, FGF8 acts as a local patterning molecule on the anteroposterior axis, SHH is involved in dorsoventral patterning. Forebrain explants that normally do not give rise to MbDA neurons, when exposed to FGF8 beads, ectopically start expressing MbDA markers. Furthermore, inhibition of SHH with a function-blocking antibody, prevents FGF8 from inducing MbDA neurons. Thus, SHH and FGF8 control the fate and position of MbDA neurons along the dorsoventral and anteroposterior axis (Ye et al., 1998). FGF8 and SHH signals determines the activation of a combination of transcription factors, such as OTX2 (Orthodenticle homeobox 2), LMX1A/B (LIM homeobox transcription factor 1 α and β), EN1/2 (Engrailed 1 and 2) in a temporal order. FGF8 represses OTX2 (Martinez et al., 1999). Transcription factor OTX2, expressed in the anterior part of the brain (forebrain and midbrain) and GBX2 (Gastrulation Brain homeobox 2), expressed posteriorly (hindbrain) interact to position the MHB and FGF8

expression (Li and Joyner, 2001)(Figure 4 A). In mutants, who ectopically express OTX2 in anterior hindbrain the MHB is shifted, leading to an expansion of MbDA progenitor domain (Brodski et al., 2003). FGF8 can induce and maintain expression of WNT1 (Wingless-related MMTV integration site 1) at the MHB and in the roof plate (Chi et al., 2003; Liu and Joyner, 2001) (Figure 4 A, C). WNT1 is important for maintaining OTX2 expression, which is required for the repression of NKX2.2 (NK2 homebox 2) (Figure 4C). The absence of this repression results in generation of 5HT neurons instead of MbDA neurons (Prakash et al., 2006). Moreover, in absence of WNT1, SHH and FGF8 are not sufficient to induce MbDA neurons (Prakash et al., 2006). WNT1 is also involved in maintaining the expression of EN1/2 genes, which are also involved in the induction and maintenance of MbDA neurons (Castelo-Branco et al., 2004; Castelo-Branco et al., 2003; Danielian and McMahon, 1996).

SHH induces FOXA2 (Forkhead box protein A2) expression, by signaling through its receptor PTCH1 (Patched-1). The SHH-PTCH binding triggers the release of SMO (Smoothened) inhibition by PTCH1 and activation of GLI proteins. SHH signaling induces the generation of a transcriptional activator form of GLI2 and suppresses the formation of a GLI3 repressor. GLI2 activator induces FOXA2 transcription factor in the ventral midline of the floor plate (Hynes et al., 1997; Matise et al., 1998). When the floor plate starts to express FOXA2 transcription factor, expression of FOXA1 is induced. FOXA1/2 induce SHH expression in the floor plate and also attenuate the SHH signaling by binding to and inhibiting the expression of GLI2 transcriptional activator (Kittappa et al., 2007; Mavromatakis et al., 2011). FOXA1/2 inhibits the NKX2.2 in ventral midbrain progenitors playing a role in neuronal commitment of MbDA progenitors (Lin et al., 2009; Mavromatakis et al., 2011). SHH expression ventrally, in the domain that give rise to MbDA neurons is flanked by NKX6.1 domain from which red nucleus (RN) progenitors arise, which is then followed by the NKX2.2 domain believed to give rise to GABAergic interneurons (Ang, 2006). The delineation of MbDA progenitors is controlled by the SHH indirect induction of MSX1 (Msh homeobox 1) expression in the ventral midbrain. MSX1 inhibits NKX6.1 (NK6 homeobox protein1) and restricts its expression to more lateral region of the ventral midbrain from where the other neuronal types are generated (Andersson et al., 2006; Fedtsova and Turner, 2001). SHH also induce the expression of LMX1A/B (LIM homeobox transcription factor 1 α and β) (Andersson et al., 2006; Fedtsova and Turner, 2001). LMX1A start to be expressed in the ventricular zone of the developing midbrain around E9.0 and forms a regulatory loop with WNT1 (Chung et al., 2009; Yan et al., 2011). In postmitotic MbDA progenitors, LMX1A/B downregulate the expression of LIM1/2 (LIM homeobox 1 and 2) and BRN3A (brain-specific homeobox / POU domain protein 3A), which are markers for neurons of the red nucleus (Ono et al., 2007). LMX1A also acts on MSX1, required for the repression of NKX6.1. Repression of NKX6.1 at the midline is important to delimit the MDA progenitor domain from the progenitor of other neuronal types (Andersson et al., 2006; Fedtsova and Turner, 2001). Subsequently,

LMX1A/B is involved in inducing the expression of other transcription factors necessary for MbDA neuronal differentiation (Andersson et al., 2006; Chung et al., 2009; Fedtsova and Turner, 2001).
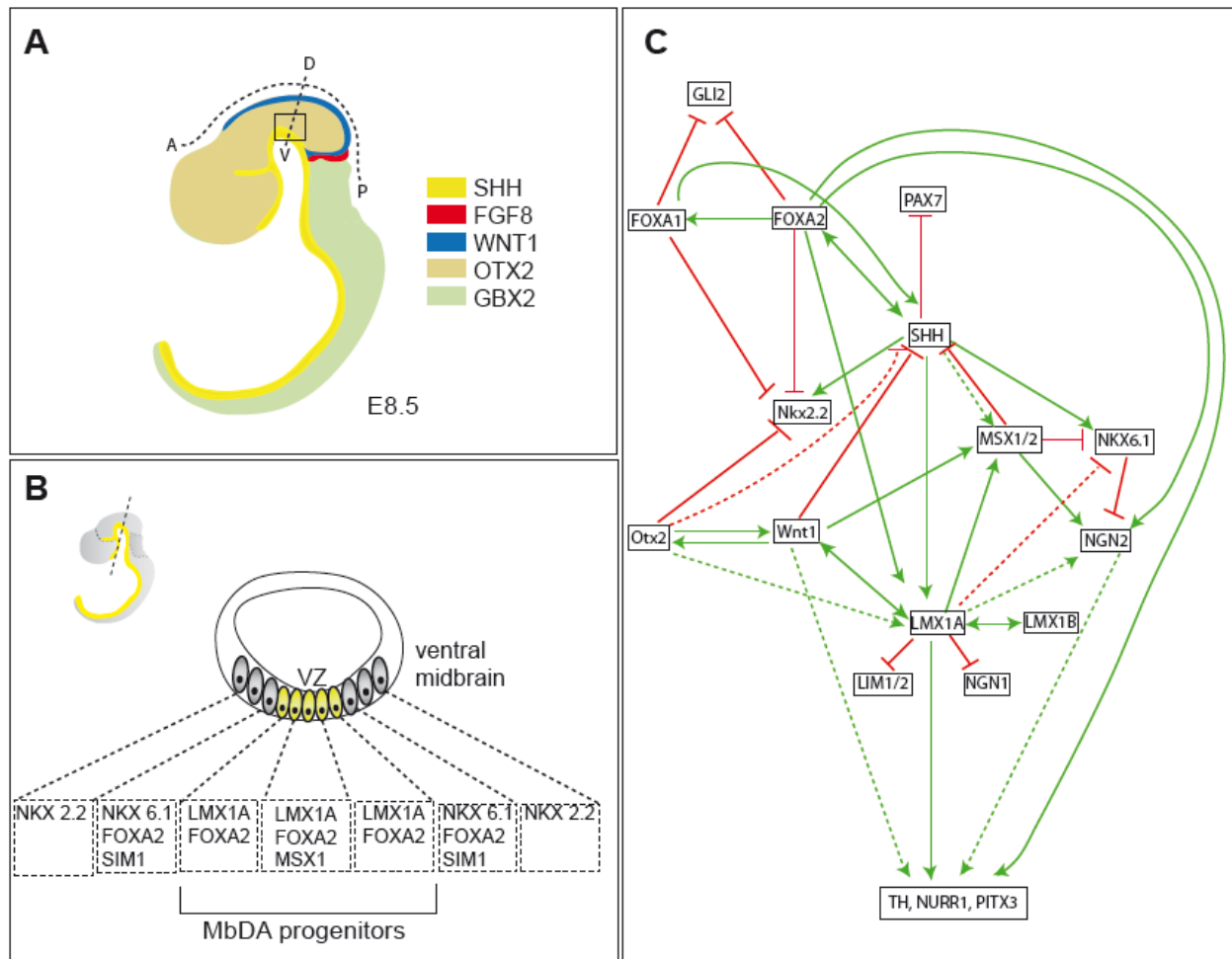
Figure 4. The induction of MbDA progenitors and their differentiation into MbDA neurons: MbDA progenitors are induced, starting at E8.5 by a combination of factors, the most important ones: SHH (Sonic Hedgehog), FGF8 (Fibroblast growth factor 8) and WNT1 (Wingless-type protein 1). The square indicates the place of MbDA neurons induction. (B) The MbDA initial domain expressing SHH will express MbDA progenitors markers, LMX1A (LIM homeobox transcription factor 1 α), MSX1 (MSH homeobox 1); whereas the adjacent domain will express SIM1 (single-minded homolog 1), NKX6.1 (NK6 homeobox 1), the red nucleus progenitors. FOXA2 (forkhead box A2) labels both progenitor domains. NKX2.2 (NK2 homebox 2) is expressed in a precursor domain that is thought to give rise to GABAergic interneurons. Modified after (Blaess et al., 2011) (C) Simplified regulatory network of MbDA neuron induction. SHH induces the expression of LMX1A, Nkx6.1, Nkx2.2 and regulates FOXA2 expression, and inhibits PAX7 (paired box gene 7). FOXA2 interacts with FOXA1 and both inhibit NKX2.2. FOXA2 activates NGN2 and the markers for differentiated MbDA neruons: TH (Tyrosine Hydroxylase), NURR1 (nuclear receptor subfamily 4, group A, member 2) and Pitx3 (paired-like homeodomain transcription factor 3). WNT1 (wingless-related MMTV integration site 1) negatively regulates SHH and induces OTX2 (orthodenticle homolog 2) and LMX1A. LMX1A represses LIM1/2 (LIM homebox protein 1 and 2) and NGN1 (neurogenin 1), regulates WNT1 and TH, NURR1 and PITX3, and indirectly activates NGN2 (neurogenin 2); WNT1. Red arrows: negative regulation, Green arrows: positive regulation (Andersson et al., 2006; Chung et al., 2009; Ferri et al., 2007; Gennet et al.; Joksimovic et al., 2009b; Lin et al., 2009; Mavromatakis et al., 2011; Nakatani et al., 2010; Omodei et al., 2008; Ono et al., 2007; Prakash and Wurst, 2006; Puelles et al., 2004; Tang et al., 2010).

1.2.2 Differentiation of MbDA progenitors into MbDA neurons

FOXA1/2 and WNT1 activate the expression of the panneural gene NGN2 (neurogenin 2), marking the beginning of MbDA neurogenesis (Ferri et al., 2007; Kele et al., 2006; Ono et al., 2007). WNT1 is further required for the proper differentiation of MbDA progenitors, since in WNT1 null mice few TH positive neurons are generated and they do not start to express PITX3 (paired-like homeodomain transcription factor 3), one of the differentiated MbDA neurons markers (Prakash et al., 2006). The WNT1-LMX1A regulatory loop controls the number of the cells expressing NURR1 (nuclear receptor subfamily 4, group A, member 2) and TH and their position in the floor plate (Andersson et al., 2013). NURR1 is necessary for the proper development of MbDA neurons. In absence of NURR1, postmitotic MbDA do not initiate TH, VMAT (vesicular monoamine transporter 2) and DAT (dopamine transporter) expression and become apoptotic (Perlmann and Wallen-Mackenzie, 2004; Prakash and Wurst, 2006). Thus, NURR1 induces the expression of TH, VMAT2 and DAT, which are required for dopamine synthesis (Saucedo-Cardenas et al., 1998; Sillitoe and Vogel, 2008; Smidt et al., 2003).

The first, differentiated MbDA neurons appear between E10.5 and E11.5. MbDA neurons continue differentiation in successive waves between E12.5 and E15.5 (Bayer et al., 1995). Neurons of SN and dorsal lateral VTA appear first with a peak at E11.5. In contrast, medial VTA neurons and more caudal MbDA neurons appear to be born later with a peak at E12.5 (Bayer et al., 1995). By E11.5 - E12.5 WNT1 is restricted to a narrow area at the VZ and together with LMX1B induces PITX3 expression (Prakash and Wurst, 2006; Smidt et al., 2000). PITX3 is expressed in all MbDA neurons and its expression is maintained till adulthood. The lack of PITX3 does not affect the formation of MbDA neurons, but leads to the loss of most of SN neurons and about 50% of VTA neurons at later stages in development. This suggested that PITX3 is important for SN terminal differentiation (Maxwell et al., 2005; Nunes et al., 2003; Smidt et al., 2004). PITX3 also cooperate with EN1, which can induce the NURR1 target genes, including TH and DAT in the anterior MbDA neurons (Veenvliet et al., 2013). The absence of EN1 leads to a similar phenotype to that observed in *Pitx3* null embryos (Veenvliet et al., 2013). EN1 starts to be expressed in postmitotic MbDA neurons by E11.5 and it has been shown to be required for MbDA neurons survival (Simon et al., 2001). Thus, in the *En 1/2* null mutants the generation of MbDA neurons is diminished and the neurons that are generated die at around E14.5. It is belived that their survival depend on signals or trophic support provided by other cells that are normally present in the ventral midbrain and which are missing in the *En 1/2* null mutants (Simon et al., 2001; Simon et al., 2004). EN1/2 can compensate for each other and are also required for maintenance of MbDA at later stages.

1.2.3 SHH expressing progenitors give rise to different MbDA neuronal subpopulations

All MbDA neurons originate from progenitors in the midbrain floor plate that express SHH,

FOXA1/2 and LMX1A/B (Ang, 2009; Blaess et al., 2011; Chung et al., 2009; Hayes et al., 2011; Nakatani et al., 2010; Yan et al., 2011). However, SHH expression in the ventral midbrain is very dynamic (Figure 5). MbDA progenitors respond to SHH signaling between E7.5 and E9.5 and express SHH between E8.5 and E11.5. SHH is expressed in a narrow medial domain at E8.5, which becomes broader by E9.5-E10.5. At E11.5 SHH expression is present even further lateral, but ceases medially (Blaess et al., 2011; Hayes et al., 2011) .
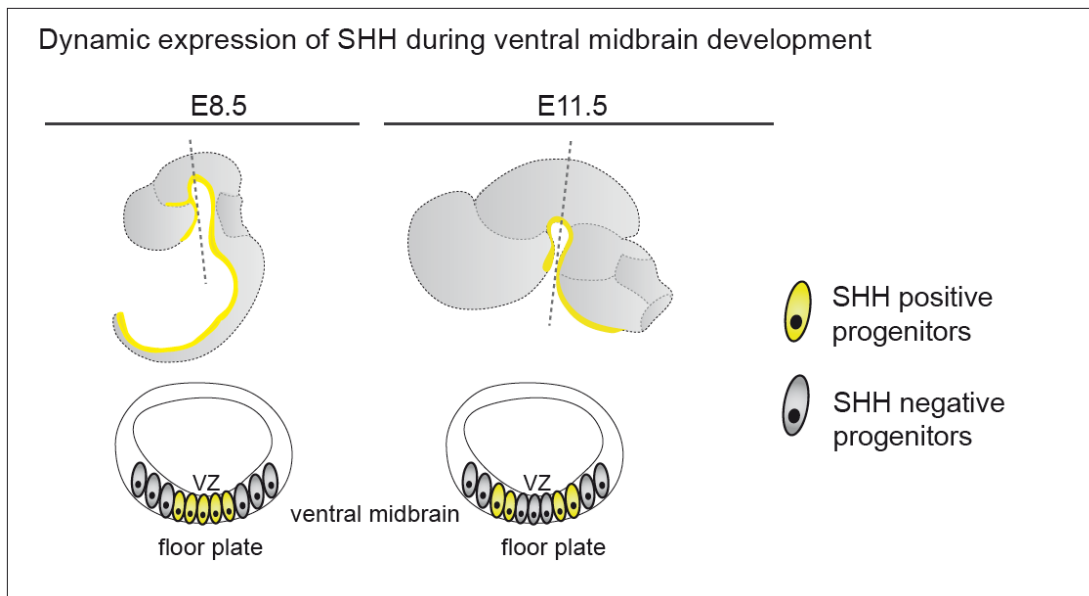
Figure 5. SHH expression (yellow) during ventral midbrain development is dynamic: initially (E8.5) it is confined to the mesencephalic ventral midline, then expands laterally (E11.5) and at later stages is downregulated in the ventral midline (after E12.5).

1.2.3.1 Genetic inducible fate mapping of SHH expressing progenitors

By employing genetic inducible fate mapping method (GIFM), which heritably marks progenitors and their descendants, several authors unraveled the contribution of SHH to MbDA neuron subpopulations. GIFM is a lineage tracing method, which establish a relationship between gene expression at a specific embryonic time point and cell fate (Joyner and Zervas, 2006). GIFM is based on an inducible Cre-loxP system, which uses a fusion protein of DNA recombinase, Cre (Causes Recombination) and a mutant estrogen receptor ligand-binding domain (ER) or progesterone receptor ligand binding domain. The mutant ER it can only be activated by the synthetic estrogen antagonist 4-hydroxy-tamoxifen (TM) and not by the endogenous estrogen (Hayashi and McMahon, 2002; Schwenk et al., 1998). The Cre estrogen receptor fusion protein (CreER) interacts with chaperone proteins, such as HSP 90 (heat shock protein 90) and forms an inactive complex, which is retained in the cytoplasm. When TM binds to the ER, the CreER fusion protein dissociates from the chaperones and the nuclear localization signal of the ER is exposed. This allows the CreER protein to enter into the nucleus, where it specifically recognizes 34 base pairs (bp) sequences named lox P (locus of x over P1). Cre mediates cleavage at the loxP sites, with the same orientation and a DNA sequence flanked by two loxP,

13

is deleted upon recombination. Knocking in a CreER cassette into the Shh locus ($Shh^{CreER/+}$ mice**)** results in CreER expression under the control of Shh specific promoter (Harfe et al., 2004). Tamoxifen (TM) administration to these mice induces Cre recombinase activity in all cells expressing SHH. A reporter line was generated by inserting a *loxP*-flanked *Stop* sequence followed by the Enhanced Yellow Fluorescent Protein gene (EYFP) into the *Gt(ROSA)26Sor* ubiquitous locus (Srinivas et al., 2001). By crossing the ShhCreER line with R26YFP, the *Stop* sequence is deleted and EYFP expression is observed in the cells expressing SHH upon TM administration at a particular embryonic stage (Figure 6 A). During embryogenesis the dose of TM that can be administrated is limited, since TM can interfere with the normal development of embryos (Joyner and Zervas, 2006). The limited dose of TM determines that SHH expressing cells to be labeled in a mosaic pattern (Figure 6 A). The time of TM administration can be chosen and the descendants of the recombined cells can be visualized at any later time point. Therefore contribution of the dynamic expression of SHH during embryonic development can be determined.

1.2.3.2 SHH expressing progenitors preferentially contribute to different MbDA neuron subpopulations over time

Using GIFM, Joksimovic and colleagues suggested that SHH expression between E7.5 and E12.5 sequentially marks three spatially distinct ventral midbrain progenitor domains that give rise to different neurons (Joksimovic et al., 2009). However, the distribution of fate mapped cells quantified and the potential contribution to other cell types, like astrocytes, was not assessed. Further studies, which also used genetic inducible fate mapping technique, quantitatively assessed the distribution of fate-mapped cells marked at different points (Blaess et al., 2011; Hayes et al., 2011). These studies show that progenitors expressing SHH between E8.5 and E12.5 give rise to MbDA neurons. The highest contribution to the MbDA neurons occurs when SHH is expressed throughout the LMX1A expressing MbDA precursor domain (Figure 4 B). Cells that express SHH between E9.5 and E10.5 also contribute to the red nucleus (RN), another midbrain neuronal population. However, the most interesting observation is that SHH expressing progenitors contribute differentially to MbDA neuronal subpopulations. Comparison of the fate of cells marked between E8.0 and E11.0 by quantitative analysis showed a continuous decrease in the relative contribution of cells expressing SHH to the most anterior region of the brain over time (see Figure 2 for anterior level). In contrast, there was a slight increase in the relative contribution of SHH-derived cells to more posterior regions (see figure 2 for intermediate level and posterior level). Additionally, cells expressing SHH after E9.5 were also found to give rise to astrocytes. SHH expression in the medial floor plate (labeling at E8.5) have a bias to contribute to the SN, while MbDA progenitors in the lateral floor plate (labeling at E11.5) contribute preferentially to MbDA neurons in the medial VTA (mVTA) (Figure 6 B). GIFM

14

can therefore be used to differentially label cells giving rise to the SN or mVTA and to follow their migratory routes and behavior from their early progenitor stage to their final location in the ventral midbrain (Figure 6B).
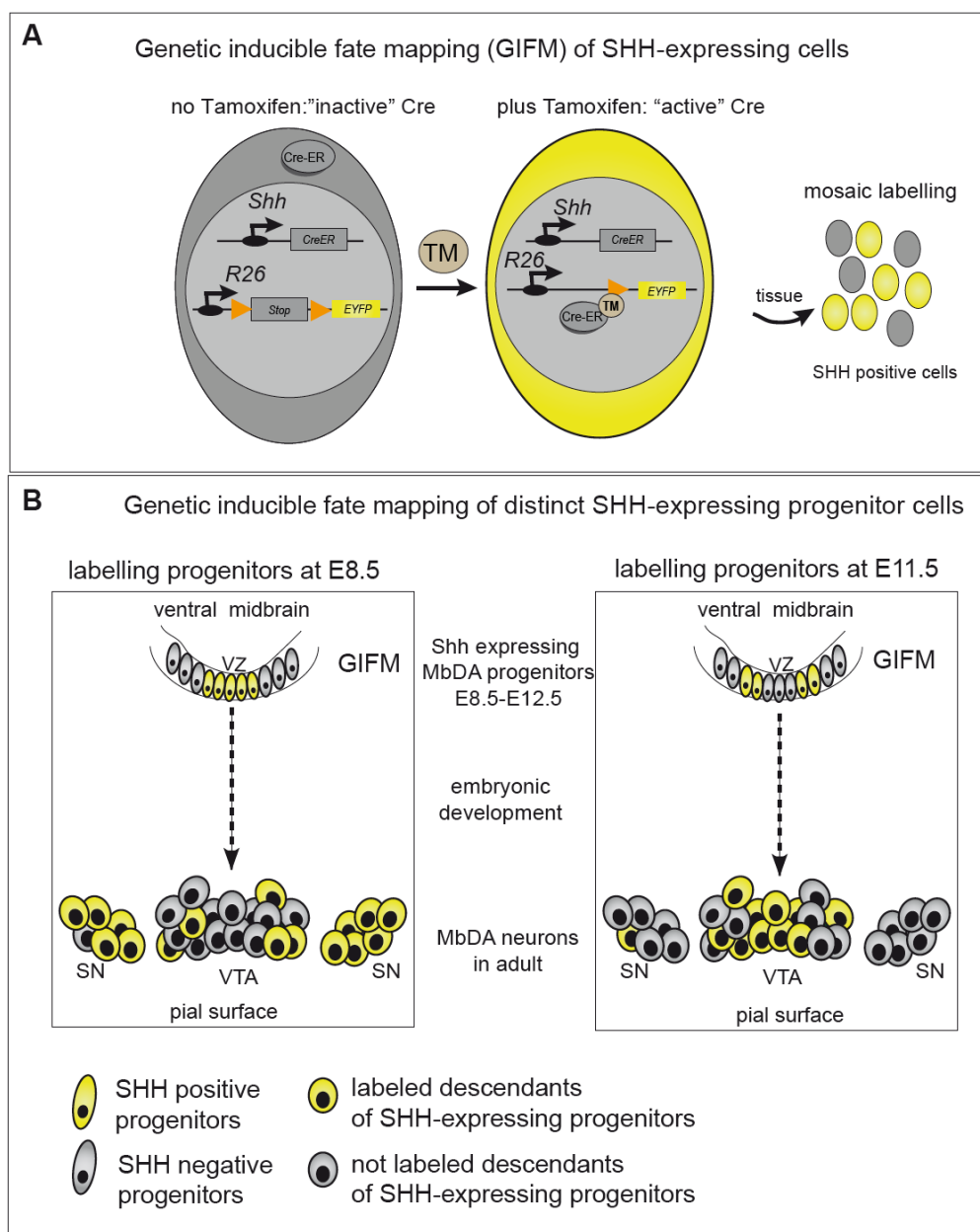
Figure 6. Fate mapping strategy to mark and follow SHH-expressing MbDA progenitors (A) Inducible fate mapping strategy. The CreER encoding sequence is inserted into the *Shh* locus. The R26 reporter allele contains a floxed *Stop* cassette upstream of *EYFP*. The *Stop* cassette is removed upon tamoxifen mediated recombination and EYFP is expressed in recombined cells. Note that the labeling is mosaic, since only a subset of cells is recombined (B) Genetic inducible fate mapping (GIFM) of SHH-expressing cells, through labeling at E8.5 results in permanent marking of medial MbDA progenitors that have a biased contribution to SN neurons. GIFM Shh-expressing cells, through labeling at E11.5 results in permanent marking of lateral MbDA progenitors that preferentially give rise to mVTA neurons.

1.2.4 MbDA neuronal migration

Once the MbDA neurons are specified, they differentiate and migrate from ventricular zone (VZ) of the ventral midbrain toward the pial surface. The differentiation and migration processes

15

occur during a similar developmental time frame (Figure 3). The end result of MbDA migration is the correct positioning of MbDA neurons within the ventral midbrain and formation of the three MbDA neuron distinct clusters: SN, VTA or RRF.

MbDA neurons subpopulations have been suggested to follow a combination of two general routes of migration: radial migration and tangential migration. These different routes of migration are largely classified by direction of migration (e.g. radial movements along the vertical plane or tangential movements in the horizontal plane).

Several studies, based primarily on immunostainings for TH, the rate-limiting enzyme in dopamine synthesis and/or birthdating of ventral midbrain cells, have suggested the following models for the different MbDA subpopulation migration:

1) VTA and SN are primarily formed through radial migration from the VZ towards the pial surface on a radial path (Hanaway et al., 1971).

2) MbDA neurons initially (E11.5) migrate radially towards the pial surface and then tangentially from the midline to form the VTA and SN (Kawano et al., 1995; Marchand and Poirier, 1983; Shults et al., 1990) (Figure 7)

3) SN is generated at the MHB and migrate first radially ventralwards and then anterior. The authors based their conclusions on the assumption that the ventral midline does not give rise to differentiated neurons and therefore the authors assume that labeled cells ventral to the floor plate are part of an anteroposterior migratory stream (Marchand and Poirier, 1983).
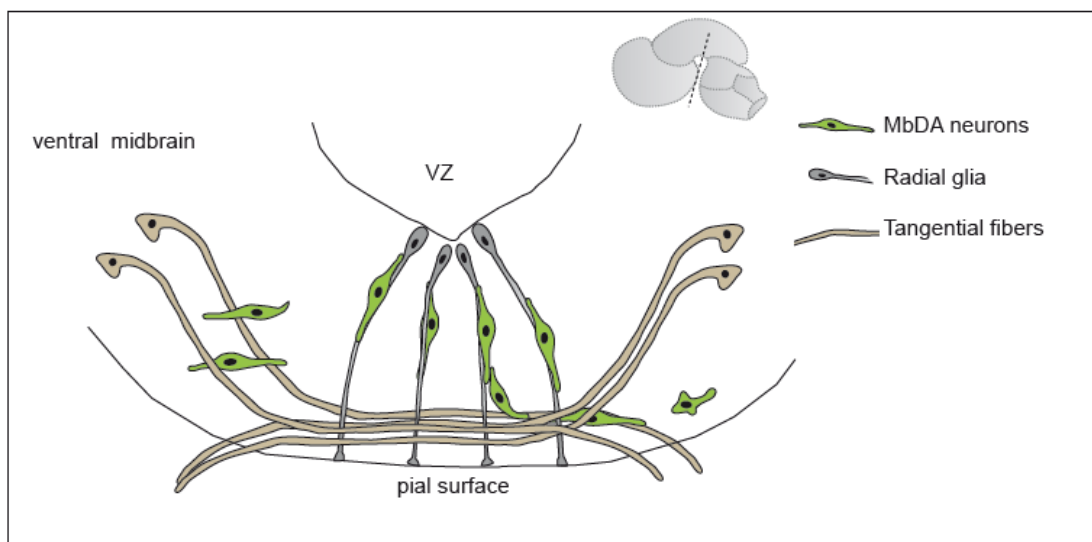
Figure 7. Proposed migratory routes of MbDA neurons. MbDA neurons generated at the VZ of the ventral midbrain migrate first toward the ventromedial part of the midbrain along radial processes and laterally in the basal part of the midbrain along tangentially arranged fibers. Modified after (Ohyama et al., 1998).

Cell adeshion molecules, proteoglycans and extracellular matrix molecules have been implicated in regulating MbDA neuronal migration. The radial migration is thought to occur along radial glia processes expressing tenascin (Figure 6) (Kawano et al., 1995). While, tangentially migrating MbDA neurons are thought to follow tangentially oriented fibers of other neurons originated from the lateral part of midbrain (Kawano et al., 1995; Shults et al., 1990). The neural

16

cell adhesion molecule L1 is expressed on the tangential fibers, whereas MbDA neurons express the ligand L1/NgCAM (cell adhesion molecule L1/neuron-glia cell adhesion molecule) and the chondroitin sulfate proteoglycan 6B4. It has been proposed that the tangential migration of MbDA is controlled by heterophilic interactions between L1 and 6B4 (Ohyama et al., 1998). Mice lacking L1 show abnormal position of MbDA neurons (Demyanenko et al., 2001; Vitalis et al., 2000).

Reelin is an extracellular matrix molecule important for neuronal migration and positioning in different brain areas, such as cortical and cerebellar cortex. In *Reeler* mice, which have a spontaneous mutation in *Reelin* gene, MbDA neurons presumably fail to migrate tangentially to form SN of and accumulate abnormally in the VTA area (Kang et al., 2010; Nishikawa et al., 2003).

Despite of all these studies, the mode of migration including cytoskeleton dynamics and the mechanisms that regulate MbDA neuron migration are not well understood. However these mechanisms were studied in detail in other brain areas, particularly in the forebrain. Since similar mechanisms might regulate migration of MbDA neurons, migration processes in other brain areas will be described in the next chapter.

1.3 Neuronal migration mechanisms

In different areas of the brain extracelular cues, guidance receptors and their downstream signaling pathways coordinate the migration of newborn neurons through the developing nervous system towards their final destination. Defects in migratory processes result in severe malformations, such as lissencephaly, which can lead to mental retardation, epilepsy, paralysis and blindness (Gleeson and Walsh, 2000; Ross and Walsh, 2001) .

Neuronal migration is a process that requires changes in the cell shape and the adhesion to an extracellular matrix. The morphological changes that occur during migration are largely related to actin cytoskeleton dynamics. Therefore, in the following subsection, the dynamic organization of cytoskeleton during neuronal migration will be discussed in detail.

1.3.1 Cytoskeleton organization during neuronal migration

Migrating neurons extend a long leading process that actively explores the environment by forming broad lamellae at their leading edges. The movement of the leading edge is closely coupled with nucleokinesis and the cell rear forms a contractile tail. The soma and nucleus jump forward in a saltatory mode, following the leading process extention (Edmondson and Hatten, 1987; O'Rourke et al., 1992; Schaar and McConnell, 2005). The saltatory mode of migration proposed by Schaar and McConnell, 2005 is caracterized by four repeting steps, as following (Figure 8): 1) the leading edge extends and explores the environment. 2) a cytoplasmic dilatation forms in the leading process, the soma translocates forward and the centrosome moves into the dilatation. 3) the nucleus moves into the dilatation. 4) the rear membrane

retracts. Contractions mediated by myosin II break off leftover adhesions and release the soma for forward movement.

These events are cyclic as the neurons migrate forward. During the migration events the leading process forms adhesion contacts with the substrate, which can be axons of other neurons or radial glia fibres. The temporal and spatial regulation of adhesion is important for the proper progression of the migratory steps.

This saltatory mode of migration was described for many radially or tangentialy migrating neurons e.g. cerebellar granule neurons migrating along glial fibers or tangentially migrating interneurons (Ang et al., 2003; Gasser and Hatten, 1990; Nadarajah et al., 2001; Solecki et al., 2009). However, different types of neurons adjust and modify this basic migratory process depending of the specific requirements of their migratory pathway, which may also change through time e.g. tangentially migrating streams of interneurons from medial ganglionic eminence switch to radial migration as they move toward specific locations within the cortical plate (Elias et al., 2010).
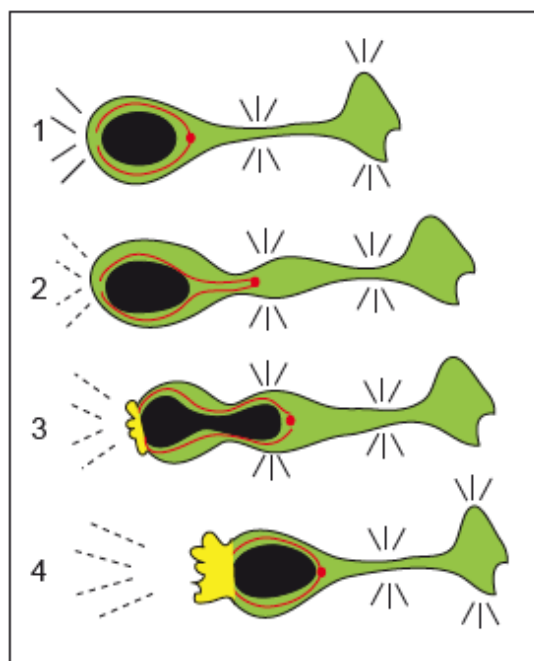
Figure 8. Coordination of the cytoskeleton during saltatory neuronal migration. The leading process extends and forms adhesive contacts with the migration substrate (1). A cytoplasmic dilatation forms at the adeshion point on the leading process. The centrosome (red) moves into the dilation (2). Nucleus (black) translocates into the dilatation, squeezed by contractions at the cell rear mediated by myosin II (yellow) (3). Adhesion contacts break off and the soma moves forward (4). Modified after (Schaar and McConnell, 2005).

1.3.1.1 Migration polarity

Migrating neurons are highly polarized in the direction of their movement. In the cerebral and cerebellar cortex, the leading processes often elongate along the radial dimension of the neuroepithelium and radial glial cells (Rakic, 1990; Rakic, 2000a; Rakic, 2000b). In the cerebral

cortex neuronal-glial interaction is mediated by integrins, which have been sugested to play a role in the interaction between the leading edge and the substrate (Anton et al., 1999).

The establishment of a leading process has been often studied in the context of axon formation, but axonal outgrowth and migration use similar mechanims. The key factors involved in setting up polarity of migrating neurons, such as the PAR3/PAR6/PKC complex are also involved in establishing polarity for axons (Brose and Tessier-Lavigne, 2000; Chen et al., 2008; Manitt and Kennedy, 2002; Tessier-Lavigne and Goodman, 1996).

Evidence that axon formation and migratory leading process extension are distinct events comes from the studies of cortical radial migration and axogenesis, which have studied the function of CDK5 (Cyclin-dependent kinase 5), the polarity protein STK11 (Serine/Threonine kinase 11) or ENA/VASP (vasodilator-stimulated phosphoprotein) proteins (Barnes et al., 2007; Kwiatkowski et al., 2007; Ohshima et al., 2007a) in mice mutants. While ENA/VASP mutants are able to properly form migratory leading and trailing processes, they do not form proper axons.

CSK5 plays critical roles in neuronal migration. CDK5 phosphorylate the microtubule-associated protein, DCX (doublecortin), which results in a lower affinity of DCX to bind microtubules and reduction of microtubule polymerization (Tanaka et al., 2004). In the *Dcx* knockdown mutants the leading processes are very active and unstable, an excessive branching occurs and radially migrating cortical neurons stop their migration. A similar phenotype occurs in mice in which *Cdk5* or the *Cdk5* activator *p35* are inactivated (Gupta et al., 2003; Ohshima et al., 2007a).

1.3.1.2 Dilatation formation and nucleokinesis

In neurons that present a dilatation, the nucleus elongates in the direction of the movement. The centrosome moves ahead of the nucleus and microtubules emerging from the centrosome form longitudinal bundles linked by cross bridges. It was believed that these bundles of microtubule stretch the nucleus, which then translocates along microtubules toward the centrosome. However, when using a microtubule disrupting agent, the nucleus was able to move forward. Myosin II was found to play a key role in nucleokinesis. When treated with a myosin inhibitor, no nucleus or soma translocation occurs, however the leading tip still extends despite the cell movement impairment (Bellion et al., 2005; Kato et al., 2008; Schaar and McConnell, 2005). Phosphorylation of DCX by CDK5 is also considered important in organizing the link between the centrosome and nucleus through its association with the microtubules (Tanaka et al., 2004).

1.3.1.3. Rear Retraction and adhesion in neuronal migration

It has been proposed that myosin constriction at the trailing edge squeezes the nucleus forward into the leading process and after nucleokinesis, the cell soma membrane that surrounded the nucleus is retracted (Higginbotham and Gleeson, 2007).

Adhesion is very important in neuronal migration as it is tightly integrated with cytoskeletal dynamics. Adhesion molecules, in contact with the migratory substrate, are also connected to the actin cytoskeleton. These contacts provide force information from the outside to the migrating neuron. Based on this information, changes are generated in the cytoskeletal structure. These changes can be used to create pulling forces, using the adhesive contacts as traction, or to attract specific intracellular components that will indicate a direction in which the neurons polarize and migrate (Schaar and McConnell, 2005).

1.3.2 Mode of migration

During their migration, neurons can switch between radial and tangential orientated migratory routes. These routes require different mechanisms for motility that are modulated by external guidance cues and substrates for migration.

1.3.2.1 Radial migration

Radial migration in brain areas, such as cortex and hindbrain, includes somal translocation (1) and glia-guided locomotion (2).

1) Radial migration through somal translocation

During somal translocation the cell soma moves along its own leading process. The young neuron maintains its primitive ventricular and pial processes, through which the cell body moves. Not many studies in the brain have been able to study somal translocation due to the lack of neuronal-specific markers that appear in the early, radially shaped cells. However, somal translocation has been shown to occur at early stages of cortical development (Nadarajah et al., 2001) and a similar mechanism has been proposed for serotonergic neurons in hindbrain (Hawthorne et al., 2010).

2) Radial migration through glia-guided locomotion

In the cortex, during glia guided locomotion neurons use the radial glial fibers as a substrate for their migration. Radial glia cells are born early during the development of the ventricular zone and extend long processes along the wall of the neural tube, which reach the pial surface (Gadisseux et al., 1989). The function of radial glia is to provide support for the migrating neuroblasts, but they also have other functions and are not only supportive elements. During cortex development, radial glia cells also undergo division to produce new neurons (Heins et al., 2002; Malatesta et al., 2000; Miyata et al., 2001; Noctor et al., 2001; Noctor et al., 2002). Neurons move with their leading process tightly wrapped around the radial glial fibre. Such a

20

mode of migration was observed for radial migration of superficial cortical neurons and cerebellar granule cell migration (Edmondson and Hatten, 1987; Gasser and Hatten, 1990; Noctor et al., 2001; Takeuchi and O'Leary, 2006).

1.3.2.2 Tangential migration

Neurons can migrate tangentially, either along tangentially oriented fibers, axons of other neurons or along other cells (Marin and Rubenstein, 2001).

Studies that showed a mechanism of tangential migration along fibres were performed on the interneurons that leave the ganglionic eminence to integrate into the cortex (Borrell and Marin, 2006; Lopez-Bendito et al., 2006; Martini et al., 2009). The chain migration of SVZ (subventricular zone) neurons into the olfactory bulb and Gonadotropin-releasing (GnRH) neurons migrate tangentially along vomeronasal axon fibers (Cariboni et al., 2007; Yoshida et al., 1995).

1.3.3 Factors regulating neuronal migration

Based on loss-of-function mouse mutants in which the formation of the SN and/or VTA is impaired, only the Netrin receptor DCC (deleted in colorectal carcinoma), the extracellular glycoprotein Reelin, and the cell adhesion molecule L1 have been implicated in the regulation of MbDA neuronal migration (Ballmaier et al., 2002; Demyanenko et al., 2001; Kang et al., 2010; Nishikawa et al., 2003). However many more signaling pathways and molecules have been implicated in regulating neuronal migration in other brain areas. In the subsequent sections only two factors: Reelin and CXCR4/CXCL12, which impact the thesis results, will be described in more detail.

1.3.3.1 Reelin signaling pathway

Reelin function in the brain has been extensively studied in the cortex, where loss of Reelin function was found to disturb the cortical lamination (Jossin, 2004; Magdaleno et al., 2002). Other studies (Goffinet, 1984; Kang et al., 2010; Nishikawa et al., 2003; Terashima et al., 1994) showed defects in Reeler mutants in ventral brain areas, such as inferior olivary complex, trigeminal motor nucleus, SN, dorsal cochlear nucleus and facial nucleus. Only two studies (Nishikawa et al., 2003 and Kang et al., 2010) showed defects in MbDA neurons positioning in Reeler mutant. However, the mechanism of Reelin role in MbDA neurons positioning remained completely unexplored.

Though the *Reelin* gene is highly conserved between mouse and human genomes, little is known about the regulation of *Reelin* mRNA expression (Tissir and Goffinet, 2003). In humans, mutations in *Reelin* gene result in lissencephaly with cerebellar hypoplasia, and reduction of *Reelin* mRNA in postmortem brains was linked to schizophrenia or bipolar illness with psychosis (Chen et al., 2002). The *Reelin* gene encodes an extracellular matrix glycoprotein, Reelin which

is secreted by different cell types in the brain, such as Cajal-Retzius cells, hippocampal GABAergic neurons, and cerebellar granule cells (Fatemi, 2005).

Reelin binds to the VLDLR (Very Low Density Lipoprotein Receptor) and ApoER2 (Apolioprotein E Receptor 2) (D'Arcangelo et al., 1999). Binding of Reelin to its receptors VLDLR/ApoER2 triggers the tyrosine phosophorylation of the cytoplasmic adaptor molecule DAB1 (Disabled 1). Reelin signaling leads to cytoskeletal changes and a change of gene expression in target neurons (Ballif et al., 2004; Bock and Herz, 2003; Bock et al., 2003; Britto et al., 2013; Fuchigami et al., 2013; Kruger et al., 2010) (Figure 9).
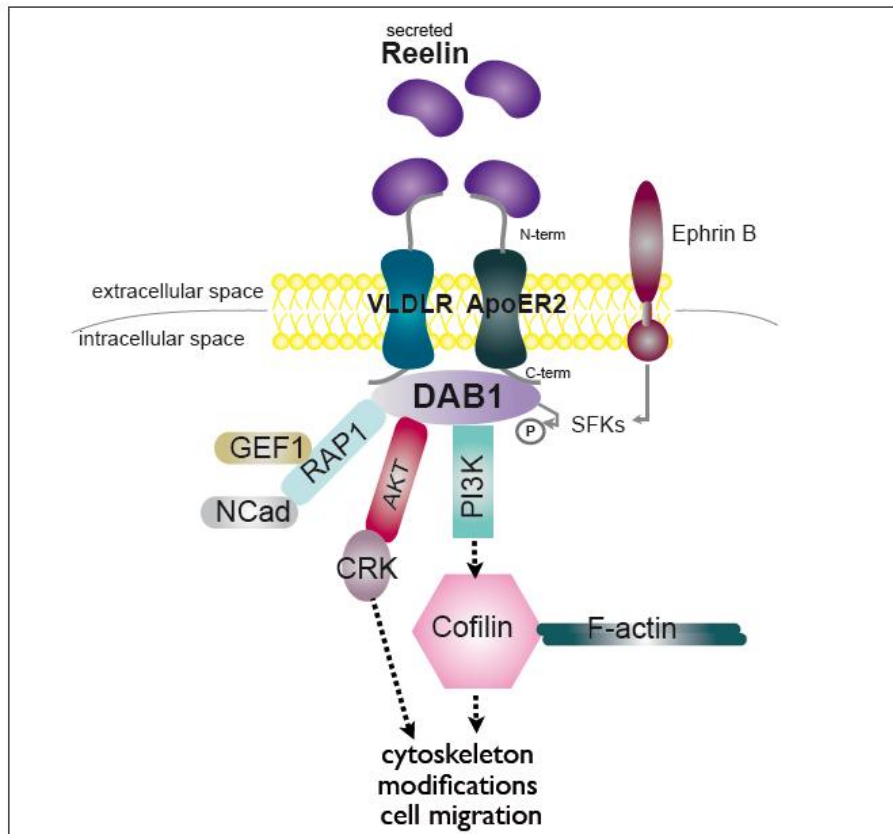
Figure 9. Reelin-mediated signaling pathway. Reelin binds to its receptors ApoER2 and VLDLR and results in dimerization/oligomerization of DAB1 protein. This process leads to activation of Src-tyrosine kinase family/Fyn-kinase (SFK) and tyrosine phosphorylation of DAB1 protein in a positive-feedback loop. Interaction between DAB1 and PI3K (phosphatidylinositol- 3-kinase) and AKT (protein kinase B) impact three other important molecules: Cofilin, CRK (v-crk sarcoma virus CT10 oncogene homolog), F-actin which indirectly lead to modification in cytoskeleton that play a role in migration. Reelin can also bind to coreceptors, such as Ephrins (Bock et al., 2003; Franco et al., 2011; Kruger et al., 2010; Senturk et al., 2011; Yip et al., 2012).

The *Reeler* mice, which have a spontaneous mutation in the *Reelin* gene that results in a *Reelin* null allele, have an abnormal laminar organization of the cerebral and cerebellar cortices and the hippocampus (Forster et al., 2006). In 1955, Falconer described for the first time the *Reeler* mouse phenotype: dystonia, tremors and a reeling gate. *Yotari* mice, which have a spontaneous mutation in *Dab1*, show similar traits as the Reeler mutants, suggesting that Reelin signals through DAB1 (Rice et al., 1998).

22

Reelin is secreted by neurons as a full-length protein and can be cleaved into 5 diffusible fragments. Whether these fragments have individual functions is unknown (Jossin et al., 2004). Reelin receptors, ApoER2 and VLDLR are not completely redundant. Either one or the other receptor appears to have a more important function depending on the brain region. Inactivation of VLDLR results in only mild defects in the cerebellum, but shows defects in the cortex and hippocampus, whereas the inactivation of ApoER leads to strong defects in cerebellum, but not in cortex and hippocampus. The *Apoer2/Vldlr* double knockout shows a phenotype similar to reeler mice (Trommsdorff et al., 1999).

In the *Reeler* neocortex, the cortical lamination is inverted and the neurons fail to pass through earlier-generated neurons, possibly because they are unable to penetrate the subplate, or because they maintain extensive contacts with the radial glial fibres. Several hypotheses exist regarding the function of Reelin in the cortex: (1) Reelin may act as a permisive factor, (2) Reelin may act as an attractant molecule for migrating neurons; (3) it may act as a stop signal (Dulabon et al., 2000; Hoffarth et al., 1995; Zhao and Frotscher, 2010). Quattrocchi and colleagues showed that Reelin has a protease activity that cleaves Laminin and Fibronectin *in vitro*, thus modifying the basal lamina, and facilitating the branching and anchoring of the leading processes important for neuronal migration (Quattrocchi et al., 2002). In *Reeler* mutant mice, the leading processes are less stable, misoriented and not attached to the marginal zone. Two studies showed that ectopic expression of Reelin could rescue the major Reeler phenotype, providing evidence for Reelin as a permissive factor. However, the inversion of cortical layers (late corticogenesis) could not be rescued, which might suggest that Reelin acts as a permissive factor for neurons undergoing somal translocation during early corticogenesis, but might be critical for glia-guided locomotion (D'Arcangelo, 2005; Jossin, 2004; Magdaleno et al., 2002).

Jossin and colleagues showed that processed fragments of Reelin could diffuse from the pial surface to the intermediate zone in the cortex, forming a gradient and acting as an attractant. In *Dab1* knockouts, neurons do not reach proper position and have a reduced speed (Jossin et al., 2007). After transfection with *Dab1* shRNA, neurons accumulate underneath the preplate (Feng et al., 2007; Sanada et al., 2004). In *Reeler* cerebellum, Purkinje cells fail to migrate out of deep locations. Transplantation of granule cells, expressing Reelin into the fourth ventricle resulted in malpositioning of Purkinje cells close to the ventricular zone (Miyata et al., 1997). These observations led to the proposal that Reelin may attract Purkinje cells (Miyata et al., 2010).

Reelin also can play a role as a stop signal. By reducing expression of integrin adhesion molecules, Reelin promotes detachment from the radial glia (Magdaleno and Curran, 2001). Another proposed way, in which Reelin acts as a stop signal, was named the polarization model, in which the location of Reelin source plays an important role. Reelin triggers polarization when neurons are at marginal zone by activating RAP1 (Ras-proximate-1 or Ras-

related protein-1) and stabilizing N-Cadherin (N-Cad). At the same time phosphorylation of DAB1 and Reelin signaling is downregulated and N-Cad is degraded when neurons migrate bipolar. In this model Reelin is suposed to act only on multipolar neurons and this implay the existence of 2 signals, one in more immature multipolar neurons and one in more mature bipolar neurons (Franco et al., 2011; Jossin and Goffinet, 2001).

Reelin has been shown to regulate neuronal migration in the cortex by interacting with Notch and stimulated DAB1 binds to NICD (Notch internal cytoplasmatic domain) and blocks its degradation. In *Reeler* mice, a low level of Notch NICD is present and loss of Notch in migrating neurons results in migration and morphological defects (Hashimoto-Torii et al., 2008). Reelin also stabilizes the cytoskeleton by regulating the phosphorylation level of actin and microtubule-associated proteins, such as Cofilin, which results in the stabilization of the actin cytoskeleton in leading process. In reeler mutant mice the level of Cofilin is reduced (Chai et al., 2009a). By stabilizing the actin cytoskeleton, Reelin can anchor the leading edge of migrating neurons to the cortical surface, a prerequisite for somal translocation (Frotscher, 2010).

1.3.3.2 CXCL12/CXCR4 signaling pathway

CXCR4 receptor is a member of the family of G protein coupled receptors (GPCRs). The CXCR4 ligand is the CXC motif chemokine stromal derived factor-1 (CXCL12 or SDF1). Data from *Cxcl12* and *Cxcr4* null mice showed that CXCR4/CXCL12 have important function in brain development. In the cerebellum of CXCR4 deficient mice, the granule cells are mislocalized (Zou et al., 1998). A similar phenotype was observed in *Cxcl12* deficient mice, suggesting that CXCL12 acts through CXCR4 to regulate cerebellar development (Ma et al., 1998).

CXCL12/CXCR4 signaling is active when CXCL12, secreted by extracellular matrix, binds to the CXCR4 receptor and activates a cascade of events, mediated through the G protein. GTP (guanosine triphosphate) replaces GDP (guanosine diphosphate) in the α subunit of the G protein. The G protein heterotrimer then dissociates from the ligand/receptor complex and signals through a number of downstream pathways, which are not fully understood in the brain, but are known to regulate migration, adhesion, and transcriptional activation of target genes (Figure 10),(Busillo and Benovic, 2007).

Proteolytic degradation and CXCR7 scavenger modulate CXCL12 availability. CXCR7 acts as a scavenger, binding and removing extracellular CXCL12 (Cubedo et al., 2009). There are 2 splice variants of CXCL12, presumably having the same function (Jahnichen et al., 2010).

Meningeal derived CXCL12 has been described to function as a short-range chemoattractant for migrating Cajal-Retzius cells, GABAergic interneurons and precerebellar neurons that express CXCR4 (Borrell and Marin, 2006; Zhu et al., 2009; Stumm et al., 2003; Tanaka et al., 2010).
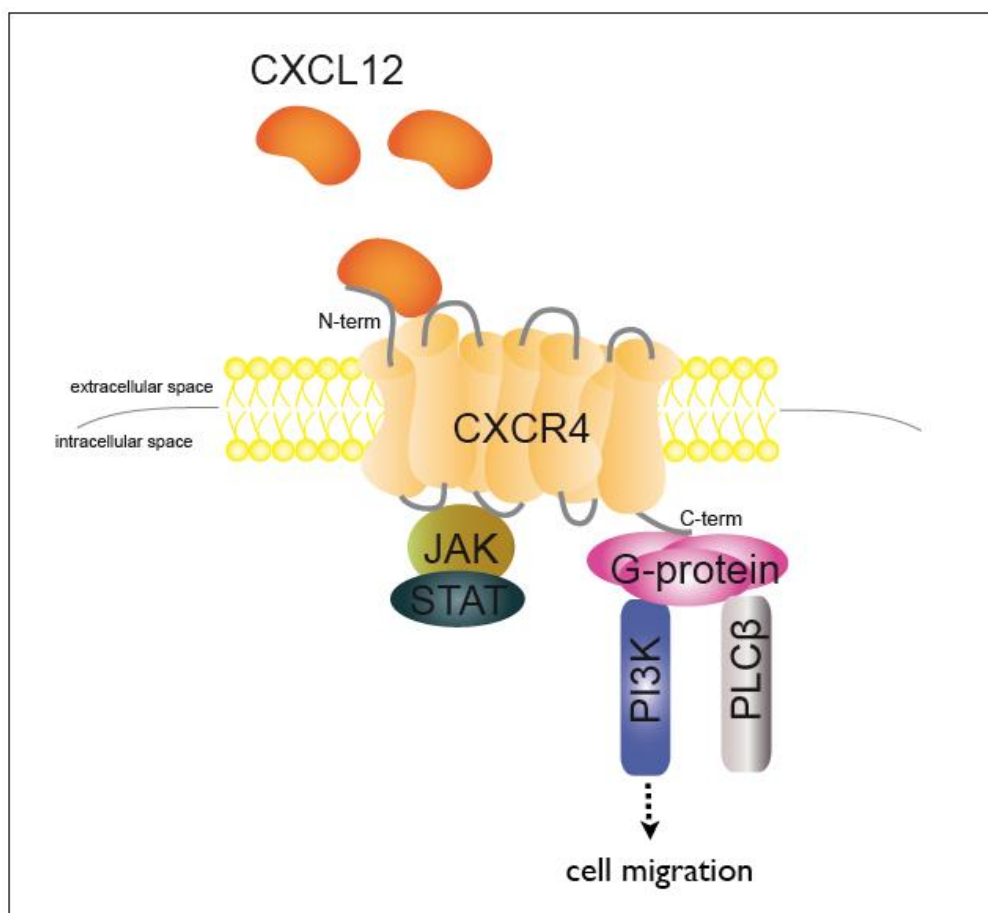
Figure 10. CXCL12/CXCR4 signaling pathway. CXCL12 binding to CXCR4 leads to the activation of multiple G protein-dependent signaling pathways. Activated G protein is able to liberate Gβγ, activate phospholipase C-β (PLC-β) and phosphoinositide-3 kinase (PI3K), ultimately leading to the regulation of processes such as cell migration. Tyrosine phosphorylation of CXCR4 results in the recruitment and activation of the JAK/STAT pathway. Modified after (Busillo and Benovic, 2007).

In the cortex, it has been shown that migrating GABAergic interneurons can respond to a diffusible gradient of CXCL12 (Stumm et al., 2003; Tanaka et al., 2010). Thus, cortical brain slices exposed to a medium containing secreted CXCL12 that perturbs the endogenous level, show an increased response of migrating interneurons with the increase in CXCL12 concentration (Liapi et al., 2008). Furthermore, it was described that CXCL12 plays a role in GABAergic interneuron migration by modulating the migration rate and branching frequency in primary cell culture (Lysko et al., 2011). Additionally, a more recent cortical study showed that CXCR7 can modify CXCR4 responsiveness in interneurons in which both are expressed (Sanchez-Alcaniz et al., 2011), suggesting a more complicated CXCL12/CXCR4 signaling pathway.

CXCL12 plays the role of an attractant on a non-diffusable gradient for gonadotropin releasing hormone neurons. Gonadotropin releasing hormone neurons migrate along the nasal mesenchymal cells that express an increasing level of CXCL12 (Schwarting et al., 2007).

CXCL12 has also been shown to act as a long-range chemoattractant in the case of hippocampal dendate gyrus granule cells migration. CXCR4 expressing granule cells are

located far from their migratory target, which expresses CXCL12. *Cxcr4* mutant mice show a mislocalization of granule cells. Furthermore, ectopic expression of CXCL12 in explant slices disrupts granule cells migration, which migrate to the ectopic location of CXCL12 insted of the normal location (Bagri et al., 2002).

Other than chemoatractant function in migration, CXCL12 has been shown to play a role as an anchor for granule cell progenitor cells in the cerebellum. CXCL12 expressed in the meninges keeps the dividing cerebellar granule cell precursosr from leaving prematurely the extrernal granule layer (Klein et al., 2001).

1.4 Objectives of the study

During embryogenesis, MbDA neurons are generated from MbDA progenitor cells in the floor plate of the ventral midbrain. From their place of origin MbDA neurons have to migrate and assemble into the laterally positioned SN and the medially located VTA. However, the precise migratory routes of MbDA neurons and the molecular mechanisms regulating MbDA migration were not understood.

The first aim of the present study was to characterize the migratory routes of different subpopulation of MbDA neurons giving rise to SN and VTA. Due to the lack of specific markers for SN and VTA neurons during their migration phase, a genetic inducible fate mapping method was used to fluorescently label the two distinct MbDA populations throughout their development. To assess their migration patterns, a detailed analysis of the position of the fluorescently labeled SN or VTA MbDA neurons had to be performed at several stages of their development. Three-dimensional analysis of the morphology of fate mapped MbDA neurons in the ventral midbrain had to be performed to assess the spatial orientation of the leading processes of individual migrating MbDA neurons. Considering the fact that migration is a time dependent, dynamic process, live imaging monitoring of the migratory behavior of MbDA neurons was required. However, the developing mouse brain is a difficult system for manipulation and imaging *in vivo* due to its inaccessibility and opaqueness. To directly monitor the MbDA neuron migratory behaviour *in vitro,* an organotypic slice culture system had to be established.

The second aim of this study was to uncover molecular mechanisms regulating MbDA neuron migration. Reelin signaling was thought to play a role in MbDA neuronal migration, since the SN does not form properly in mouse mutants, in which Reelin signaling is inactivated. To assess whether and how Reelin signaling regulates MbDA neuronal migration it had to be examined whether components of the Reelin signaling pathway were expressed in MbDA neurons during their migration phase. Secondly, the function of Reelin had to be investigated by monitoring the migratory behavior of MbDA neurons in slice cultures upon inhibition of Reelin signaling and by assessing the distribution and morphology of MbDA neurons in in mouse mutants, in which Reelin signaling is inactivated. CXCR4/CXCR12 signaling plays a role in neuronal migration in several brain areas. Therefore, the potential involvement of CXCR4/CXCR12 signaling in MbDA neuronal migration was explored. The expression pattern of CXCR4 and its ligand, CXCL12 was analyzed in the ventral midbrain. Subsequently, the function of CXCR4/CXCR12 signaling in MbDA neuronal migration was investigated by blocking CXCR4 function in slice cultures and by analyzing the distribution of MbDA neurons in *Cxcr4* and *Cxcl12* knockout animals.

This study was performed to gain a better understanding of the development of MbDA neurons and to provide new insights into the routes and molecular mechanisms driving MbDA migration.

2. MATERIALS AND METHODS

2.1 Materials

2.1.1 Technical Equipment

Appliance	Model/Cat. No.	Manufacturer	Registered Office
10x air objective (ultramicroscopy)	CFI Plan Fluor 10x NA 0.3 wd 16 mm	Nikon	Dusseldorf, DE
10x objective (ApoTome)	EC PlnN 10x/0.3 DICI 1.11µm	Carl Zeiss	Jena, DE
20x air objective (ultramicroscopy)	CFI Plan Fluor 20x NA 0.5 wd 2.1 mm	Nikon	Dusseldorf, DE
20x objective (ApoTome)	EC PlnN 20x/0.5 DIC II 0.67 µm	Carl Zeiss	Jena, DE
40x long working distance water immersion objective (ultramicroscopy)	CFI Apo LWD Lambda S 40x NA 1.15 wd 0.60 mm	Nikon	Dusseldorf, DE
40x objective (ApoTome)	Pln Apo 40x/1.3 Oil DIC III 0.26 µm	Carl Zeiss	Jena, DE
40x objective (confocal)	PLAPO 40x WLSM NA 0.90	Olympus	Hamburg, DE
63x objective (ApoTome)	Pln Apo 63x/1.4 Oil DIC II 0.24µm	Carl Zeiss	Jena, DE
Autoclave	DX-150 benchtop	Systec	Wettenberg, DE
Balance	AC211S	Sartorius	Göttingen, DE
Balance	ATL-822-1	Sartorius	Göttingen, DE
Centrifuge	Pico 17	Thermo Fisher Scientific	Schwerte, DE
Centrifuge	Labofuge 400R 75008-162	Thermo Fisher Scientific	Schwerte, DE
Confocal microscope	Olympus IX81	Olympus	Hamburg, DE
Dry bath	FB15103	Thermo Fisher Scientific	Schwerte, DE
Fluorescence Lamp	Illuminator HXP120C	Carl Zeiss	Jena, DE
Gel chambers	Model 41-1525 Model 40-1515	Peqlab	Erlangen, DE
Heating Block	Dry bath Typ15103	Thermo Fisher Scientific	Schwerte, DE
Heating Plate	flattening table OTS 4001 - 4002 - 00	Medite	Burgdorf, DE
Hot plate	Hi1220	Leica	Wetzlar, DE
Hybridization oven	InSlide Out 241000	Boekel Scientific	Feasterville, USA
Incubator (bacteria)	AL01-07	Advantage-Lab	Schilde, BE
Incubator (cell culture)	HERAcell 150i CO2 50115191 A	Thermo Fisher Scientific	Langenbold, DE
Laminar Flow Cabinet	51012197	Heraeus	Meckenheim, DE
Magnetic stirrer	AGE 1200 rpm	VELP Scientifica	Usmate, IT
Micro-centrifuge	Pico17	Thermo Fisher Scientific	Schwerte, DE

Microscope body, inverted (ultramicroscopy)	TI-Eclipse	Nikon Instruments	Dusseldorf, DE
Microscope camera (ultramicroscopy)	CMOS Orca Flash 4.0	Hamamatsu	Herrsching am Ammersee, DE
Microscope Camera (stereomicroscope)	DFC290	Leica Microsystems	Wetzlar, DE
Microscope Camera (ApoTome)	AxioCam MRm	Carl Zeiss	Jena, DE
Microscope Color Camera (ApoTome)	AxioCam MRc	Carl Zeiss	Jena, DE
Microscope, with ApoTome	AxioObserver Z1 SIP66732	Carl Zeiss	Jena, DE
Microwave	MW7809	Severin	Sundern, DE
Mini-centrifuge	3722L	Thermo Fisher Scientific	Schwerte, DE
Motorized sample stage (ultramicroscopy)	M-112.12S	Physik Instrumente	Karlsruhe, DE
pH Meter	FE20 FiveEasy	Mettler Toledo	Giessen, DE
Piezo driven mount (ultramicroscopy)	P-721 PIFOC	Physik Instrumente	Karlsruhe, DE
Pipette-boy Accu-jet pro	26300	Brand	Wertheim, DE
Pipettes (10, 20, 200,1000µL)	FA10002M FA10003M FA10005M FA10006M	Gilson	Middleton, USA
Power supply electrophoresis	EV231	Peqlab	Erlangen, DE
Power Units	Power Supply 231	Carl Zeiss	Jena, DE
Refrigerators Freezers 4°C, -20°C, -80°C	G 2013 Comfort HERAfreeze	Liebherr Kendro	Lindau Hanau, DE
Rocking Platform	4440148	VWR	Darmstadt, DE
Spectrophotometer	Nanodrop 1000	Peqlab	Erlangen, DE
Stereomicroscope with fluorescence	Model MZ10F 10446377	Leica Microsystems	Wetzlar, DE
Thermoblock	230-1.00AT	Peqlab	Erlangen, DE
Thermocycler	DANN engine PTC-200	BioRAD	München, DE
Vacuum pump	Vacuubrand	Brand	Wertheim, DE
Vibratome	HM650V	Microm	Dresden, DE
Vortexer	Vortex mixer Rx3	VELP Scientifica	Usmate, IT
Vortexer	Vortex genius	IKA	Staufen, DE
Water bath	10679808	GFL	Burgwedel, DE
Water bath (paraffin)	WB Typ1012/1013	GFL	Burgwedel, DE
Water bath (cell culture)	Typ 1003 11212101K	Labortechnik	Burgwedel, DE

2.1.2 Data acquisition and data analysis

Computing	Software	Producer	Registered Office
DNA sequence analysis	DNA strider 1.4f18	CEA	Saclay, FR
Gel documentation	Quantity One	Bio-Rad	München, DE
Image acquisition	Axiovision 4.8	Carl Zeiss	Jena, DE
Image acquisition	Leica Application Suite 3.3.0	Leica	Wetzlar, DE
Image acquisition	Olympus Fluoview ver.3.1	Olympus	Hamburg, DE
Image editing	Illustrator CS3	Adobe Systems	München, DE
Image processing	Adobe Photoshop CS3	Adobe Systems	München, DE
Image processing	ImageJ 1.46k	Wayne Rasband, National Institutes of Health	Bethesda, USA
Image processing	ImageJ 1.47n (Fiji)	Wayne Rasband, National Institutes of Health	Bethesda, USA
Image processing	Imarisx64 7.6.1	Bitplane	Zürich, CH
Image processing	MATLAB	The Mathworks	Ismaning, DE
Statistical analysis	GraphPad Prism 5.0	GraphPad Software	San Diego, USA
Statistical analysis	IBM SPSS Statistics 20.0	International Business Machines Corp.	Ehningen, DE

2.1.3. Laboratory consumables

Consumables	Model/Cat. No.	Manufacturer	Registered Office
12-well culture plate	353043	BD Biosciences	Heidelberg, DE
24-well culture plate	353047	BD Biosciences	Heidelberg, DE
6-well culture plate	353046	BD Biosciences	Heidelberg, DE
Autoclave tape	SteriClin sticky tape	VP group	Feuchtwangen, DE
Blades	Apollo	Apollo Herkenrath GmbH & Co KG	Solingen, DE
Cover glasses	LAME110071	Labomedic	Bonn, DE
Culture dishes 100x20mm	831802003	Sarstedt	Sarstedt, USA
DermaClean gloves	PFC 4303971	Ansell	München, DE
Embedding cassettes	Histosette	VWR	Darmstadt, DE
Embedding molds	Peel-A-Way	Polysciences Inc.	Eppelheim, DE
Eppendorf tubes 1.5mL	72690	Sarstedt	Nümbrecht, DE
Filter tips	ART 100/200/1000 barrier tips	Thermo Fisher Scientific	Schwerte, DE
Forceps Dumont (#5)	11252 – 30	Fine Science Tools	Heidelberg, DE
Graefe Forceps (0.8mm)	11050-10	Fine Science Tools	Heidelberg, DE
Iris scissors (11 cm)	14060-11	Fine Science Tools	Heidelberg, DE

Iris Scissors (9 cm)	14060-09	Fine Science Tools	Heidelberg, DE
Lens Cleaning Tissue 105	2105841	Whatman	Dassel, DE
Liquid scintillation vials	Z190527	Sigma-Aldrich	Steinheim, DE
Microcentrifuge tubes 1.5mL	780400	BIO-CERT	Wertheim, DE
Microtome/Cryostat blades	819	Leica	Wetzlar, DE
Millicell membrane insert	PIGMORG 50	Merck Millipore	Darmstadt, DE
Perforated spoon	Moria MC17BIS 10370 -18	Fine Science Tools	Heidelberg, DE
Noyes Spring Scissors (14 mm)	15012-12	Fine Science Tools	Heidelberg, DE
Parafilm	PM-996	Bemis	Köln, DE
Pasteur plastic pipettes 1mL	2655181	VWR	Darmstadt, DE
Pasteur-Plastic Pipette	2655181	VWR	Darmstadt, DE
PCR strip tubes	732-0551	VWR	Darmstadt, DE
PCR strip tubes individual cap	732-0545	VWR	Darmstadt, DE
PCR tubes 0.2mL	81-38440	PEQLAB	Erlangen, DE
Petri dishes 100x15mm	351029	BD Biosciences	Heidelberg, DE
Petri dishes 35x10mm	351008	BD Biosciences	Heidelberg, DE
Polypropylene conical tubes 1.5mL	352096	BD Biosciences	Heidelberg, DE
Polypropylene conical tubes 50mL	352070	BD Biosciences	Heidelberg, DE
Razor Blade	121-6	Plano GmbH	Wetzlar, DE
Rein Rotmarder Brush 770	149-2120	VWR	Darmstadt, DE
Round bottom tubes – 17x100mm	352059	BD Biosciences	Heidelberg, DE
Serological pipettes	4487 (5mL) 4488 (10mL) 4489 (25mL)	Corning Life Sciences	Kaiserslautern, DE
Single use feeding needle	18061-20	Fine Science Tools	Heidelberg, DE
Slides boxes	HS15994E	Carl Roth	Karlsruhe, DE
Sterifilp Sterile Disposable Vacuum	9479650	Merck Millipore	Darmstadt, DE
Student Surgical Scissors	91401-12	Fine Science Tools	Heidelberg, DE
Surgical Blade no.10	0201000010	Feather Safety Razor co.LTD	Köln, DE
Syringes – 1mL	300013	BD Biosciences	Heidelberg, DE
Tissue Wipers	05511	Kimtech	Surrey, UK
Winged Needle	P295A05	Venisystems	Hospira, USA
µ-Dishes, 35 mm low	80136	Ibidi	Martinsried, DE

2.1.4 Chemicals

Chemicals	Catalog no.	Manufacturer	Registered Office
Acetic anhydride	1.00639.1000	VWR	Darmstadt, DE
Ampicillin	A5354	Sigma-Aldrich	Steinheim, DE
Agarose	16500-500	Life Technologies	Darmstadt, DE
AMD3100 octahydrochloride	A5602	Sigma-Aldrich	Steinheim, DE
Ampuwa water	40676.00.00	Ampuwa, Fresenius	Bad Homburg, DE
Aqua-PolyMount	18606	Polysciences Inc.	Eppelheim, DE
Ascorbic acid	A4403	Sigma-Aldrich	Steinheim, DE
Benzyl alcohol	402834	Sigma-Aldrich	Steinheim, DE
Benzyl benzoate	B6630	Sigma-Aldrich	Steinheim, DE
Bisbenzimide H33258 (Hoechst 33258) 10mg/mL	B2883	Sigma-Aldrich	Steinheim, DE
BM purple AP substrate	11442074	Roche	Penzberg, DE
Bromphenol blue	A1120.005	AppliChem	Darmstadt, DE
CaCl	22322.295	VWR	Darmstadt, DE
Chlorophorm	22711.260	VWR	Darmstadt, DE
Corn Oil	C8267	Sigma-Aldrich	Steinheim, DE
Denhardt's Solution 50x concentrate	D2532	Sigma-Aldrich	Steinheim, DE
Dextran sulfate	A4970.0250	AppliChem	Darmstadt, DE
Digoxigenin-labeled NTPs	11277073910	Roche	Penzberg, DE
DMEM	41966-029	Life Technologies	Darmstadt, DE
DMSO	D8418	Sigma-Aldrich	Steinheim, DE
DNA ladder (1kb)	10787-018	Life Technologies	Darmstadt, DE
DNAse I	LS002138	Cell Systems	Kirkland, USA
dNTPs (100mM)	28-4065-52	GE Healthcare	Dornstadt, DE
EDTA	E6511	Sigma-Aldrich	Steinheim, DE
Ethanol	20821.321	VWR	Darmstadt, DE
Ethidium bromide	2218.2	Carl Roth	Karlsruhe, DE
Formamide	155-15026	Life Technologies	Darmstadt, DE
Gel red	41003	Biotium	Hayward, USA
Glucose	G7528-250g	Sigma-Aldrich	Deisenhofen, DE
Glue	Roti coll 1 0258.1	Carl Roth	Karlsruhe, DE
Glycerol	BP 229-1	Thermo Fisher Scientific	Schwerte, DE
Goat serum	G9023519	Sigma-Aldrich	Steinheim, DE
Hanks'Balanced Salts solution	H9394-100mL	Sigma-Aldrich	Steinheim, DE
Hexane	21390.293	VWR	Darmstadt, DE
Histoacryl glue	BRAU9381104	Braun Aesculap	Tuttlingen, DE
Horse Serum	26050-088	Life Technologies	Darmstadt, DE
Immersol	TM518F	Carl Zeiss	Jena, DE
Isoflurane	Forane 2594.00.00	Abbott	Wiesbaden, DE
Isopropanol	P/7500/15	Thermo Fisher Scientific	Schwerte, DE

Propidium Iodide	P4864	Sigma-Aldrich	Steinheim, DE
KCl	26764.260	VWR	Darmstadt, DE
Luria-Bertani-Medium	A0954	AppliChem	Darmstadt, DE
MgCl	25108.260	VWR	Darmstadt, DE
Na$_2$HPO4	28028.298	VWR	Darmstadt, DE
NaCl	27808.297	VWR	Darmstadt, DE
NaH$_2$PO4	28013.264	VWR	Darmstadt, DE
NaHCO$_3$	27775.293	VWR	Darmstadt, DE
NaOH	31627.290	VWR	Darmstadt, DE
Normal donkey serum	017-000-121	Jackson ImmunoResearch	Suffolk, UK
Paraffin Remover	41-5600-00	Medite	Burgdorf, DE
Paraformaldehyde	0335.2	Carl Roth	Karlsruhe, DE
PBS tablets	18912-014	Life Technologies	Darmstadt, DE
PCR purification kit	28104	Qiagen	Hilden, DE
Penicillin-Streptomicin 100x	P4333	Sigma-Aldrich	Steinheim, DE
Phenol	A0889.0100	AppliChem	Darmstadt, DE
Polyethyleneglycol	P5413	Sigma-Aldrich	Steinheim, DE
Plasmidial DNA isolation	Maxiprep Pure Link K210017	Life Technologies	Darmstadt, DE
Progesterone	P-3972	Sigma-Aldrich	Steinheim, DE
Ribonucleic acid, transfer, from Bakers Yeast	R5636	Sigma-Aldrich	Steinheim, DE
Rnase inhibitor	13398800	Roche	Penzberg, DE
Sarcosyl	L9150	Sigma-Aldrich	Steinheim, DE
SDF1alpha/CXCL12	250-20A	PeproTech	Hamburg, DE
Sodium azide	S2002	Sigma-Aldrich	Deisenhofen, DE
Sucrose	27480.360	Sigma-Aldrich	Deisenhofen, DE
Tamoxifen	T5648	Sigma-Aldrich	Deisenhofen, DE
Taq DNA polymerase recombinant	10342-020	Life Technologies	Darmstadt, DE
Tetramisole hydrochloride	L9756	Sigma-Aldrich	Steinheim, DE
ThermoClean	25220100	Bioanalytic	Freiburg, DE
Tissue Tek O.C.T.	4583	Sakura	Alphen aan den Rijn, NL
Triethanolamine	28746290	VWR	Darmstadt, DE
Tris-HCl	108219.1000	Merck Millipore	Darmstadt, DE
TritonX100	1.08603.1000	Merck Millipore	Darmstadt, DE
Tween20	28829.183	VWR	Darmstadt, DE
UltraPure LMP Agarose	15517-022	Life Technologies	Darmstadt, DE
Xylene	CN80.2	Carl Roth	Karlsruhe, DE

2.1.5 Antibodies

2.1.5.1 Primary antibodies

Primary Antibodies	Cat. No.	Manufacturer	Registered Office
Anti-DIG-AP Fab fragments	11093274910	Roche	Penzberg, DE
Mouse anti-BrdU	555627	BD Biosciences	Heidelberg, DE

Mouse anti-Brn3a	Sc-8429	Santa Cruz Biotechnology	Heidelberg, DE
Mouse anti-Reelin (CR-50)	D223-3	MBL	Eching, DE
Mouse anti-TH	MAB318	Merck Millipore	Darmstadt, DE
Mouse Biotynilated anti-Cxcr4	AB097	BD Biosciences	Heidelberg, DE
Rabbit anti-Calbindin	CB38	Swant	Bellinzona, CH
Rabbit anti-cleaved Caspase-3	9664S	Cell Signaling	Leiden, NL
Rabbit anti-CXCR4 (UMB-2)	Kindly provided by R.Stumm laboratory (Fischer et al., 2008)		
Rabbit anti-GFP	A11122	Life Technologies	Darmstadt, DE
Rabbit anti-GIRK2	APC-006	Alomone labs	Jerusalem, IL
Rabbit anti-Lmx1a	AB10533	Merck Millipore	Darmstadt, DE
Rabbit anti-Nurr1	Sc-990	Santa Cruz Biotechnology	Heidelberg, DE
Rabbit anti-TH	AB152	Merck Millipore	Darmstadt, DE
Rat anti-GFP	04404-26	Nacalai Tesque	Kyoto, JP

2.1.5.2 Secondary antibodies

Secondary Antibodies/ Conjugates	Cat. No.	Manufacturer	Registered Office
Alexa Flour 488-conjugated donkey anti-rabbit IgG	A21206	Life Technologies	Darmstadt, DE
Alexa Flour 488-conjugated donkey anti-rat IgG	AB150149	Life Technologies	Darmstadt, DE
Biotynilated anti-guinea pig	706-065-148	Jackson ImmunoResearch	Suffolk, UK
Biotynilated anti-rabbit	711-065-152	Jackson ImmunoResearch	Suffolk, UK
Biotynilated anti-rat	712-065-150	Jackson ImmunoResearch	Suffolk, UK
Biotynilated donkey anti-mouse	715-065-150	Jackson ImmunoResearch	Suffolk, UK
Cy3- conjugated Streptavidin	016-160-084	Jackson ImmunoResearch	Suffolk, UK
Cy3-conjugated donkey anti-goat IgG	05-165-147	Jackson ImmunoResearch	Suffolk, UK
Cy3-conjugated donkey anti-ms IgG	715-165-150	Jackson ImmunoResearch	Suffolk, UK
Cy3-conjugated donkey anti-rabbit IgG	11-165-152	Jackson ImmunoResearch	Suffolk, UK
DyLight 488-conjugated donkey anti-Guinea Pig IgG	706-485-148	Jackson ImmunoResearch	Suffolk, UK
DyLight 488-conjugated donkey anti-rat IgG	712-485-150	Jackson ImmunoResearch	Suffolk, UK
DyLight 647-	712-606-150	Jackson	Suffolk, UK

conjugated donkey anti-rat IgG		ImmunoResearch	

2.1.6 Enzymes

General enzymes	Cat. No.	Manufacturer	Registered Office
Proteinase K	03115879001	Roche	Penzberg, DE
Deoxyribonuclease (DNAse)	M610A	Promega Corp	Mannheim, DE
Ribonuclease (RNAse A)	PureLink 12091-021	Life Technologies	Darmstadt, DE
Restriction enzymes	**Cat. No.**	**Manufacturer**	**Registered Office**
BamHI	RO189S	New England Biolabs	Frankfurt am Main, DE
EcoRV	RO195S	New England Biolabs	Frankfurt am Main, DE
NotI	RO189S	New England Biolabs	Frankfurt am Main, DE
SphI	RO182S	New England Biolabs	Frankfurt am Main, DE

2.1.7 RNA and DNA Polymerases

Polymerase	Cat. No.	Manufacturer	Registered Office
Taq DNA Polymerase Recombinant (500U)	10342-020	Roche	Penzberg, DE
Taq RNA SP6 Polymerase (1000U)	10810274001	Roche	Penzberg, DE
Taq RNA T3 Polymerase (1000U)	11031163001	Roche	Penzberg, DE
Taq RNA T7 Polymerase (1000U)	10881767001	Roche	Penzberg, DE

2.1.8 RNA *in situ* probes

RNA Probe	Gene name	Description	Restriction Enzyme	RNA Polymerase	Provided by
RELN	Reelin	pCRII-Topo vector, 0.64 kb (cDNA)RELN inserted fragment	NotI	Sp6	Mengqing Xiang lab, Rutgers University
ApoER2	Low-density lipoprotein receptor-related protein 8	pCRII-Topo vector, (cDNA)ApoER2	BamHI	T7	Mengqing Xiang lab, Rutgers University
DAB1	Disabled-1	pYX-Asc vector with 0.66 kb (cDNA)DAB1 inserted fragment	NotI	T7	Source Bioscience ID 6410411
VLDLR	very-low-density-lipoprotein receptor	pCRII-Topo vector, 0.56kb (cDNA)VLDLR inserted fragment	BamHI	T7	Mengqing Xiang lab, Rutgers University

CXCR4	C-X-C chemokine receptor type 4	pCRII-Topo vector,1kb (cDNA)CXCR4 inserted fragment	EcoRV	SP6	Fadel Tissir, *Université catholique de Louvain*
CXCL12	C-X-C motif chemokine 12	pCRII-Topo vector, 1kb (cDNA)CXCL12 inserted fragment	EcoRV	SP6	Fadel Tissir, *Université catholique de Louvain*
CXCR7	C-X-C chemokine receptor type 7	pGEM T easy vector, 1.3 kb (cDNA)CXCR7 inserted fragment	SphI	SP6	Ralf Stumm, University of Jena

2.1.9. PCR primers used for genotyping mice

Primer	Sequence 5'- 3'
ApoER2	MT R: GCTTGTTGGAATTCAGCCAGTTACC WT R: CCACAGTGTCACACAGGTAATGTG WT F: ACGARGACCCCAATGACAGCAGCG MT F: GATTGGGAAGACAATAGCAGGCATGC
Cre	F: TAAAFATATCTCACGTACTGACGGTG R: TCTCTGACCAGAGTCATCCTTAGC
Cxcl12	F: ACGCCAAGGTCGTCGCCGZGCTGG R: GTTAGGGTAATACAATTCCTTAGA
Cxcr4	WT F: CTGTCATCCCCCTGACTGAT WT R: TTCTCATCCTGGCCTTCATC MT: CACGAGACTAGTGAGACGTG
Dab1	WT F: CGGCAGGGAGTAGTAGATCG WT R: AGGAGCGAAATCACTCAAGC MT R: AGACTGCCTTGGCAAAAGCG
Reeler	WT F: CTGCTACACACTTGACATACCTTAATCTAC WT R: AGAGCCTAGAGGTTAGGGACACAACTCTTC MT F: TAAGGGAGTCCTGGTCTCTTTCTGTCTTTA
R26	RR1: AAAGTCGCTCTGAGTTGTTAT RR2: GCGAAGAGTTTGTCCTCAACC RR3: GGAGCGGGAGAAATGGATATG
Vldlr	WT F: TGGTGATGAGAGGCTTGTATGTTGTG WT R: TTGACCTCATCGCTGCCGTCCTTG MT F: CGGCGAGGATCTCGTCGTGACCCA MT R: GCGATACCGTAAAGCACGAGGAAG

2.1.10 Buffers and solutions

Buffers /Solutions	Content
Solutions for genotyping	
Lysis Buffer (for genotyping)	333 µL 1.5 M Tris, pH 8.8 (50 mM), 20 µL 0.5 M EDTA (1 mM), 500 µL 10% Tween, 9.1 mL dH$_2$O
Solutions for RNA *in situ* hybridization	
Triethanolamine (TEA)-HCl 0.1M	650 µL TAE in 50 mL Ampuwa H$_2$O, 130 µL 12M HCl
RNAse A	100 mg RNAse A, 100 µl Tris-HCL (pH 7.5), 30 µl 5 M NaCl (15 mM), 9.8 mL
SSC 20X	88.2 g NaCitrate (C$_6$H$_5$Na$_3$O$_7$), 174 g NaCL in 1 L Ampuwa H$_2$O (pH 7.0)

RNase Buffer	100 mL 5 M NaCl (0.5 M), 10 mL 1 M Tris-HCl (pH 7.5, 10 mM), 10 mL 0.5 M EDTA (pH 8, 5 mM), 880 mL dH$_2$O
NTMT	2 mL 5 M NaCl (100 mM) 10 mL 1 M Tris-HCl, pH 9.5 (100 mM) 5 mL 1 M MgCl$_2$ (50 mM) 0.1 mL Tween 20 (0.1%) 82.9 mL dH$_2$O
Hybridization Solution	50 mL Formamide (deionized), 20 mL 50% Dextran sulfate, 2 mL 50x Denhardt's, 2.5 mL yeast tRNA (10 mg/mL), 6 mL 5 M NaCl, 2 mL 1 M Tris-HCl (pH 8.0), 1 mL 0.5 M EDTA, 1 mL 1 M NaPO$_4$ (pH 8.0), 5 mL 20% Sarcosyl, 11.5 mL Ampuwa H$_2$O
TE buffer pH8.0	1mL 1M Tris-HCl pH8, 200µL 0.5M EDTA; up to 100mL with dH$_2$O
Washing solution	Tween 0.1% in PBS (1x)
Solutions for bacteria transformation	
LB medium	25 g of powder of LB medium according to Miller in 1 L dH$_2$O, autoclaved and cooled to RT, added 1mg/mL Ampicillin, stored at 4°C
TSB buffer, pH 6.5	5g Polyethyleneglycol (10%), 2.5 mL 1M MgCl$_2$ (50mM), 2.5 mL DMSO (5%), up to 50 mL in dH$_2$O, pH 6.7; filtered sterile and stored at 4°C.
Agar-LB medium	40 g of powder of LB agar according to Miller in 1 L dH$_2$O, pH 7.5, autoclaved and cooled to 50°C, added 1mg/mL Ampicillin, stored at 4°C
Solutions for organotypic slice culture preparation	
Culture medium	48.73% DMEM high glucose, 25% Horse serum, heat inactivated, 25% HBSS 1X, 1.27%Glucose, Penicillin/Streptomycin1x, filtered sterile and stored at 4°C
Krebs (10x)	252 mL NaCl 5M, 25mL KCl 1M, 12mL NaH$_2$PO$_4$ 1M, 12mL MgCl$_2$ 1M and 3,68 g CaCl$_2$ up to 1L with dH$_2$O, stored at 4°C up to 3 months
Krebs (1x)	100mL Krebs buffer (10x), 50mL NaHCO$_3$ 0.5M, 1,98 g Glucose, up to 1L with dH$_2$O, used fresh
LMP-agarose (4%)	4 g LMP agarose in 100 mL dH$_2$O, melted in a microwave and kept at 45°C in a water bath.
Solutions for immunofluorescence	
PBS (5x)	40 g NaCl (137 mM) 1 g KCl (2,7 mM) 7.1 g Na2HPO4 (10 mM) 1.36 g KH2P4 (2 mM) in 1 L dH2O
PBS-azide (0.1%)	0.1% sodium-azide in PBS
PFA (20%, Paraformaldehyde)	500 g PFA 2.0 L ddH2O 8.0 mL NaOH, filtered through 0.4 µm filter and stored at -20°C
Fixation solution (4% PFA)	10 mL 20% PFA in 50mL PBS
PBT (0.1%)	10 mL 10% Triton-X (0.1 %), 990 mL PBS (1x)
PBT (0.2%)	20 mL 10% Triton-X (0.2 %), 980 mL PBS (1x)
Washing solution	0.1% Triton-100x in PBT
Blocking solution	10% NDS in PBT
Citrate Buffer, 10 mM, pH 6.0 (for paraffin sections)	1.92 g Citric acid (anhydrous), 0.05%Tween 20 in 1 L dH$_2$O
Borate Buffer, 0.1 M, pH 8.5 (for BrdU staining)	3.10 g Boric acid, 4.8 g Sodium tetraborate· 10 H$_2$O in 1 L dH$_2$O
Solutions for gel electrophoresis	
50 x Tris-acetate-buffer (TAE)	242g Tris-base, 100mL 0.5M EDTA (pH 8.0), 57.1mL glacial acetic acid in 1L H$_2$O, stored at room temperature
1 x TAE	50 x TAE was diluted 1:50 with H$_2$O, stored at room temperature

10x Loading buffer	50%Glycerol, 0.4%; Bromphenol blue 0.4%; Xylene Cyanol, Mixed and stored at 4°C

2.2 Mice

2.2.1 List of mouse lines

Common symbol	Allele symbol and name	Allele type	Provided by/ Purchased from	Reference
Apoer2 KO	*LRP8^{tm1Her}* Targeted mutation 1, Joachim Herz	Targeted (Knockout)	Amparo Acker-Palmer lab, Goethe University Frankfurt	(Trommsdorff et al., 1999)
CD1	Wild-type	Wild-type	Charles River Laboratories	
Cxcl12 KO	*Cxcl12^{tm1Tng}* Targeted mutation 1, Takashi Nagasawa	Targeted (Knockout)	Ralf Stumm lab, Jena University	(Nagasawa et al., 1996)
Cxcr4 KO	*Cxcr4^{tm1Qma}* Targeted mutation 1, Qing Ma	Targeted (Knockout)	Ralf Stumm lab, Jena University	(Ma et al., 1998)
Dab1 KO	*Dab1^{tm1Cpr}* Targeted mutation 1, Jonathan A Cooper	Targeted (Knockout)	Amparo Acker-Palmer lab, Goethe University Frankfurt	(Howell et al., 1997)
R26^{EYFP}	*Gt(ROSA)26Sor^{tm1Sor}* Targeted mutation 1, Philippe Soriano	Targeted (Reporter)	Frank Costantini lab, Columbia University	(Srinivas et al., 2001)
Reeler	*Reln^{rl}* Reeler	Spontaneous	Amparo Acker-Palmer lab, Goethe University Frankfurt	(Bar et al., 1995)
Shh^{CreER}	*Shh$^{tm2(cre/ERT2)}$* Targeted mutation 2, Clifford J Tabin	Targeted (Knock-in)	Clifford Tabin lab, Harvard University	(Harfe et al., 2004)
Vldlr KO	*Vldlr^{tm1Her}* Targeted mutation 1, Joachim Herz	Targeted (Knockout)	Amparo Acker-Palmer lab, Goethe University Frankfurt	(Frykman et al., 1995)

2.2.2 Mice breeding and maintenance

All transgenic mouse lines were bred into a CD1 background strain. To reduce genetic drift, transgenic mice were intercrossed every second generation with outbred CD1 mice. The mice were housed and bred in a controlled environment, with 12 hours light/night cycles. Food and water supply was available *ad libidum.* All animal experiments were performed in accordance with the regulations approved by the University of Bonn Animal Care and Use Committee.

2.2.3 Mouse genetics

2.2.3.1 Genetic inducible fate mapping system

Shh$^{CreER/+}$ allele was generated by knocking in a CreER cassette into the *Shh* locus (Harfe et al., 2004). Tamoxifen administration to these mice induces Cre recombinase expression in all cells expressing Shh. *R26$^{EYFP/EYFP}$* reporter mice were generated by inserting a *loxP*-flanked STOP sequence followed by the Enhanced Yellow Fluorescent Protein gene (EYFP) into the *Gt(ROSA)26Sor* locus (Srinivas et al., 2001). When bred to mice expressing Cre recombinase, the *Stop* sequence is deleted and EYFP expression is observed in the *Cre*-expressing tissue(s) of the double mutant offspring. The Shh$^{CreER/+}$ mice were crossed to *R26$^{EYFP/EYFP}$* reporter mice to generate *Shh$^{CreER/+}$; R26$^{EYFP/+}$* descendants. The *Shh$^{CreER/+}$; R26$^{EYFP/EYFP}$* males were mated with CD1 wild-type females to generate *Shh$^{CreER/+}$; R26$^{EYFP/+}$* progeny.

Embryonic day 0.5 (E 0.5) was considered the noon of the day when a vaginal plug was detected. Tamoxifen (TM) was dissolved in corn oil at 20 mg/mL. To reduce miscarriages, 5 mg/mL Progesterone was added into the TM solution. Pregnant females were given 3-4 mg TM through oral gavage with animal feeding needles at 12 pm of E8.5 or E11.5. The Shh$^{CreER/+}$ and *R26^{EYFP}* allele was identified by PCR-based genotyping using specific oligonucleotides, as previously described (Kimmel et al., 2000; Soriano, 1999). For primer sequences and genotyping procedure see sections 2.1.9 and 2.2.7.

2.2.3.2 Inactivation of the Reelin signaling pathway

The *Vldlr*, *Apoer2* and *Dab1* knockout (KO) mice were developed in the laboratory of Dr. Joachim Herz. Brains of adult and embryo *Reeler* mice, adult brains of *Vldlr*, *Apoer2*, *Dab1* knockouts and *Apoer2/Vldlr* double knockout, together with control littermates were kindly provided by the laboratory of Prof. Amparo Acker-Palmer, Goethe University Frankfurt. Genotyping, perfusion and dissection of the brains were performed in the laboratory of Prof. Amparo Acker-Palmer.

Reeler mice have a spontaneous mutation in the *Reeler* gene (*Reln^{rl}*), which encodes for the Reelin protein (Bar et al.1995). Therefore no Reelin protein is produced. The *Vldlr, Apoer2* and *Dab1* KO mice were produced by disrupting the gene's reading frame via inserting a neomycin-resistance cassette through gene targeting. The *Vldlr* KO mice were generated by inserting the neomycin-resistance cassette into exon 5, which encodes a part of the ligand binding region of *Vldlr* (Frykman et al., 1995). The *Apoer2* KO mice were generated by inserting the neomycin-resistance cassette into exons 17 and 18, encoding for the transmembrane segment and part of the cytoplasmic tail of the *Apoer2* (Trommsdorff et al., 1999). The *Dab1* KO mice were generated by inserting the neomycin-resistance cassette into exon 2, encoding for the first aminoacids of the phosphotyrosine-binding domain of *Dab1* (Howell et al., 1997).

2.2.3.3 Inactivation of CXCL12/CXCR4 signaling pathway

Generation of *Cxcr4* KO and Cxcl12 KO mice was performed by inserting a neomycin-resistance cassette in exon 2 of the *Cxcr4* or *Cxcl12* genes, which encodes for the fourth transmembrane domain of *Cxcr4* (Ma et al., 1998) or for the *Cxcl12* binding region, respectively (Nagasawa et al., 1996). The insertion of the neomycin-resistance cassette disrupts the reading frame and no protein product is detectable by western blot analysis. Brains of *Cxcr4* and *Cxcl12* KO embryos, together with control littermates were kindly provided by the laboratory of Prof. R. Stumm, Jena University. Dissection, genotyping and PFA fixation of the brains was performed in the laboratory of Prof. R. Stumm.

2.3 Molecular biology

2.3.1 Genotyping of the mice

2.3.1.1 Tissue lysis

For identification of genetically modified animals in a litter, a small piece of tissue from the ear (ear punch), the tail tip (for E11.5-18.5 and postnatal mice) was collected for genotyping.

The tissue was digested in 100 µL lysis buffer with 1 µL proteinase K at 60°C overnight, followed by heat inactivation of proteinase K at 95°C for 10 min. 1 µl of the clear superficial layer of the digest-solution, which contained the genomic DNA, was analyzed by PCR.

2.3.1.2 PCR protocols

The following PCR protocols were performed:

Rosa26			
Amount of reaction component	Thermal cycler Program		
1.00 µL sample			
2.00 µL PCR rxn buffer (1x)		Temp. °C	Time min.
0.16 µL dNTPs (25 nM)	Steps		
1.00 µL R26-RR1 (5 µM) primer	1) 1st Denaturing	94	2:00
1.00 µL R26-RR2 (5 µM) primer	2) Denaturing	94	1:00
1.00 µL R26-RR3 (5 µM) primer	3) Annealing	61	1:00
0.60 µL MgCl$_2$ (1.5 mM)	4) Extension	72	10:00
13.04 µL dH$_2$O	5) Last Extension	72	10:00
0.2 µL Taq Polymerase (1 U)	6) Incubation	8	hold
20.00 µL volume (total)	Repeat steps 2 – 4 for 30 cycles		
Gel electrophoresis – 1.5% agarose, wild-type: 500 bp, mutant: 220 bp			

Cre

Amount of reaction component	Thermal cycler Program		
1.00 µL sample			
2.00 µL PCR rxn buffer (1x)	Steps	Temp. °C	Time min.
0.16 µL dNTPs (25 nM)			
1.00 µL F (5 µM) primer	1) 1st Denaturing	95	2:00
1.00 µL R (5 µM) primer	2) Denaturing	95	0:40
0.60 µL MgCl$_2$ (1.5 mM)	3) Annealing	59	1:00
14.04 µL dH$_2$O	4) Extension	72	0:50
0.2 µL Taq Polymerase (1 U)	5) Incubation	8	hold
20.00 µL volume (total)	Repeat steps 2 – 4 for 30 cycles		
Gel electrophoresis – 1.5% agarose, mutant: 300bp			

Reeler

Amount solution / sample	Thermal cycler Program		
1.00 µL sample			
2.00 µL PCR rxn buffer (1x)	Steps	Temp. °C	Time min.
0.16 µL dNTPs (25 nM)			
1.00 µL WT-F (5 µM) primer	1) 1st Denaturing	95	2:00
1.00 µL WT-R (5 µM) primer	2) Denaturing	95	0:30
1.00 µL MT-F (5 µM) primer	3) Annealing	63	0:30
0.60 µL MgCl$_2$ (1.5 mM)	4) Extension	72	1:00
14.04 µL dH$_2$O	5) Last extension	72	10:00
0.2 µL Taq Polymerase (1 U)	6) Incubation	8	hold
20.00 µL volume (total)	Repeat steps 2 – 4 for 30 cycles		
Gel electrophoresis – 1.5% agarose: MT band 300bp			

Dab1 protocol 1

Amount of reaction component	Thermal cycler Program		
2.00 µL sample			
2.40 µL PCR rxn buffer (5x)	Steps	Temp. °C	Time min.
0.24 µL dNTPs (10 mM)	1) 1st Denaturing	94	2:00
0.30 µL WT (20 µM) primer	2) Denaturing I	94	0:20
0.30 µL MT-R (20 µM) primer	3) Annealing WT-F	65	0:15
0.96 µL MgCl$_2$ (25 mM)	4) Annealing MT-R	68	0:10
5.75 µL dH$_2$O	5) Denaturing II	94	0:15
0.05 µL Taq Polymerase (5U/µL)	6) Annealing	60	0:15
12.00 µL volume (total)	7) Extension	72	0:10
	8) Last extension	72	2:00
	9) Incubation	10	hold
Gel electrophoresis – 1.5% agarose MT Wild-type: 344 bp; Mutant band: 150 bp	Repeat steps 2 – 4 for 10 cycles Repeat steps 5 – 7 for 28 cycles		

Dab1 protocol 2

Amount of reaction component	Thermal cycler Program		
2.00 µL sample	Steps	Temp. °C	Time min.
2.40 µL PCR rxn buffer (5x)			
0.24 µL dNTPs (10 mM)	1) 1st Denaturing	94	2:00
0.30 µL WT (20 µM) primer	2) Denaturing I	94	0:20
0.30 µL WT-R (20 µM) primer	3) Annealing WT-F	65	0:15
0.96 µL MgCl$_2$ (25 mM)	4) Annealing MT-R	68	0:10
5.75 µL dH$_2$O	5) Denaturing II	94	0:15
0.05 µL Taq Polymerase (5U/µL)	6) Annealing	60	0:15
12.00 µL volume (total)	7) Extension	72	0:10
	8) Last extension	72	1:00
Gel electrophoresis – 1.5% agarose	9) Incubation	10	hold
Wild-type: 344 bp	Repeat steps 2 – 4 for 10 cycles Repeat steps 5 – 7 for 28 cycles		

Apoer2

Amount of reaction component	Thermal cycler Program		
2.00 µL sample			
1.20 µL PCR rxn buffer (10x)	Steps	Temp. °C	Time min.
0.96 µL dNTPs (2.5 mM)			
0.60 µL WT-F (20 µM) primer	1) 1st Denaturing	94	1:50
0.60 µL WT-R (20 µM) primer	2) Denaturing	94	0:30
0.30 µL MT-F (20 µM) primer	3) Annealing	56	0:45
0.30 µL MT-R (20 µM) primer	4) Extension	72	0:45
0.72 µL MgCl$_2$ (25 mM)	5) Last extension	72	2:00
4.78 µL dH$_2$O	6) Incubation	10	hold
0.06 µL Taq Polymerase (5U/µL)	Repeat steps 2 – 4 for 35 cycles		
12.00 µL volume (total)			
Gel electrophoresis – 1.5% agarose, wild-type: 602 bp, mutant: 420 bp			

Vldlr

Amount of reaction component	Thermal cycler Program		
2.00 µL sample	Steps	Temp. °C	Time min.
1.20 µL PCR rxn buffer (10x)			
0.96 µL dNTPs (2.5 mM)	1) 1st Denaturing	94	3:00
0.30 µL WT-F (20 µM) primer	2) Denaturing	94	0:20
0.30 µL WT-R (20 µM) primer	3) Annealing	65	0:15* (*0.5°C/cycle)
0.30 µL MT-F (20 µM) primer	4) Extension	68	0:10
0.30 µL MT-R (20 µM) primer	5) Denaturing	94	0:15
0.96 µL MgCl$_2$ (25 mM)	6) Annealing	60	0:15
5.64 µL dH$_2$O	7) Extension	72	0:10
0.04 µL Taq Polymerase (5U/µL)	8) Last extension	72	2:00
12.00 µL volume (total)	9) Incubation	10	hold
2.00 µL sample	Repeat steps 2 – 4 for 10 cycles		
1.20 µL PCR rxn buffer (10x)	Repeat steps 5 – 7 for 25 cycles		
Gel electrophoresis – 1.5% agarose, wild-type: 400 bp, mutant: 200 bp			

Cxcr4			
Amount of reaction component	Thermal cycler Program		
2.00 µL sample			
1.20 µL PCR rxn buffer (10x)		Temp. °C	Time min.
0.96 µL dNTPs (2.5 mM)	Steps		
0.40 µL WT-F (20 µM) primer	1) 1st Denaturing	94	3:00
0.40 µL WT-R (20 µM) primer	2) Denaturing	94	0:30
0.80 µL MT (20 µM) primer	3) Annealing	62	1:00
	4) Extension	72	1:00
0.96 µL MgCl$_2$ (25 mM)	5) Last extension	72	2:00
5.22 µL dH$_2$O	6) Incubation	10	hold
0.06 µL Taq Polymerase (5U/µL)	Repeat steps 2 – 4 for 35 cycles		
12.00 µL volume (total)			
Gel electrophoresis – 1.5% agarose, wild-type: 193 bp, mutant: 305 bp			

Cxcl12			
Amount of reaction component	Thermal cycler Program		
2.00 µL sample			
1.20 µL PCR rxn buffer (10x)		Temp. °C	Time min.
0.96 µL dNTPs (2.5 mM)	Steps		
0.40 µL Cxcr4 F (20 µM) primer	1) 1st Denaturing	94	3:00
0.40 µL Cxcr4 R (20 µM) primer	2) Denaturing	94	0:30
0.96 µL MgCl$_2$ (25 mM)	3) Annealing	62	1:00
6.02 µL dH$_2$O	4) Extension	72	1:00
0.06 µL Taq Polymerase (5U/µL)	5) Last extension	72	2:00
12.00 µL volume (total)	6) Incubation	10	hold
Gel electrophoresis – 1.5% agarose, mutant: 539 bp	Repeat steps 2 – 4 for 40 cycles		

For primer sequences see section 2.1.9

2.3.1.3 DNA electrophoresis

The agarose gel was prepared by heating 1.5% standard agarose in TAE buffer until dissolved and then allowed to cool down (aprox. 40°C). Ethidium bromide (10 µg/mL) or gel red (1:10000) was added and the solution poured into a gel chamber. The PCR mix and 6x loading buffer were loaded onto the gel and run for 40 min at 120 V. After electrophoresis, the gel was illuminated with a UV lamp of a Gel Doc transilluminator and a picture was captured.

2.3.2 Molecular cloning

2.3.2.1 Generation of competent bacteria

The plasmids were transformed into competent *Escherichia coli* (*E.coli*) DH5α bacteria. Competent *E.coli* were generated following a protocol adapted from Chung and Miller, 1988. Bacteria were cultivated on a LB-agar plate without antibiotic at 37°C overnight. Several emerging colonies were picked from the plate and grown at 37 °C in 20 mL LB without antibiotic

overnight. The following day, 2 µL of overnight culture was used to inoculate 200 mL LB medium. Cells were grown at 37°C overnight, until they reached an OD of 0.4-0.45 at 600 nm. Next, bacterial culture was centrifuged at 4°C and 4000 rpm for 8 min. The pellet was resuspended in 1/10th volume of TSB buffer, then incubated on ice for 10 min. The competent cells were aliquoted in a volume of 100 µL and stored at -80°C. To verify the transformation efficiency, a 100 µL aliquot of bacteria was mixed with 100 pg plasmid DNA having an antibiotic resistance gene. The cells were incubated on ice for 30 min. Next, cells were grown in 900 µL TSB buffer with 200 mM glucose at 37°C and 225 rpm for 1 h, to permit expression of the antibiotic resistance gene. The cells were plated agar plates, containing the appropriate antibiotic for selection of transformants. A transformation efficiency of 2 x 10^5 transformants per µg DNA was obtained.

2.3.2.2 Bacteria transformation

100 µL of competent bacteria were thawed on ice for 5 min. 1 µL of desired plasmid was added to the competent bacteria. Bacterial cells were then incubated on ice for 30 min. Subsequently, bacterial cells were incubated at 42°C for 45 sec using a water bath and then on ice for 2 min. 900 µL of LB medium without antibiotic was added and the cells were grown at 37°C and 225 rpm for 1 h using a thermo-block. The cells were centrifuged for 2 min at 2000 rpm and 900 µL supernatant were removed. The cells were resuspended in the remaining 100 µL supernatant and plated on a LB-agar plate supplemented with the appropriate antibiotic. Bacteria cells were cultivated at 37°C overnight.

2.3.2.3 Preparation of DNA

Colonies cultivated on LB-agar plate were used to inoculate 3 mL of LB medium supplemented with the appropriate antibiotic. The 3 mL cultures were grown at 37°C and 225 rpm for 6 h. Next, 200 µL of the 3 mL cultures were used to inoculate 200 mL of LB medium with antibiotic. Cells were grown at 37°C and 225 rpm overnight. The following day, bacterial cells were centrifuged at 4000 rpm. Pelted cells were resuspended and lysed, and DNA was extracted and purified using the PureLink HiPure Plasmid Maxiprep kit according to the manufacturer's protocol.

2.3.3 Measurement of DNA concentration

For the measurement of DNA content, the NanoDrop system from Peqlab was used. DNA concentration was determined measuring at a wavelength of 260nm (nucleic acids peak of absorption). Additionally a measurement at a wavelength of 280 nm was done to determine eventual protein contamination. A ratio of OD 260/280 > 1.80 was regarded as pure.

2.4 Organotypic slice cultures

2.4.1. Organotypic slice preparation

To directly monitor the migratory behavior of neurons, an organotypic slice culture protocol was established. Generation of organotypic brain slices, which allow the normal development of ventral MbDA neurons at early developmental stages (E12.5-E14.5) involves a number of critical steps, as follows: dissection of the embryonic brain, vibratome sectioning and culturing (Figure 11).

2.4.1.1 Dissection and embedding of the embryonic brain

Pregnant female mice (gestation day 12.5) were anesthetized using isoflurane and sacrificed by cervical dislocation. Embryos were dissected out of the uterus and placed on ice in Krebs buffer (1x). To dissect the brains, heads of the embryo were removed and fixed by piercing with forceps through the eye level. Another pair of forceps was used to carefully remove the skin and skull. Next, brains were lifted out and transferred into fresh ice-cold Krebs buffer (1x). Subsequently, the tissue was briefly washed in 4% LMP-agarose at RT and then embedded in fresh 4% LMP-agarose. Brains were oriented in a position horizontal to the bottom of the agarose block, using a Pasteur pipette with a fire-polished round tip. The 4% LMP-agarose with tissue was then placed on ice for 3 min to solidify. Next, the agarose surrounding the tissue was trimmed and the brain-agarose blocks were glued onto the specimen stage of a vibratome. The ventral side of the brain (for horizontal sectioning) or the lateral side of the brain (for sagittal sectioning) was positioned parallel to the stage. The stage with the glued brain blocks was submerged into cold Krebs buffer (1x).

2.4.1.2 Vibratome sectioning

Brains were sectioned on a vibratome at 300 μm. The Krebs buffer (1x) was maintained at 4°C during the sectioning. A frequency of 50 Hz, blade amplitude 1.1 mm and a speed of 25 mm/sec were used. Brain slices were collected using a fine paintbrush by moving the slices into a mini perforated spoon.

2.4.2 Organotypic slice culture

Slices were placed on a semi-porous membrane and cultured in serum-supplemented medium at 37°C, 5% CO_2. Brain slices received medium from below and air from above. The slices were maintained *in vitro* for up to 3 days. 50% of the culture medium was changed on the second day of culturing.

2.4.3. Organotypic slice culture treatments

To inhibit Reelin function in slice cultures, 4 µg/mL CR-50 antibody was added to the culture medium prior to imaging (Utsunomiya-Tate et al., 2000). The antibody was kept in the medium during the entire imaging time, without medium renewing.

To block CXCL12 signaling, slices were treated with the CXCR4 – antagonist, AMD3100 (120µM, Sigma) (Borrell and Marin, 2006). The inhibitor was prepared in the culture medium and was added to the slices prior to imaging and kept in the medium during the entire imaging time.
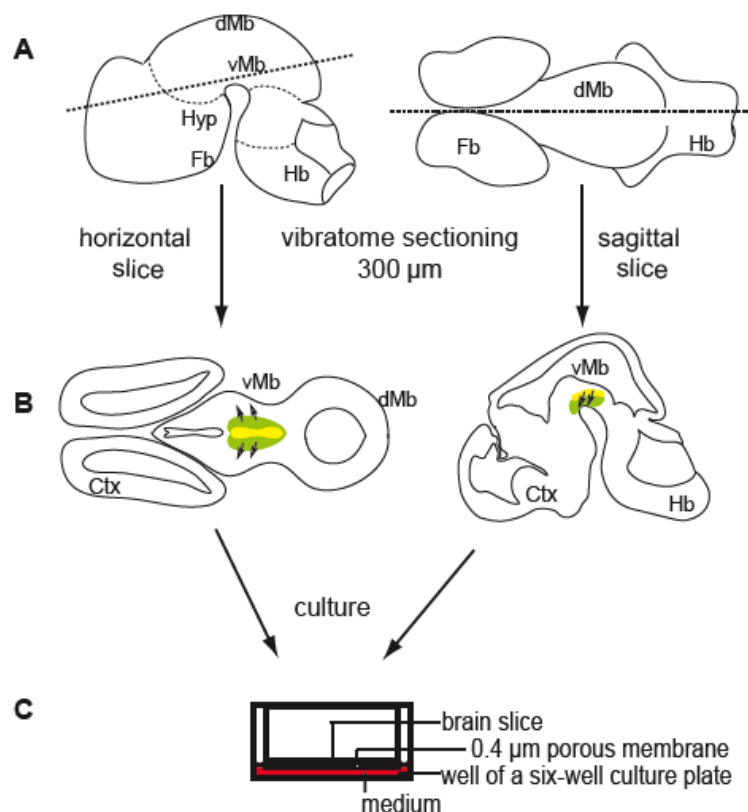
Figure 11. Schematic illustrating the preparation of organotypic slice cultures. 300 µm horizontal and sagittal brain slices was prepared by sectioning an E12.5 brain using a vibratome. (A) Schematic sagittal and top views of an E12.5 mouse brain. Levels of sections are indicated. (B) Schematics of the slices that can be obtained by horizontal and sagittal sectioning and that contain both forebrain (Fb) and midbrain (Mb). The area containing MbDA neurons is indicated in green, the area containing MbDA precursors is depicted in yellow, black arrows indicate routes of migration. (C) The slices containing dopaminergic neurons are cultured on membrane inserts. Abbreviations: vMb, ventral midbrain; dMb, dorsal midbrain; Hyp, hypothalamus; Hb, hindbrain.

2.5 Histology

2.5.1 Tissue fixation and perfusion

Pregnant animals were first anesthetized with isoflurane and then sacrificed by cervical dislocation. Embryos were removed and placed in ice cold PBS. Embryo heads or brains were dissected and washed with ice cold PBS. The heads (E11.5-E16.5) or the brains (E17.5-E18.5) were fixed in 4% PFA for 30 - 120 min and washed with PBS.

Postnatal and adult animals were perfused. The animals were first anesthetized with isoflurane and then perfused transcardially under anesthesia, first with PBS and then with 4% PFA. After perfusion the brains were dissected, post-fixed in 4% PFA overnight at 4°C and then washed with PBS.

2.5.2 Tissue embedding

For cryo-embedding the fixed tissue was incubated in 15% sucrose, until submerged (6 h to overnight) at 4°C. Subsequently, the tissue was incubated in 30% sucrose overnight at 4°C. After the tissue was submerged in 30% sucrose, it was embedded in OCT TissueTek, then frozen on dry-ice and stored at –80°C.

For paraffin embedding, the specimen was dehydrated in graded ethanol series (from 70% ethanol to 100% ethanol) at room temperature (RT), for 20-30 min for each incubation step. To clear the tissue, the specimen was transferred to 100% Xylene at RT. Subsequently, the specimen was incubated in three changes of paraffin at 60°C. The tissue was embedded in molds filled with fresh paraffin, placed on a hot plate at 64°C. The paraffin blocks were left at RT to solidify and then stored at RT.

2.5.3 Tissue sectioning

Cryosectioning

The cryo-blocks were sectioned on a cryostat at a knife temperature of -22 to -24°C and an object temperature of -20 to -22°C. 12 μm embryonic brain sections were collected on superfrost ultra plus adhesion slides in series of ten slides, dried at RT for 2 hours and then stored at -20°C. For adult brains, 40 μm sections were collected in a 96 well plate and stored at 4°C in PBS with 0.01% sodium azide.

Paraffin-sectioning

The paraffin blocks were sectioned at a thickness of 7 μm on a microtome. The sections were mounted on superfrost ultra plus adhesion slides, dried overnight on a heating plate at 37°C and then stored at RT.

2.5.4 Immunostaining

Immunostaining is commonly used to detect antigens in cells and tissue. Antibodies conjugated with fluorescent dyes bind to specific antigens.

2.5.4.1 Immunostaining of frozen and paraffin embryonic brain sections

Frozen sections were thawed in PBS, briefly fixed in 4% PFA, and then rinsed in PBS and PBT (0.1%) at RT for 10 min.

Paraffin sections were incubated 3 times in Xylene for 3 min each at RT to deparaffinize. Then the sections were rehydrated in graded ethanol series (from 100% ethanol to 70% ethanol) at RT, 2 min for each incubation step. Subsequently, the paraffin sections were submerged in 10 mM citrate buffer (pH 6.0) and boiled for 5 min in a pressure cooker.

Both frozen and paraffin sections were transferred into a humidified chamber and incubated in blocking solution (10% NDS/PBT) at RT for 1 h. Sections were incubated in primary antibody solution at 4°C overnight or at RT for 2 h. The following primary antibodies and dilutions were used: rabbit anti-TH (1:500), rat anti-GFP (1:1500), rabbit anti-LMX1A (1:3000), rabbit anti-NURR1 (1:200), mouse anti-BRN3A (1:50), rabbit anti-CXCR4 (UMB-2, undiluted), biotinylated rat anti-mouse CXCR4 (1:500). Subsequently, the primary antibody solution was removed. The sections were washed three times with PBT and then incubated with secondary antibody solution at RT for 2 h. The following secondary antibodies and dilutions were used: donkey anti-rabbit IgG-Alexa 488 (1:500), donkey anti-rabbit Cy3 (1:200), donkey anti-rat IgG-DyLight 488 (1:100) or donkey anti-rat Alexa 488 (1:500), donkey-anti mouse Cy3 (1:200). For the detection of CXCR4, Cy3-labeled streptavidin was used (1:1000). For Hoechst fluorescent counterstaining of nuclei, Hoechst solution (1:10000) was added to the secondary antibody solution. Sections were washed three times with PBT, air dried for 2 min and then mounted with Aqua Polymount. Subsequently, the sections were dried at RT for several hours in the dark and then stored at 4°C. All washing steps were carried out in Coplin jars. To prepare the primary and secondary antibody solutions, the antibodies were diluted in PBT with 3% NDS.

2.5.4.2 Immunostaining of adult frozen brain sections

40 µm floating adult brain sections were washed in PBS and then PBT (0.2%) at RT for 10 min. each. Next, sections were stained using the protocol descried in 2.3.4.1. The following primary antibodies and dilutions were used: mouse anti-TH (1:500), rabbit anti-Girk2 (1:500) and rabbit anti-Calbindin (1:5000). Donkey anti-rabbit IgG-Alexa 488 (1:500) and donkey-anti mouse Cy3 (1:200) secondary antibodies were used. All washing steps and antibody solutions preparation were performed using PBT (0.2%). All steps were carried out in a 12 well plate.

2.5.4.3 Immunofluorescence staining of embryonic organotypic slice cultures

Organotypic slice cultures were fixed in 4% PFA at RT for 30 min, then rinsed in PBS and PBT (0.2%) for 10 min. Slices were incubated in blocking solution (NDS/PBT (0.2%)) at RT for 2 h.
48

Subsequently, slices were incubated with primary antibody solution at 4°C overnight. The following primary antibodies and dilutions were used: rabbit anti-TH (1:500), rat anti-GFP (1:1000), mouse anti-BrdU (1:200), rabbit anti-cleaved caspase 3 (1:200). The primary antibody solution was removed; slices were washed and then incubated in secondary antibody solution, at RT for 3 h. The following secondary antibodies were used: donkey anti-rabbit Cy3 (1:200), donkey anti-rat Alexa 488 (1:500). For the detection of BrdU, biotinylated anti-mouse antibody (1:200) and Cy3-labeled streptavidin (1:1000) were used. All washing and incubation steps were performed using PBT (0.2%). All steps were carried out in a 6 well plate.

For BrdU staining, the same protocol as above was used, with the following modifications: between fixation an blocking steps, slices were incubated with 4M HCl at RT for 10 min, neutralized with 0.1M borate buffer at RT for 5 min and washed three times with PBS.

Throughout the procedure NDS was replaced by goat serum.

2.5.4.4 Whole mount immunostaining for ultramicroscopy

Brains from E12.5 embryos were fixed in 4% PFA for 1 h, washed with PBS, incubated with blocking solution 10%NDS/ PBT at 4°C overnight. The brains were incubated with primary antibodies: rabbit anti-TH (1:500) and rat anti-GFP (1:1000) at 4°C for 2 days. Next, the primary antibody solution was removed and the brains were washed three times with PBT at RT for 15 min. The tissue was incubated with secondary antibodies: donkey anti-rat IgG-DyLight 647 (1:100) and donkey anti-rabbit Cy3 (1:200) at RT for 1 day. Subsequently, the tissue was washed three times with PBT and three times with PBS for 20 min. All washing steps and antibody solutions preparation were performed using PBT with 0.2% Triton X-100. All steps were carried out in 12 well plates.

2.5.5 RNA *in situ* hybridization

RNA *in situ* hybridization (ISH) is a commonly used method to detect mRNA localization in tissue sections and cells. A labeled anti-sense riboprobe (RNA probe) is generated and hybridized with the complementary mRNA, upon proteinase K permeabilization of the cellular membranes. The stable and labeled RNA/mRNA complex is visualized by immunohistochemistry.

2.5.5.1 RNA probe preparation

Single-stranded labeled RNA probes were used for ISH. Plasmids containing the complete or partial cDNA of the gene of interest were used for generating an antisense RNA probe.

2.5.5.1.1 DNA linearization and purification

The plasmids were linearized with restriction enzymes (see section 2.1.8). A concentration of 2 to 5 unites of enzyme was used for 1 µg DNA. All reactions were performed in the appropriate buffers supplemented with 1% BSA when recommended, at 37°C for 2 h.

For purifying the liniarized DNA, the PCR purification kit from Qiagen was used, according to the manufactures protocol. The DNA sample solution was run through a column, where DNA is able to bind to a silica membrane in the presence of chaotropic salts. All contaminants, which are not able to bind remain in the solution and are washed out. The DNA was eluted using 10 mM Tris-HCl, pH 8.5 and was used for in vitro transcription.

2.5.5.1.2 RNA *in vitro* transcription

RNA probes were transcribed from the linearized DNA templates described in section 2.4.5.1.1, using DNA-dependent RNA polymerases from the bacteriophage SP6, T3 or T7. DIG-labeled NTP mix was used as a substrate. DIG was included in the mix for detection of the RNA probe with anti-DIG-AP Fab fragments antibody upon hybridization.

In vitro transcription mix		protocol
1.5 µL	Purified DNA (1-2 µg)	- incubate 3 hours at 37°C
2 µL	Transcription buffer (10x)	- add 1 µL DNase I
2 µL	DIG-NTP labeling mix (10x)	- incubate 15 min., 37°C - add 2 µL EDTA (4mM), 2.5 µL LiCl (100mM) and
0.5 µL	RNase inhibitor (10U)	75 µL 100% EtOH to precipitate RNA
0.5 µL	RNA polymerase (30U)	- incubate 15 min, -80°C
12.5 µL	ddH$_2$O	- centrifuge max. speed, 15 min
20 µL volume final		- air-dry 3-5 min at RT - add 50 µL ddH$_2$O with 1% RNase inhibitor - measure concentration and store at -20°C

DNA purification was performed by phenol extraction and ethanol precipitation according to the previously described protocol (Sambrook and Russell, 2001)

Dr. M. Xiang kindly provided *Reelin, Dab1, Vldlr and Apoer2* cDNA for generating anti-sense RNA probes (Haas et al., 2000; Trommsdorff et al., 1999). Prof. Dr. R. Stumm kindly provided cDNA for generating *Cxcr7* RNA probes (Stumm et al., 2003). Prof. Dr. F. Tissir kindly provided cDNA for generating *Cxcl12* and *Cxcr4* anti-sense RNA probes (Tissir et al., 2004).

2.5.5.2 ISH procedure

Paraffin embryonic sections were deparafinized and rehydrated in graded ethanol series (see section 2.4.4.1) prior to the ISH protocol. The sections were post-fixed in 4% PFA, rinsed in PBS and incubated with 5 µL proteinase K (20 µg/µL)/50 mL PBS. Next, the sections were washed with PBS and acetylated in 50 mL 0.1 M TEA-HCl with 125 µL acetic anhydride. Washing in PBS and dehydration in 70% and 95% EtOH followed this step. The RNA probe (aprox. 1 µg) of interest was added to 1 mL hybridization buffer and incubated 2 min at 80°C. After air drying, the sections were transferred to a humidified hybridization cassette (formamide:H$_2$O-1:1, v/v). 300 µL hybridization solution containing RNA probe was added to each slide with sections, covered with RNase-free coverslips and incubated at 55°C overnight. On the following day, coverslips were removed in prewarmed SSC 5X. To reduce unspecific

hybridization the slides were incubated in a high stringency wash (formamide - 2xSSc (1:1 v/v)) at 65°C for 30 min. Next, the slides were washed with RNAse buffer, containing 0.1% RNase A at 37°C for 10 min to remove the non-hybridized RNA. Subsequently, the slides were washed twice with high stringency solution at 65°C for 20 min, then one time in SSC (2x) and SSC (0.1x) at 37°C for 15 min. The slides were placed in a humidified chamber and incubated with blocking solution (washing solution with 10% goat serum) at RT for 1 h. Sections were incubated with primary antibody: anti-DIG-AP Fab fragments (diluted 1:5000 in 1% goat serum/ washing solution) for 3 hours or overnight. When the antibody was removed, the slides were washed several times in washing solution, followed by two washes in NTMT (containing 1 mg/mL levamisole to reduce background of endogenous alkaline phosphatase activity) at RT for 10 min. In the last step the slides were incubated in BM purple, a substrate for alkaline phosphatase (with 0.5 mg/mL levamisole) at RT. After staining became visible (24 – 72 h), the slides were washed, briefly post-fixed in 4%PFA and mounted with Aqua Polymount. Stained sections were stored at RT.

2.5.6 Combined ISH and immunostaining

For combined ISH and immunostaining, the ISH protocol was modified as following: after 4% PFA fixation and PBS wash, frozen or paraffin sections were acetylated (without proteinase K incubation). Next, sections were dehydrated in graded ethanol series (from 70% to 100% ethanol) and incubated in chloroform for 5 min. The hybridization buffer containing the RNA probe was incubated for 5 min at 80°C and then cooled on ice for 2 min. After hybridization with DIG labeled RNA probes and detection of DIG with anti-DIG-AP Fab fragments antibody, sections were incubated with BM purple. The color reaction was stopped in TE buffer and post-fixed in 4% PFA at RT for 20 min. Subsequently, the sections were processed for immunostaining (protocol described in section 2.3.4.1). Blocking steps and incubation with primary and secondary antibodies were carried out in PBS containing 0.2% Triton X100.

2.6 Imaging

2.6.1 Imaging of paraffin and frozen sections

2.6.1.1 Immunostaining

Images of sections labeled with immunostaining were taken on a Zeiss AxioObserver Z1 inverted microscope with an ApoTome set-up, using a 20x air objective. The ApoTome system allows the acquisition of optical sections of thin specimens (10-50 µm) by computationally removing out-of-focus light in each image plane. Images were acquired using Zeiss AxioVision software. To image larger tissue areas the AxioVision Mosaix module was used. Several

individual images were automatically stitched together, creating a single picture from a large area.

2.6.1.2 Combined ISH and immunostaining

Pictures were taken for brightfield (ISH) and fluorescence channels using the Zeiss AxioObserver Z1 with a 20x air objective. The ApoTome was active only for the fluorescence channel. To present the RNA *in situ* hybridization and the immunofluorescence signal in one image, brightfield images of the RNA in situ hybridization signal were assigned to a RGB channel in Axiovision software; the channel was then inverted in Adobe Photoshop.

2.6.2 Time-lapse imaging of organotypic slice cultures

Slices were let to recover overnight before starting the time-lapse. In the following day after preparation, slices were transferred to an Ibidi μ-dish with 1 mL culture medium and 1.5 μL ascorbic acid (200 nM). Ascorbic acid was used to protect the slices against phototoxicity. For time-lapse imaging the slices were transferred to an environmental chamber at 37°C, 5%CO_2. Images of EYFP-labeled fate mapped neurons were acquired at 100X magnification with 10 min intervals for 8–12h on a Zeiss Axio-Observer inverted microscope with a live-cell imaging system.

2.6.3 Ultramicroscopy

Ultramicroscopy is a relatively new technique (Dodt et al., 2007), that allows high-resolution imaging of large tissues such as a whole mouse brain with fast data acquisition and little photo-bleaching. It utilizes a thin, horizontal, light sheet that penetrates the tissue. In this study ultramicroscopy was used to create a 3D reconstruction of the ventral midbrain.

Since mouse brain is not transparent, the tissue cannot be imaged without prior clearing.

2.6.3.1 Tissue clearing

Brains from E12.5 *Shh*$^{CreER/+}$*; R26*$^{EYFP/+}$ mice were immunostained as described in section 2.3.4.4. For tissue-clearing, brains were dehydrated in graded ethanol series (from 30% to 100% ethanol) at RT for 15 min. Next, the tissue was incubated in fresh 100% ethanol at 4°C overnight. The following day, brains were placed in hexane for 1 hour at RT and then transferred into a clearing solution of 1 part benzyl alcohol with 2 parts benzyl benzoate. The clearing solution has a similar refractive index as the fixed tissue, so that the light passing through the medium is not scattered by the different refractive index of the tissue (Spalteholz, 1914; Steinke and Wolff, 2001).

The samples were kept in the clearing solution at RT for 2 days preceding imaging (protocol modified after (Dodt et al., 2007).

2.6.3.2 Imaging set-up[1]

Optically sectioned volumetric imaging was performed using a previously described light sheet microscope (Spille et al., 2012) based on an inverted microscope body 8 (Figure 12). Cleared specimen was placed in a custom-made sample cuvette with coverslip bottom (Hellma, Müllheim). The cuvette with inner dimensions of 20 mm x 4 mm x 2 mm was filled with clearing solution and sealed with a coverslip. For fluorescence excitation, laser light was focused into the specimen orthogonal to the detection path through the optical grade sidewall of the cuvette. The excitation beam was tailored to form a thin sheet of light with a thickness of 2 - 6 µm (Ritter et al., 2010) and a width of 700 µm (FWHM) within the sample. Fluorescence was collected from below by either a 10x air objective or a 40x long working distance water immersion objective and imaged onto a scientific grade CMOS camera. 3D image data were acquired by moving the sample through the light sheet in steps of 1 µm using a motorized sample stage) controlled by ImSpector software (LaVision BioTec). Focal shift occurred during acquisition of image stacks due to the refractive index mismatch between clearing solution (n = 1.56) and immersion medium (air, n = 1.00 or water, n = 1.33). Instead of moving the light sheet with the detection focus (Mertz and Kim, 2010) to compensate for this effect, we employed a piezo driven objective mount. Its displacement was coupled linearly to the motion of the sample stage z-axis. Empirically we found a displacement ratio between objective mount and sample stage z-axis of 180/500 for air objectives and 75/500 for water immersion objectives.
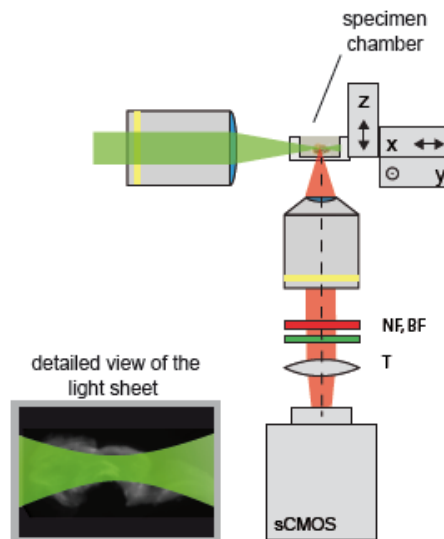
Figure 12. Ultramicroscopy set-up. The sample is illuminated from one side by a green laser forming a thin sheet of light. The cleared specimen is placed in a sample cuvette, submerged in clearing solution.

According to the laws of Gaussian optics, a thin light sheet has a high divergence angle resulting in a loss of optical sectioning towards the image borders along the optical axis of

---

[1] *Kindly provided by J.-H.Spille, Prof. U. Kubitschek laboratory, University of Bonn*

illumination. This is characterized by the Rayleigh length $x_R = \pi w_0^2 n/\lambda$. For a 3 µm thin light sheet, x_R = 70 µm at λ = 640 nm in clearing solution. To avoid this effect and acquire optically sectioned full frame images, typically 8 image stacks of the same sample volume were acquired consecutively with the light sheet focus displaced along the optical axis by approximately 140 µm between them. Using the 10x objective, a sample volume of 1.33 mm x 1.33 mm x 1.00 mm could thus be acquired in 8 x 100 seconds at a typical exposure time of 100 ms per frame and a voxel size of 0.65 µm x 0.65 µm x 1.00 µm. Using higher laser powers, this value could be reduced by a factor of 10 using the maximum camera frame rate. Light sheet microscopy was especially useful for volumetric imaging not only because of the high image rate, but especially because of its efficient use of the photon budget. Each slice within the sample was exposed to illumination light once per light sheet focus position, i.e. typically 8 times per data set. In contrast, using e.g. confocal microscopy each part of the sample would be exposed to illumination light once per z slice, i.e. 100 times more often than with light sheet microscopy if 800 z slices were acquired.

2.6.3.3 Image processing[2]

Instead of stitching the optically sectioned parts of the images the following post-processing steps were applied: To eliminate out of focus information contained in the images and numerically increase the sectioning effect, for each frame within a stack a floating minimum z-projection running over ± 4 frames was applied. This resulted in stacks containing in focus information in an image area with a width of approximately $2x_R$ = 140 µm around the light sheet focus position and only little information outside of this area. Full image frames were reconstructed from a maximum intensity projection of all frames from the same sample plane illuminated with different light sheet focus positions. This approach bears some similarity to TSLIM (Schacht et al., 2011) and the image processing in early implementations of structured illumination microscopy (Neil et al., 1997). However, in contrast to TSLIM, the illumination focus and not the sample is displaced along the optical axis. Further, instead of taking two images – one in and one out of focus – of a sample plane as in (Neil et al., 1997), only in focus images were acquired here. The out of focus information to be subtracted was obtained from neighboring slices in a z-stack which were acquired anyways, thus reducing the number of exposures by a factor of two. Image processing was performed using MATLAB functions written for this purpose.

2.7 Quantifications

---

[2] *Kindly provided by J.-H.Spille, Prof. U. Kubitschek laboratory, University of Bonn*

54

2.7.1 Fate mapped MbDA neurons

The distribution of MbDA neurons was quantified on sections at three anteroposterior midbrain levels of at least three embryos for each time point. For each level, the medial-lateral distribution of fate-mapped MbDA neurons (double-positive for TH and EYFP, $TH^{pos}/EYFP^{pos}$) was determined by dividing the ventral midbrain into bins of 100 µm thickness along the mediolateral axis (N=3). Statistical significance was analyzed using two-ways ANOVA, with Bonferroni post-hoc multiple comparison test (GraphPad).

2.7.2 Organotypic slice culture migration assay

The velocity (total distance traveled per time) of the moving cells in organotypic slice cultures was assessed using Fiji, MTrack2 (Schindelin et al., 2012). Based on their velocity the migrating cells were divided in three categories: low speed (2-10 µm/h), medium speed (10-25 µm/h) and high speed (>25 µm/h). The percentage of cells out of the total number of cells for each category was determined (N=9 slices). Statistical significance was analyzed with Student's t-test. Migration trajectories of $EYFP^{pos}$ cells were manually tracked with Fiji MtrackJ plugin. The midline of a horizontal slice was assigned as x-axis. The best-fit tangential path was considered as being perpendicular to the x-axis and was assigned as y-axis. The trajectory in reference to the x- and y-axes was obtained by tracking somal coordinates through the imaging sequence. Deviations from the best-fit trajectory (0°) were represented in degrees (0°– 90°).

2.7.3 *Cxcl12* and *Cxcr4* KO analysis

The area containing TH^{pos} MbDA neurons was divided into 2 bins along the dorsoventral axis (from the ventricle to the ventral pial surface) and into 8 (E14.5) or 10 (E16.5) bins along the mediolateral axis (from the midline to the lateral pial surface, on either side of the midline). For each side, the number of TH^{pos} cells was determined in each bin and normalized for the total number of TH^{pos} cells (expressed in percentage) (Table 1). To take into account TH^{pos} neurons on both sides of the midline, an average was formed between the left and the right side. Statistical significance was analyzed with one-way ANOVA and LSD post-hoc multiple comparison test (SPSS, IBM).

2.7.4 Ultramicroscopy

3D-volume renderings of the MbDA neuron-containing area ($TH^{pos}/EYFP^{pos}$) were generated from image stacks at 10x magnification (Fiji-3D viewer plugin). Cell bodies and processes were traced in image stacks acquired at 30x magnification with Surpass Scene FilamentTracer (Imaris, Bitplane). Statistical significance was analyzed with Student's t-test.

3. RESULTS

3.1 Fate mapping strategy to follow the migration of MbDA neurons contributing to the SN or medial VTA

In this study, genetic inducible fate mapping method (GIFM), was used to differentially label distinct SHH-expressing progenitor cells and follow their fate and migratory routes from their early progenitor stage to their final location in the ventral murine midbrain. A knock-in mouse line that expresses *CreER* from the *Shh* locus (Harfe et al., 2004) was used in conjunction with a reporter line in which enhanced fluorescent protein (EYFP) reporter gene was under the control of the Gt(*ROSA)26Sor* (*R26*) ubiquitous promoter (Joyner and Zervas, 2006). The *R26* allele contains a floxed *Stop* sequence upstream of *EYFP* (*R26^EYFP*) (Srinivas et al, 1999). EYFP can only be expressed after excision of the *Stop* sequence by Cre-mediated recombination (Figure 13A). Temporal control was achieved by administrating tamoxifen at chosen time points (Figure 13B). Since the CreER nuclear translocation occurs within 6 h after TM administration and is maintained for approximately 24 h, cells expressing SHH from 6 to 36 h after TM administration can be genetically marked (active labeling) (Hayashi and McMahon, 2002; Zervas et al., 2004). Once marked, the cell labeling is retained (retained labeling) (Figure 13B).
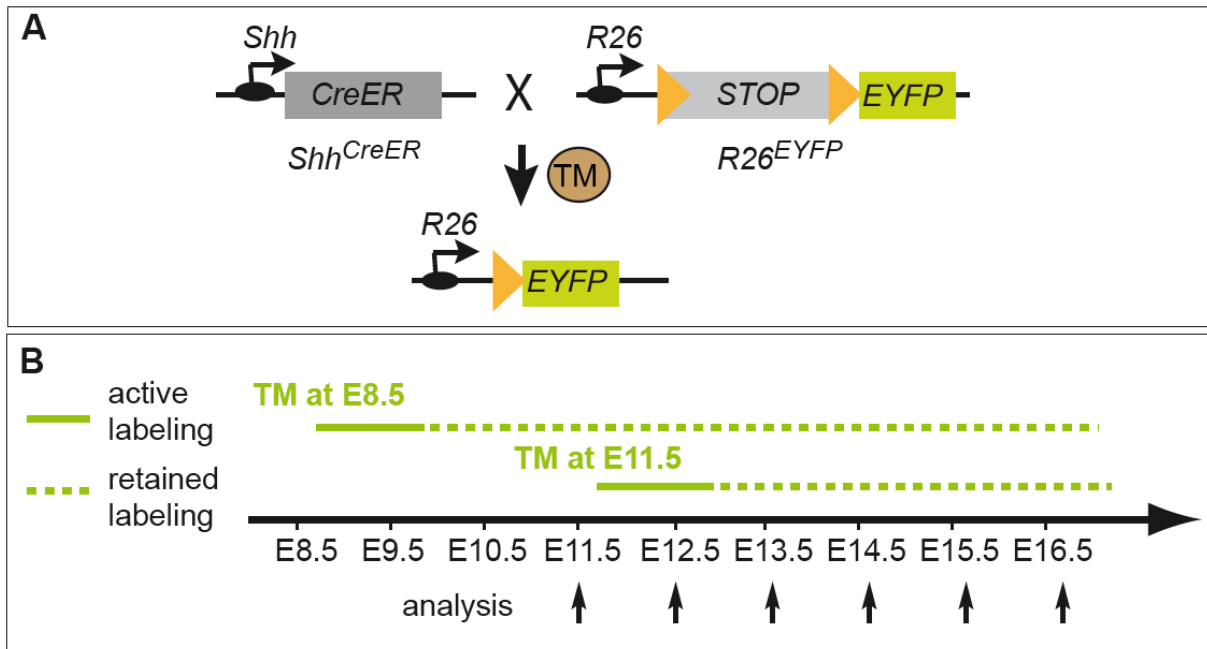
Figure 13. Recombination scheme in *Shh^CreER/+; R26^EYFP/+* mice. A) Fate mapping strategy to mark and follow SHH-expressing cells and their descendants. The *CreER* encoding sequence is inserted into the *Shh* locus. The R26 reporter allele contains a floxed *Stop* cassette upstream of *EYFP*. This *Stop* cassette is removed upon tamoxifen induced Cre mediated recombination and EYFP is permanently expressed in recombined cells. TM: tamoxifen, orange triangle: *loxP* site. B) Recombination results in active labeling within 24 h. After this, the labeling is retained and transmitted to the descendant cells.

SHH is expressed in MbDA progenitors in the medial floor plate between E8.5 and E9.0, but at E11.5, it is excluded from the medial domain and restricted to lateral MbDA progenitors (Blaess et al., 2011; Hayes et al., 2011; Joksimovic et al., 2009; Legue and Joyner, 2010). When GIFM of SHH-expressing cells is induced at E8.5, medial MbDA progenitors and their descendants are marked; these cells show a biased contribution to the SN (marking scheme 1) (Figure 14). Induction at E11.5 marks lateral MbDA progenitors and their descendants; this population contributes preferentially to the medial VTA consisting of the paranigral and intrafasicular nucleus (marking scheme 2) (Figure 14) (Blaess et al., 2011; Hayes et al., 2011; Joksimovic et al., 2009). Progenitor populations labeled with the marking scheme 1 or 2 give also rise to neurons of the lateral VTA (parabrachial nucleus) and contribute a few cells to the mVTA or SN, respectively. Nevertheless the two populations are sufficiently distinct to separately examine the migratory routes and behavior of MbDA neurons contributing to the SN or the mVTA (Figure 14).
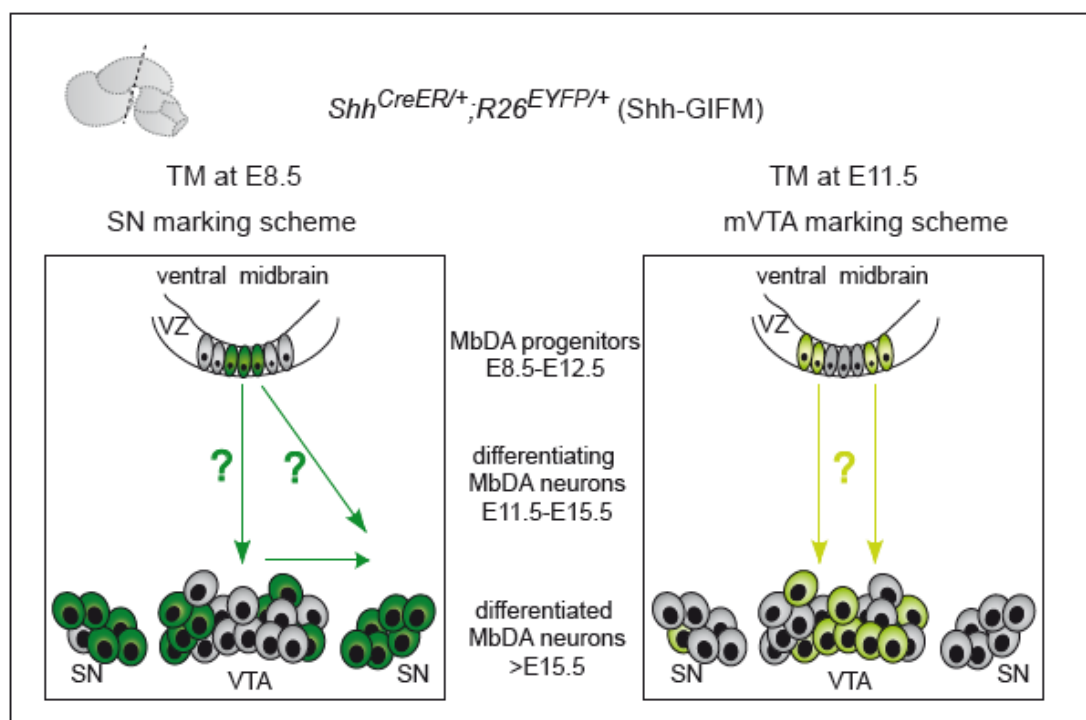
Figure 14. Genetic inducible fate mapping (GIFM) of MbDA neurons. GIFM of SHH-expressing cells through TM administration at E8.5 (TM at E8.5) results in labeling of medial MbDA progenitors that have a biased contribution to SN neurons (SN marking scheme). TM administration at E11.5 results in labeling of lateral MbDA progenitors that preferentially give rise to mVTA neurons (mVTA marking scheme). Arrows indicate possible models for the migration of differentiating MbDA neurons: radial migration of neurons destined for the SN and VTA; radial migration followed by tangential migration of neurons destined for the SN.

Fate mapped differentiated MbDA neurons were identified by immunostainings for TH and EYFP. This double-labeling approach was necessary, since, in addition to MbDA progenitors and MbDA neurons, some non-MbDA neurons are labeled with the SN and mVTA marking scheme in the ventral midbrain (Blaess et al., 2011). Quantification of EYFP positive (EYFP[pos]) and EYFP[pos]/TH^{pos} cells at E13.5 and E14.5 showed that within the areas that contain

differentiated MbDA neurons, more than 70% of EYFP^{pos} cells were also TH^{pos} (Figure 15 C).
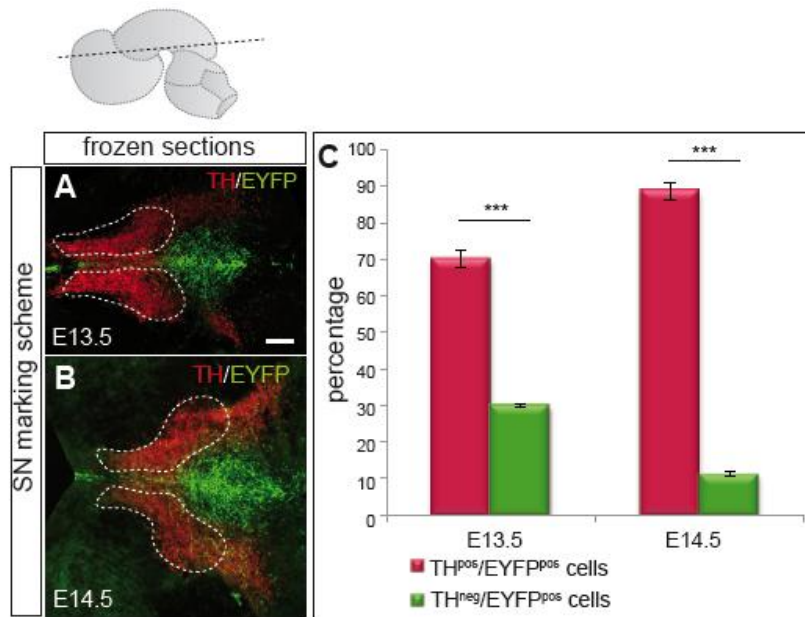

Figure 15. More than two-thirds of differentiated cells labeled with the SN marking scheme express Tyrosine Hydroxylase (TH). (A, B) Immunostaining for EYFP and TH on horizontal sections. Outlined areas contain differentiated MbDA neurons (TH^{pos}). (C) Quantification of TH^{pos}/EYFP^{pos} in the areas outlined in A and B. Significance was determined by Student's t-test, p<0.001.

3.2 Distribution of MbDA neurons destined for the SN shifts from medial to lateral during embryonic development

To investigate the migratory routes of MbDA neurons, the distribution of fate mapped MbDA neurons labeled with the SN or mVTA marking scheme was determined between E11.5 and E16.5. The detailed analysis at E11.5 for MbDA neurons labeled with the SN marking scheme and the analysis at E13.5 and E15.5 for MbDA neurons labeled with both the SN and the mVTA marking scheme, are shown as examples (Figure 16, 17). The distribution of the fate-mapped MbDA neurons (EYFP^{pos}/TH^{pos}) was analyzed at three levels along the anteroposterior axis of the developing ventral midbrain (referred to as anterior, intermediate and posterior) (Figure 17 O). From anterior to posterior these areas correspond to the following MbDA nuclei in the adult brain: the anterior SN; the intermediate SN and the anterior VTA; the posterior SN, posterior VTA, SN and RRF (Figure 17 P).

At anterior levels, MbDA neurons labeled with the SN marking scheme were distributed lateral relative to the midline at E11.5, E13.5 and E15.5 (Figure 16 A; Figure 17 C,C', I, I'). At intermediate levels, MbDA neurons labeled with the SN marking scheme were medial at E11.5 and E13.5, but located in a lateral position at E15.5 (Figure 16B, 17 E, E', K, K'). At posterior levels, the MbDA destined for the SN were located medially at all the stages analyzed. In contrast, MbDA neurons labeled with the mVTA marking scheme were located medially at both intermediate and posterior levels (Figure 17 F-H', 17 L-N'). Very few neurons labeled with the mVTA marking scheme were located at anterior levels, corresponding with the localization of

MbDA labeled with the VTA marking scheme in the adult brain (Figure 17 D, D', J, J', P).
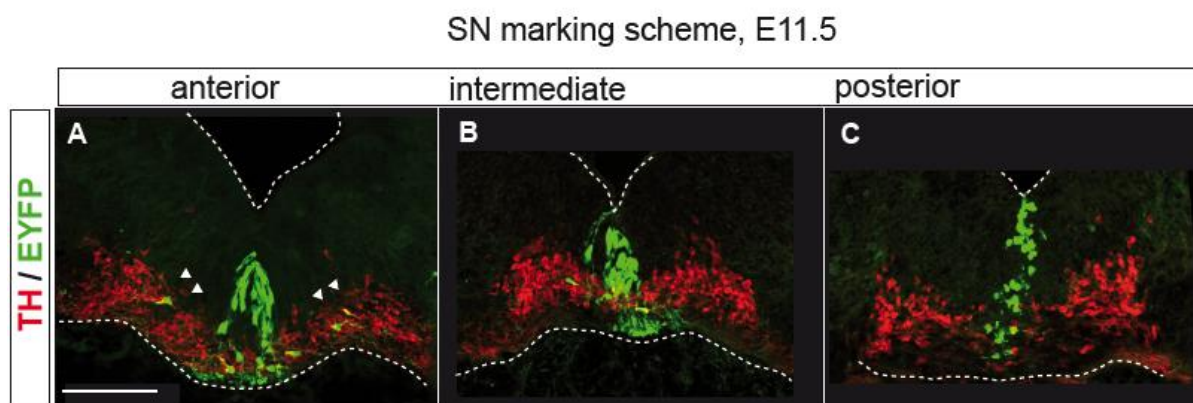

Figure 16. Cells labeled with the SN marking scheme at E11.5 show lateral positions at anterior levels and medial positions at intermediate and posterior levels. (A, B, C) Coronal sections at three anteroposterior levels were immunostained for EYFP (green) and TH (red). Arrowheads show MbDA neurons at anterior levels located at some distance from the midline. The ventricle and the pial surface are outlined. Scale bars: 100 µm

To quantify the mediolateral position of the fate-mapped MbDA neurons, the ventral midline in each section was determined. The ventral midbrain was divided into bins of 100 µm along the mediolateral axis (Figure 18 A-D). The number of fate-mapped MbDA neurons per bin was counted and expressed as percentage of the total number of fate-mapped MbDA neurons per section (Figure 18 E,F, 19 A-C).

At anterior levels, MbDA neurons labeled with the SN marking were located in increasingly lateral positions at subsequent stages (Figure 16 A, 19 A). Analysis at intermediate and posterior levels showed that MbDA neurons labeled with both marking schemes are located close to the midline (0-300µm) between E11.5 and E13.5 (Figure 18 E, F; 19, B, C). At later stages (E15.5-E16.5), intermediate and posterior levels analysis showed the MbDA neurons labeled with the SN marking scheme in increasingly more lateral positions, while MbDA neurons labeled with the mVTA marking scheme maintained a relative medial position (0-400 µm) (Figure 18 E, F; 19 B, C). Statistical significance was determined by ANOVA and post-hoc Bonferroni analysis.
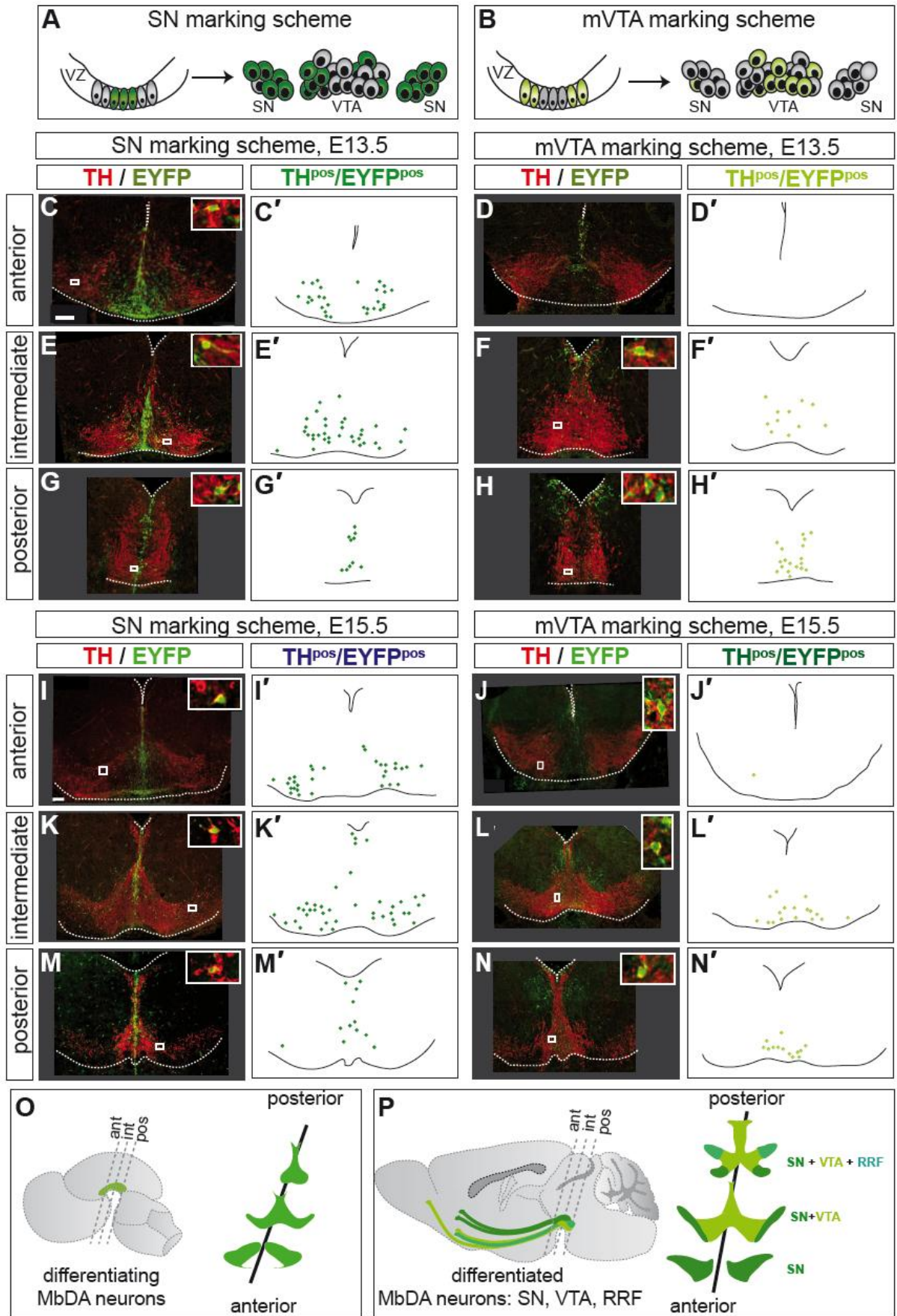
Figure 17. Distinct distribution of MbDA neurons destined for the SN or mVTA (Figure legend continues on the following page)

60

Figure 17. (A, B) Drawing showing the SN or mVTA marking scheme. (C-H) E13.5 and (I-N) E15.5 coronal sections at three anteroposterior levels were immunostained for EYFP (green) and TH (red) to visualize fate-mapped MbDA neurons. Only a subset of cells is labeled at any given SHH-expressing domain due to the mosaic recombination pattern. Upper right corner: higher magnification of the boxed area. (C´-N´). Schematics show the distribution of fate-mapped cells (blue or green dots). Note that E13.5 and E15.5 images and schematics are not to scale. MbDA neurons labeled with the SN marking scheme are located in or close to the midline at E13.5, and are found in more lateral positions at anterior and intermediate levels at E15.5 (C, E, I, K). In contrast, MbDA neurons labeled with the mVTA marking scheme remain in a medial position (F, L). Hardly any neurons labeled with the mVTA marking scheme are located at anterior levels (D, J) (O) Schematic indicating the plane of section shown in C-N. Green: MbDA neuron-containing area. (P) Schematic indicating the corresponding levels in the adult brain. Scale bar: 100 µm, Insets scale bar: 25 µm

Statistical analysis for MbDA neurons labeled with the SN marking scheme at intermediate levels, showed that the change in distribution of neurons from medial (0-100 µm) to lateral (>600 µm) ventral midbrain was highly significant ($p < 0.001$) when comparing E12.5 with E15.5 or E12.5 with E16.5 ($p < 0.001$). Further, there was a significant change ($p < 0.01$) in distribution of neurons from medial (100-200 µm) to lateral (>600 µm) when comparing E12.5 with E16.5. These differences are probably due to MbDA movement from medial to lateral positions in the ventral midbrain between E12.5 and E15.5-E16.5. Statistical analysis for MbDA labeled with the mVTA marking scheme, at intermediate levels, showed highly significant differences ($p < 0.001$) in distribution of neurons from medial (0-100 µm) to slightly more lateral (100-200 µm) ventral midbrain when comparing E12.5 with E13.5, E14.5, E15.5 and E16.5, which probably accounts for tissue expansion over time.
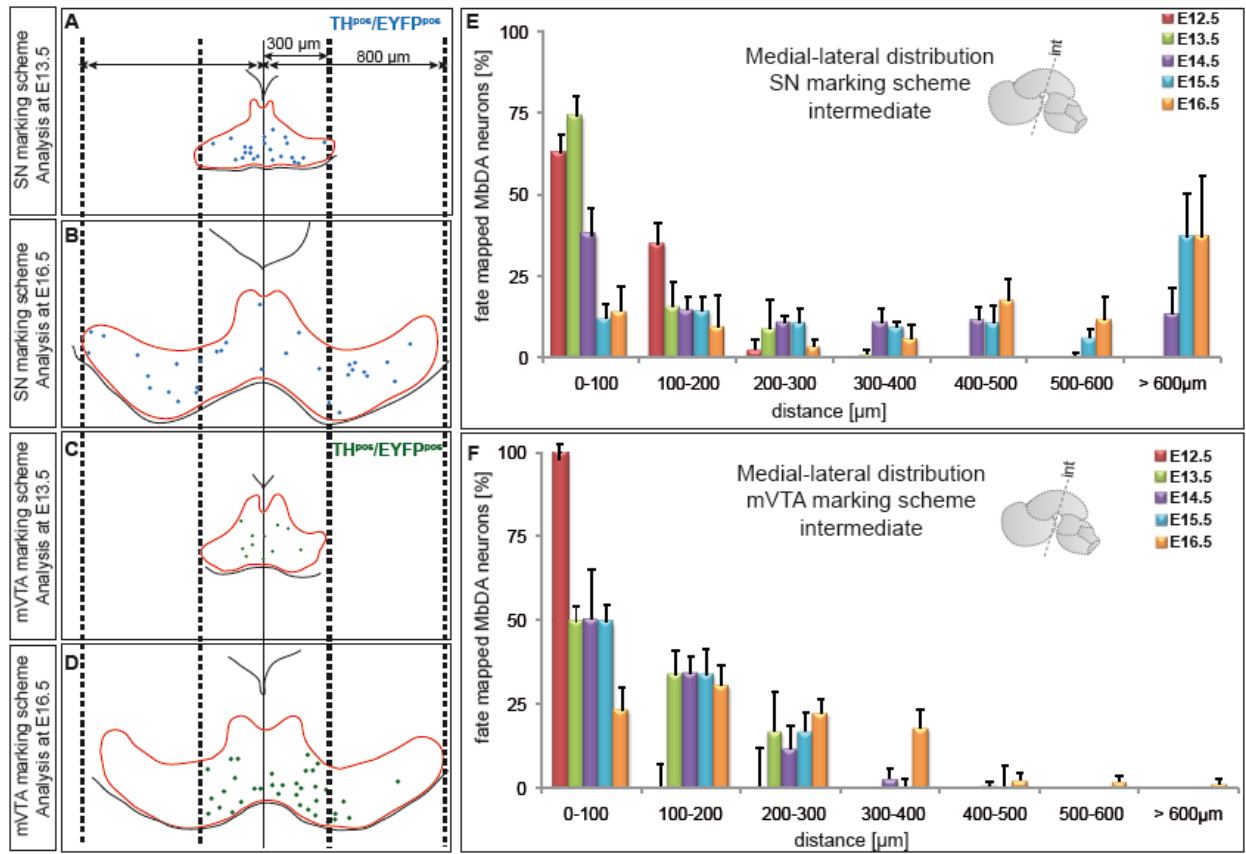
Figure 18. MbDA neurons destined for the SN take increasingly lateral positions over time on intermediate sections. (A-D) To-scale-analysis of the distribution of MbDA neurons labeled with the SN or mVTA marking scheme at E13.5 and E16.5. Blue or green dots indicate fate-mapped MbDA neurons (TH[pos]/EYFP[pos]). The solid line indicates the midline; dashed lines indicate the maximum lateral position of MbDA neurons at E13.5 or E16.5. (E, F) Medial-lateral distribution of fate-mapped MbDA neurons was quantified between E12.5 and E16.5 at intermediate section levels. (E) There was highly significant shift from medial (0-100µm) to lateral (≥ 600 µm from the midline) in the distribution of MbDA neurons labeled with the SN marking scheme between E12.5 and E15.5/E16.5, indicating a lateral movement of these cells. (F) In contrast MbDA neurons labeled with the mVTA marking scheme remain in a relative medial area. Data presented as ± SEM, N=3.
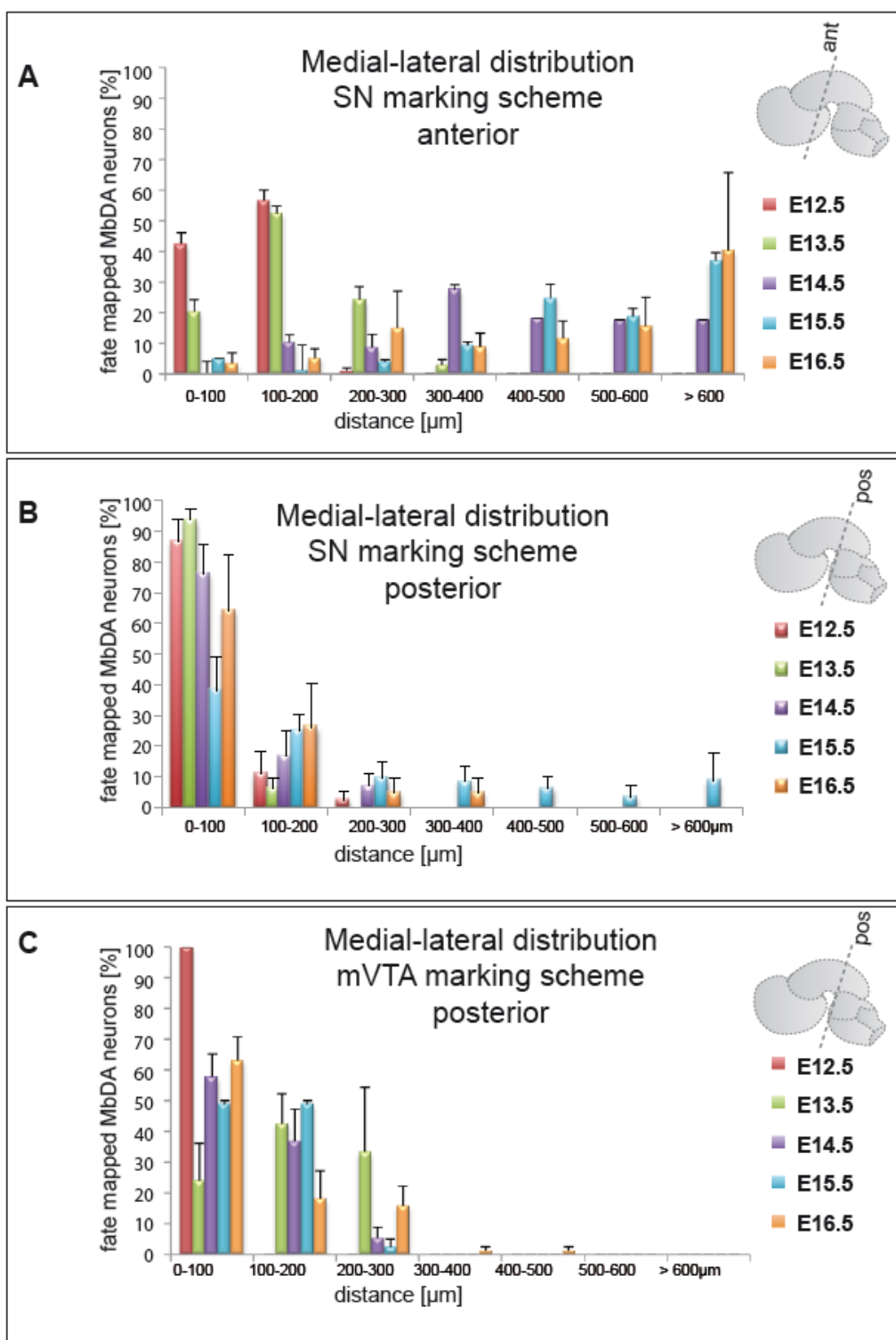
Figure 19. Distribution of fate-mapped MbDA neurons at anterior and posterior section levels (A, B) Medial-lateral distribution of MbDA neurons labeled with the SN marking scheme between E12.5 and E16.5 at anterior and posterior section levels. The ventral midbrain was divided in 100 µm wide bins from medial to lateral; fate-mapped MbDA neurons were counted in each bin. There is a shift from medial to lateral ($\geq$ 600 µm from the midline) in the distribution of MbDA neurons between E12.5 and E16.5 in anterior sections. In posterior sections, only few MbDA neurons were found in lateral positions. (C) Medial-lateral distribution of MbDA neurons labeled with the mVTA marking scheme between E12.5 and E16.5 at posterior section levels. There is no significant lateral shift over time. Data are presented as ± SEM, N=3.

3.3 MbDA neurons giving rise to the SN or VTA have different orientation of their leading process

The leading process selects the orientation of migrating neurons in response to chemotactic cues in the environment and its orientation can serve as an indicator for the direction of migration (Rakic, 1990; Yee et al., 1999). Cells labeled with the SN marking scheme in brain sections correlating with the lateral displacement of MbDA neurons appear to have tangentially-oriented leading processes (Figure 20 A-D). The MbDA neurons labeled with the mVTA marking scheme showed predominantly radially-oriented leading processes. This suggests that MbDA destined to VTA migrate mainly radially, from the VZ towards the pial surface (Figure 20 E-G).
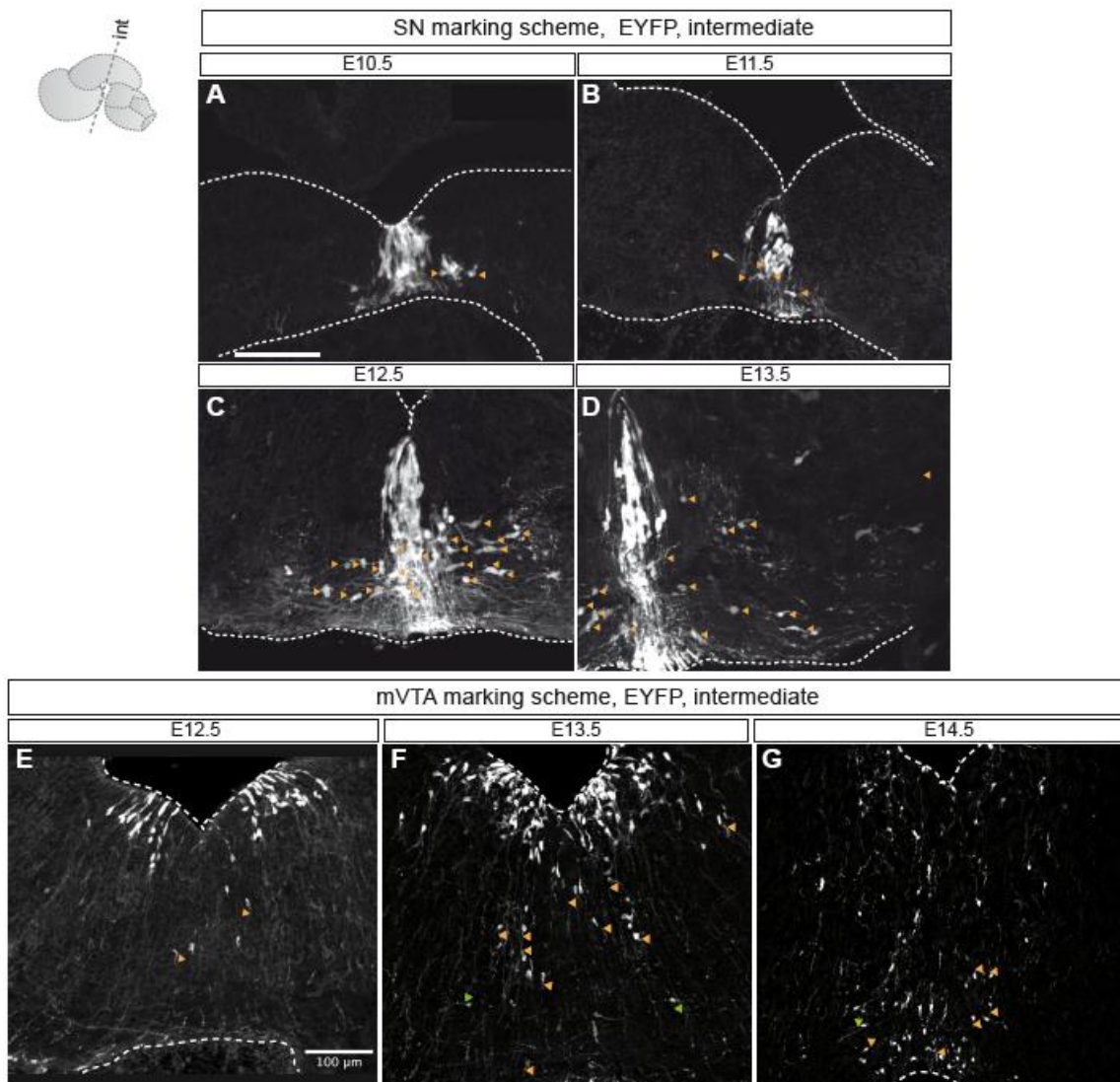
Figure 20. MbDA neurons labeled with the SN marking scheme show laterally oriented processes, whereas MbDA neurons labeled with the mVTA marking scheme show mainly radially oriented processes. (A-G) Coronal sections at an intermediate level were stained with antibodies against TH and EYFP, but only EYFP immunostaining is shown to visualize processes. (A-D) SN marking scheme at intermediate level, immunostaining for EYFP on coronal sections of E10.5-E13.5 embryos. (E-G) mVTA marking scheme at intermediate level, immunostaining for EYFP on coronal sections of E12.5-E14.5 embryos. The ventricle and the pial surface are outlined. (A-G) Orange arrowheads indicate radially oriented TH^{pos} neurons, green arrowheads indicate tangentially oriented TH^{pos} neurons. Scale bar: 100 μm

64

To investigate the morphology of fate-mapped MbDA neurons (EYFP[pos]/TH[pos]) more precisely, the entire midbrain was imaged using ultramicroscopy[3] (Figure 21). Unlike widefield and confocal fluorescence microscopy, ultramicoscopy allows fast multidimensional data acquisition of entire tissues with minimal photo-bleaching and with good optical resolution. Before subjecting the whole brains to ultramicroscopy, the entire E12.5 brain was immunostained for TH and EYFP and then the tissue was cleared as described in section 2.5.
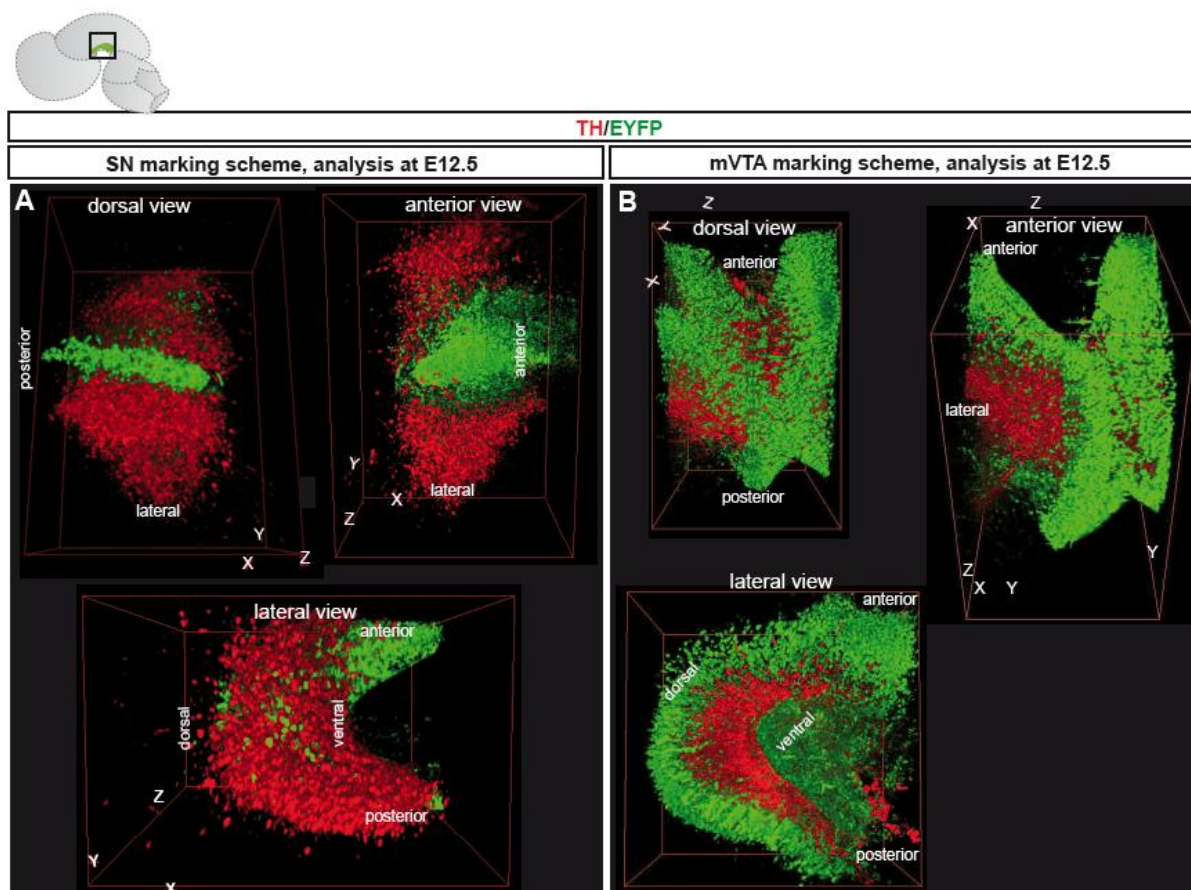
Figure 21. Ultramicroscopy and 3D renderings of the ventral Mb labeled with the SN or mVTA marking scheme[1]. (A) 3D rendering of the ventral midbrain (vMb) for the SN marking scheme. Cells immunostained for EYFP (green) and TH (red). Top, anterior and lateral views of the vMb show the medial precursor domain and EYFP, fate mapped cells positioned laterally, outside the progenitor domain, within the TH[pos] area. (B) 3D rendering of the vMb for the mVTA marking scheme. Top, anterior and lateral 3D views of the vMb show the two lateral precursor domains and EYFP, fate mapped cells spread medially within the TH[pos] domain.

Analysis of 3-D reconstructions of the acquired image stacks showed that most MbDA neurons had a bipolar morphology (Figure 22 B, D). MbDA neurons labeled with the SN marking scheme displayed radially-oriented processes when located close to the VZ, but tangentially-oriented processes after reaching the mantle layer (Figure 22 A, B, E). In contrast, MbDA neurons labeled with the mVTA marking scheme had predominantly radially-oriented processes and only few tangentially-oriented processes (6 out of 72 cells) (Figure 22 C, D, E). Classification of the

---

[3] *Ultramicroscopy performed by J-H.Spille, Prof. U. Kubitscheck laboratory, University of Bonn*

processes into trailing processes (radially-oriented towards the ventricular zone or tangentially-oriented toward the midline) and leading processes (radially-oriented towards the pial surface or tangentially-oriented, away from midline) showed that neurons labeled with both marking schemes had leading and trailing processes (Figure 22 F). In summary, MbDA neurons destined for the SN have first radial and then tangential leading/trailing processes supporting a model in which they initially undergo radial migration to reach the mantle layer and subsequently switch to tangential migration to form the SN. In contrast, neurons giving rise to the mVTA have almost exclusively radial leading/trailing processes, consistent with a simple radial mode of migration.
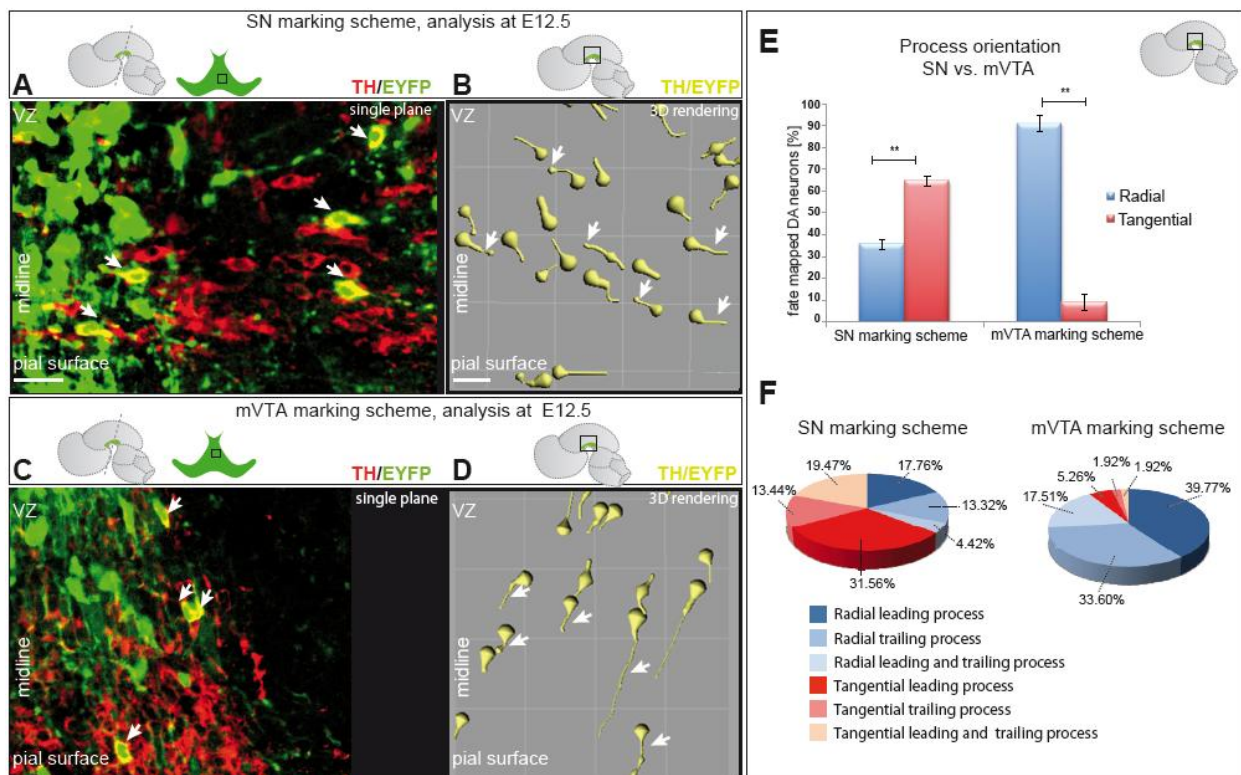
Figure 22. MbDA neurons destined for the SN have tangentially oriented processes. Ultramicroscopy to monitor the morphology of fate-mapped MbDA neurons. (A, C) Single plane from a 3D-reconstruction of the ventral midbrain at E12.5, immunostained for EYFP (green) and TH (red). The medial progenitor domain (EYFP^{pos}) is visible. Fate-mapped MbDA neurons (EYFP^{pos}/TH^{pos}) indicated by arrows. (B, D) Fate-mapped MbDA neurons traced in 3-D reconstructions to assess their morphology. Arrows indicate tangentially trailing or leading processes (B) and radially leading processes (D). (E) Quantification of radial vs. tangential orientation of the leading process. MbDA neurons labeled with the SN marking scheme have leading processes with both tangential and radial orientation. Leading processes of MbDA neurons labeled with the mVTA marking scheme have a predominantly radial orientation. (F) Classification of neuronal process orientation into trailing processes (radially oriented toward VZ or tangentially oriented toward midline) and leading processes (radially oriented towards pial surface or tangentially oriented away from midline). Scale bar (A, C): 100 μm; (B, D): 20 μm

3.4 Organotypic slice cultures of embryonic ventral midbrain: a system to study MbDA neuron migration live *in vitro*

Live-cell imaging allows the analysis of spatial dynamics of cells over time. This approach is particular suitable for studying cell migration, which is mediated by dynamic change in the cytoskeleton. However, the developing mouse brain is not suitable for easy manipulation and live cell imaging, *in vivo* since the mouse embryo is inaccessible and opaque. Organotypic slice cultures of embryonic brains are therefore widely used to study murine neuronal migration, *in vitro*. Time-lapse imaging in slice cultures has been particularly successful for studying cortical neuronal migration (Noctor et al., 2004; Martini et al., 2009, Marin et al., 2010; Ayala et al., 2007). Embryonic organotypic slice culture systems in brain regions outside of the cortex are less well established. Therefore an organotypic slice culture system of the ventral midbrain was established to study the MbDA neurons migration.The onset of migration of MbDA neurons is at embryonic day (E) 12.5. Therefore E12.5 mouse ventral midbrain was used for slice preparation.

A major challenge of live cell imaging *in vitro* is keeping cells alive and functioning as naturally as possible for the duration of the experiment. A number of steps were required in order to obtain slices that allow the normal development of MbDA neurons. The most critical step was the dissection of the embryonic brain, which had to be both fast and precise. In contrast to the generation of adult brain slices, it is crucial to section the brains on a vibratome equipped with a cooling system and to use a low frequency combined with a high speed sectionning to obtain intact slices of E12.5 brains. Details of the organotypic slice culture protocol are provided in section 2.4.

3.4.1 MbDA neurons require the presence of the projection target area for proper development in organotypic slice cultures

To visualize the radial and tangential migration of MbDA, coronal vibratome slices of ventral midbrain were prepared. Immunostainings for TH indicate the development of MbDA neurons in organotypic slice cultures. In coronal slices, the forebrain target areas of MbDA neurons are absent and subsequently the neurons formed aberrant projections to the dorsal midbrain (Figure 23). These aberrant projections were considered an abnormal development of MbDA neurons in the slice cultures, and coronal slice cultures were not used for further analysis of migration. Horizontal and sagittal brain slices were generated instead. This sectioning approach allows the forebrain target areas of MbDA projections to be included in the slice.
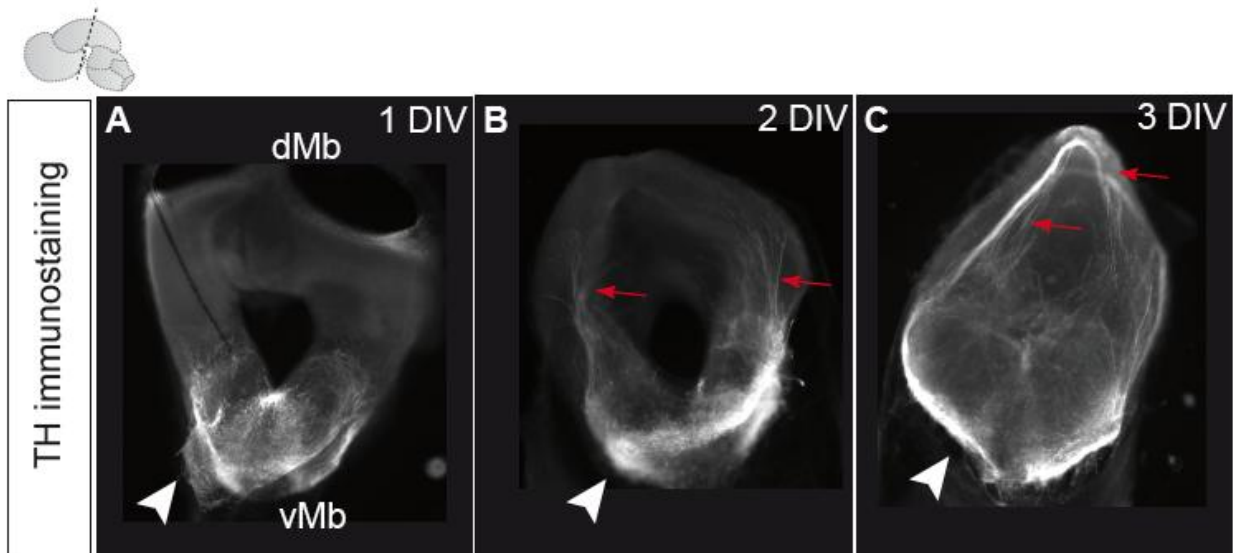
Figure 23. Midbrain coronal slice cultures stained for TH to label MbDA neurons. (A-C) Slices after 1, 2 or 3 DIV (days in vitro). MbDA neurons develop aberrant projections towards the dorsal midbrain (red arrows). Arrowheads show the location of the MbDA cell bodies.

3.4.2 Projections of MbDA neurons in organotypic slice cultures are dependent on the integrity of the forebrain

Horizontal organotypic slices (acute and after several days in culture) obtained from E12.5 mouse brain are shown as an example (Figure 24). The horizontal slices were compared with frozen brain sections at the equivalent developmental stages (Figure 24). MbDA neurons were visualized with immunohistochemistry for TH in horizontal slices. Fixed horizontal sections show that MbDA project to targets in the forebrain (Figure 24 B). These projections start to form at E12.5 and extend towards the forebrain during the subsequent days both in fixed horizontal sections and live horizontal slices (Figure 24 A, B). After 3 DIV or when the forebrain target area was damaged, aberrant projections extended towards the dorsal midbrain in the horizontal slices.
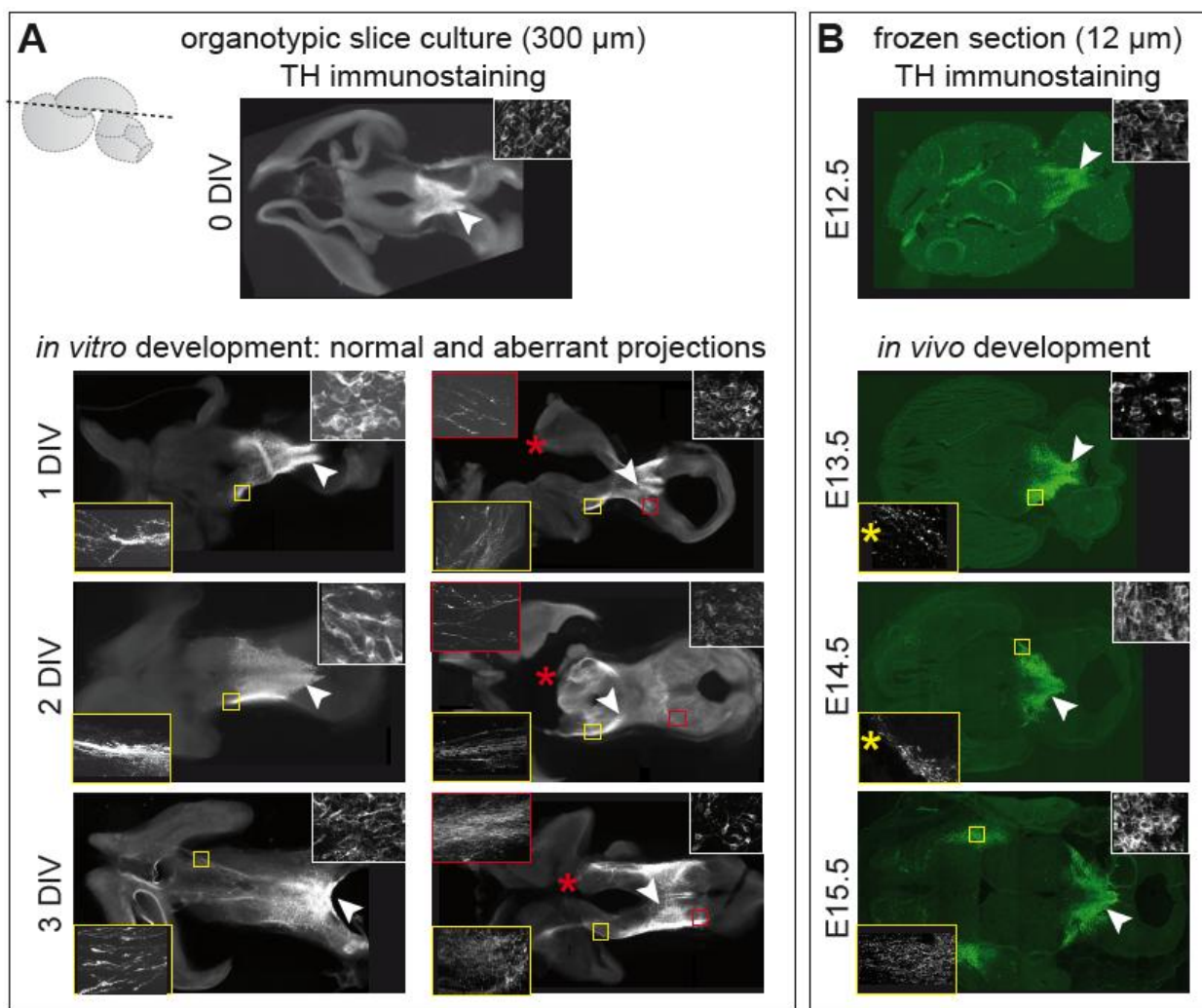
Figure 24. Projections of MbDA neurons in organotypic slice cultures are dependent on the integrity of the forebrain. (A) An acute slice (0 DIV) shows the normal location of MbDA neurons in the ventral midbrain. The white arrowhead indicates the area that is shown in higher magnification in the inset. Projections to the forebrain have not yet developed. After 1 DIV, projections to the forebrain start to form. Projections extend into the forebrain at 2-3 DIV. White arrowheads indicate the location of the cell bodies shown in higher magnification in the insets (white frame). Yellow squares highlight the normal projections in intact slices shown in higher magnification in the insets (yellow frame). Aberrant projections develop in slices with damaged forebrain. Red squares indicate the aberrant projections to the dorsal midbrain shown in higher magnification in the insets (red frame). Damage is indicated with red asterisks. After 3 DIV, most slices (n=5/7) had aberrant projections towards the dorsal midbrain. (B) TH immunostaining on horizontal frozen brain sections at different developmental stages show the development of dopaminergic projections *in vivo*. White arrowheads indicate the location of the cell bodies shown in higher magnification in the insets (white frame). Yellow squares highlight the position of the projections shown in higher magnification in the insets (yellow frame). The level of the frozen sections was chosen to closely match the level of the organotypic slice cultures. Note that a single frozen sections (12 μm) does not represent the entire organotypic slice (300 μm). Therefore, projections shown at E13.5 and E14.5 were observed on sections 120 μm more ventral than the section containing the cell bodies (yellow asterisks).

3.4.3 Organotypic slice cultures of the ventral midbrain can be maintained in culture for a limited period of time

Fluorescence illumination, especially in the UV range, is harmful for cells and causes photobleaching and phototoxicity. In the ventral midbrain organotypic slice cultures presented here, the slices could be maintained *in vitro* for maximum three days. Analysis of proliferating, necrotic and apoptotic cells in the organotypic slice cultures was performed to verify the viability of cells in the slice culture system. BrdU immunostaining to visualize proliferating cells demonstrated that cells proliferated under culture conditions after 1 DIV. Proliferation was reduced after 4 DIV (Figure 25A). After 3 DIV, many cells in the ventral midbrain undergo necrosis (propidium iodide staining) and apotosis (immunostaining for cleaved caspase-3) (Figure 25B,C). In conclusion, the slices can be maintained *in vitro* for maximum 3 days. During this time the proliferative capacity of the VZ progenitors is maintained throughout the slice and MbDA neurons maintain their normal projections and positions.
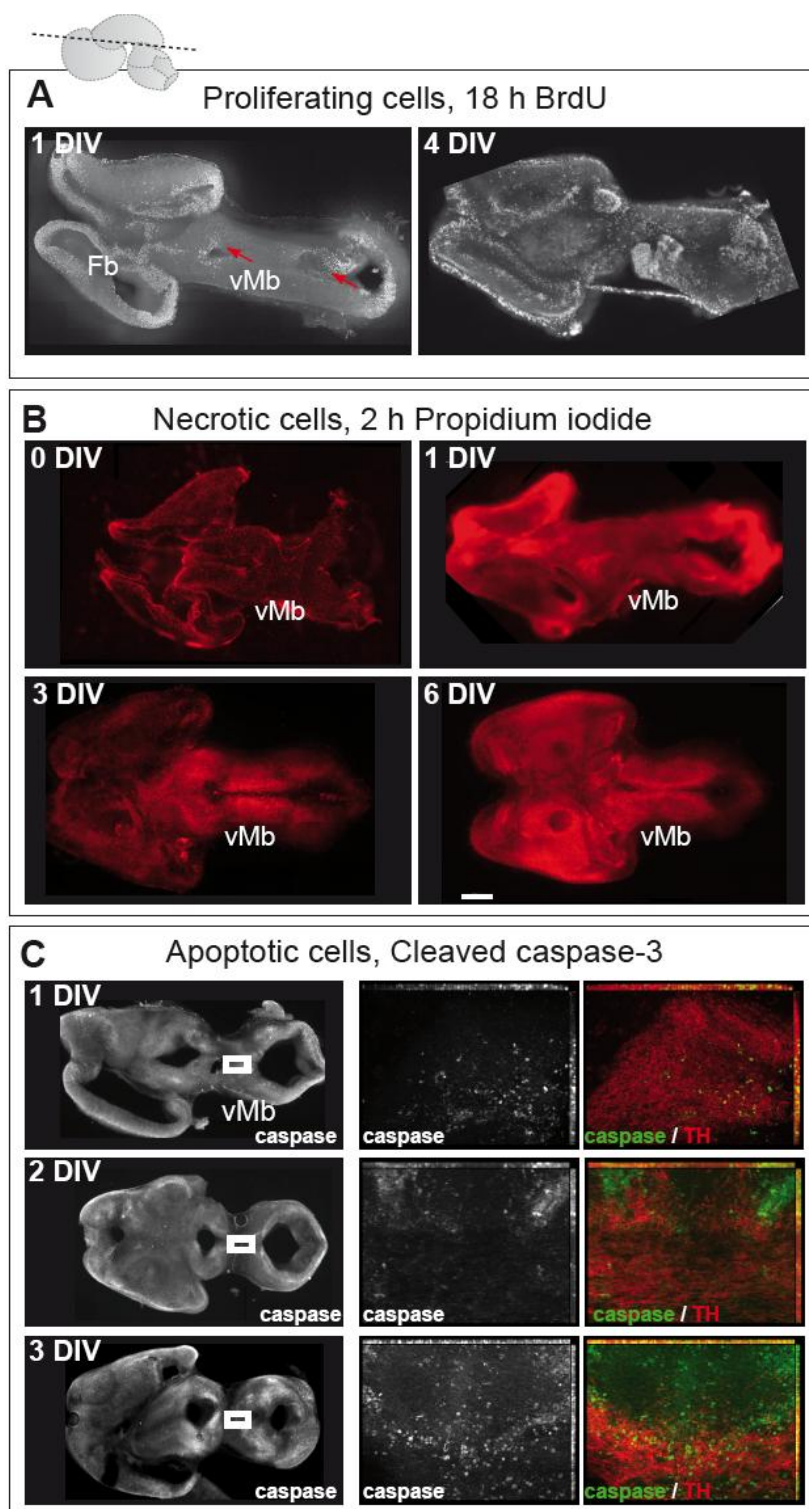
Figure 25. Cell proliferation and cell viability in midbrain organotypic slice cultures. (A) Proliferating cells were labeled by the addition of BrdU (50 ng/mL) to the culture medium for 18 h and subsequently immunostained for BrdU. After 1 DIV, BrdU labeled cells are located in the VZ (red arrows). After 4 DIV, proliferating cells are more scattered and a distinct VZ is no longer maintained. (B) Necrotic cells were labeled by addition of propidium iodide (1μg/μL) to the culture medium for 2 h and visualized by fluorescence microscopy. After 1DIV, the ventral midbrain is not necrotic, but many propidium iodide labeled cells can be seen in the dorsal midbrain and forebrain. After 3 DIV the cell viability decreases in the ventral midbrain. Scale bar: 500 μm (C) Immunostaining for cleaved caspase-3 to visualize apoptotic cells. At 1 or 2 DIV, only few MbDA neurons are apoptotic, but after 3 DIV, MbDA neurons start to undergo apoptosis. Panels in the middle and on the right are higher magnifications of the boxed area in the left panels.

3.5 Time-lapse imaging demonstrates distinct migratory routes for MbDA neurons destined for the SN or medial VTA

To examine the migratory behavior of neurons labeled with the SN or mVTA marking scheme directly, the migration of fluorescently marked cells in organotypic slice cultures was monitored using time-lapse imaging. GIFM of SHH-expressing cells results in mosaic labeling, therefore only some of the MbDA neurons originating in either the medial or lateral MbDA progenitor domain are marked. This is advantageous for live imaging, since single migrating neurons can be observed and traced (Blaess et al., 2011; Bodea and Blaess, 2012). The E12.5 horizontal or sagittal brain slices were cultured for 1 day to allow the tissue to adapt to the culture conditions. Subsequently, the slices were imaged for at least 8 hours. Imaging of cells labeled with the mVTA marking scheme in sagittal slices showed that they are undergoing radial migration (5 slices) (Figure 14F). Cells labeled with the SN marking scheme, but not the mVTA marking scheme, underwent tangential migration in horizontal slices (SN marking scheme: 4 slices, mVTA marking scheme: 3 slices) (Figure 26 C). During tangential migration, soma translocation followed the extension of a leading process (Figure 26 C). The observed cells showed transient trailing processes (5/10 cells) and short backward movements (3/10 cells). In addition, some tangentially migrating neurons underwent a phase of active forward movement followed by a resting period (4/10 cells). The average migration speed of migrating cells was 25 µm/h, but ranged between 2 µm/h and 40 µm/h (Figure 26 B, C). These data demonstrate that neurons that contribute to the SN undergo tangential migration, while neurons destined for the mVTA only follow a radial migration route.
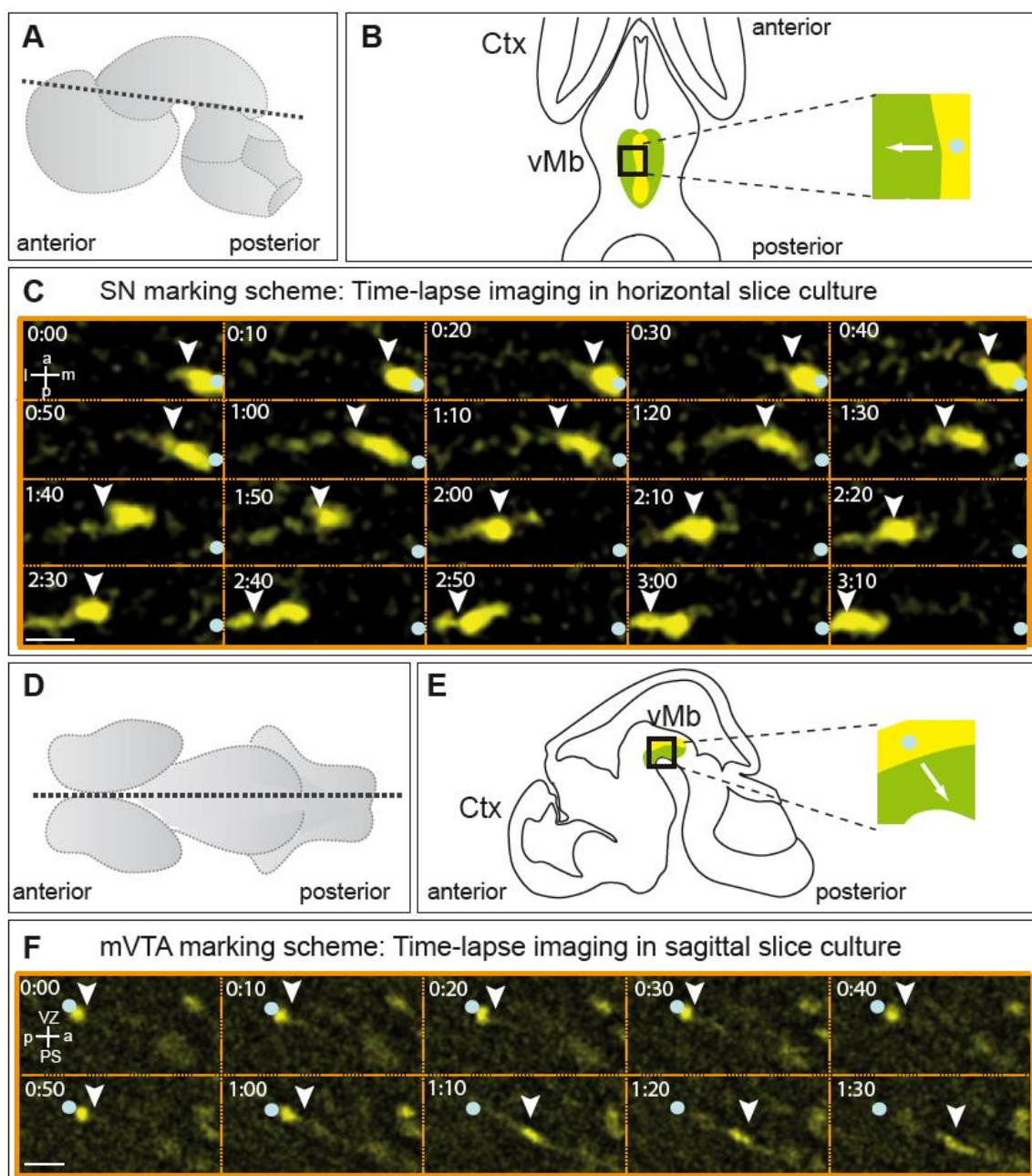
Figure 26. MbDA neurons destined for the SN undergo tangential migration. Time-lapse imaging of fate-mapped MbDA neurons in organotypic slice cultures. (A) The plane of section for horizontal slice preparations. (B) Schematic showing the tangential migratory route of MbDA neurons (white arrow) labeled with the SN marking scheme (yellow) in a horizontal slice. Blue dot indicates the initial position of the neuron. Green area: differentiated MbDA neurons. Ctx: cortex, vMb: ventral midbrain. (C) Example for time-lapse imaging of EYFP^{pos} neurons labeled with the SN marking scheme in an E12.5 horizontal slice after 1DIV. Images were taken every 20 min. The neuron migrates laterally (arrowhead) from its initial position in the ventral midline. See schematic in B for the imaged area. (D) Plane of section for sagittal slice preparations. (E) Schematic showing the migratory route of MbDA neurons (white arrow) labeled with the mVTA marking scheme (yellow) in a sagittal slice. Blue dot indicates the initial position of the neuron. Green area: differentiated MbDA neurons. (F) Example for time-lapse imaging of EYFP^{pos} neurons labeled with the mVTA marking scheme in an E12.5 sagittal slice after 1 DIV. Images taken every 10 min. The neuron migrates radially (arrowhead) from its initial position. See schematic in E for the imaged area. Scale bar: 12.5 µm

3.6 Reelin signaling regulates tangential migration of MbDA neurons destined for the SN

It has been reported previously that the Reelin pathway could play a role in regulating tangential migration of MbDA neurons, since the SN does not form and MbDA neurons accumulate in the VTA of *Reeler* mutants. (Kang et al., 2010; Matsuzaki et al., 2007; Nishikawa et al., 2003). Reelin regulates migration in several brain areas via the transmembrane receptors ApoER2 and VLDLR. Upon binding of Reelin to its receptors the cytoplasmic adaptor protein, DAB1 is phosphorylated and mediates downstream Reelin signaling (Ballif et al., 2004; D'Arcangelo et al., 1999).

To determine a possible role of Reelin in MbDA neuronal migration, the expression of components of the Reelin signaling pathway was analyzed. RNA *in situ* hybridization at E13.5 showed that *Vldlr* and *Apoer2* were expressed at low levels throughout the region containing MbDA neurons at intermediate levels (Figure 27 C, D, G, and H). In contrast, *Dab1* expression was largely restricted to the area where tangentially migrating MbDA neurons destined for the SN are located (Figure 27 B, F, I-N; 28 B, E). Reelin was expressed immediately dorsally to the *Dab1*-expressing cells, in an area positive for the red nucleus marker BRN3a (Brain-specific homebox/POU domain protein 3A) (Figure 27 E, E').
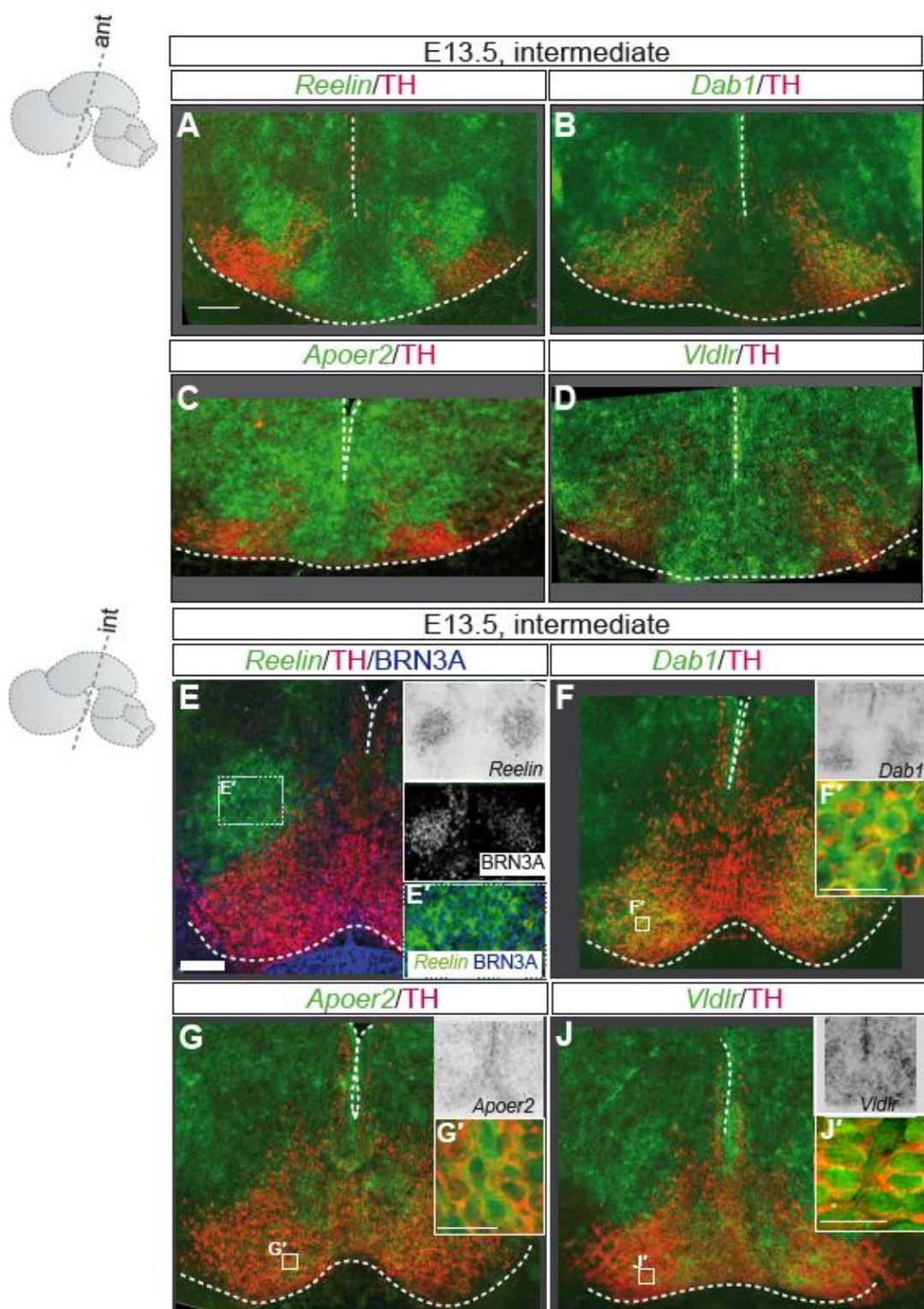
Figure 27. Reelin and its components are expressed in MbDA neurons. (A-H) RNA *in situ* hybridization for components of the Reelin signaling pathway and immunostaining for TH. *Dab1, Vldlr* and *Apoer2* are expressed in the anterior SN (A-D). *Reelin* is expressed dorsal to the *Dab1^{pos}* cells. (E) RNA *in situ* hybridization for *Reelin* and immunohistochemistry for BRN3A, a marker for red nucleus. Neurons shows overlap staining, indicating that the red nucleus is the source of Reelin in the region adjacent to the MbDA neurons. (E-J) RNA *in situ* hybridization for components of the Reelin pathway on intermediate sections. (F) *Dab1* is specifically present in the lateral population of MbDA neurons. *Apoer2* and *Vldlr* receptors are broadly expressed in MbDA neurons (G-J). Brightfield in situ hybridization images are presented in the insets.
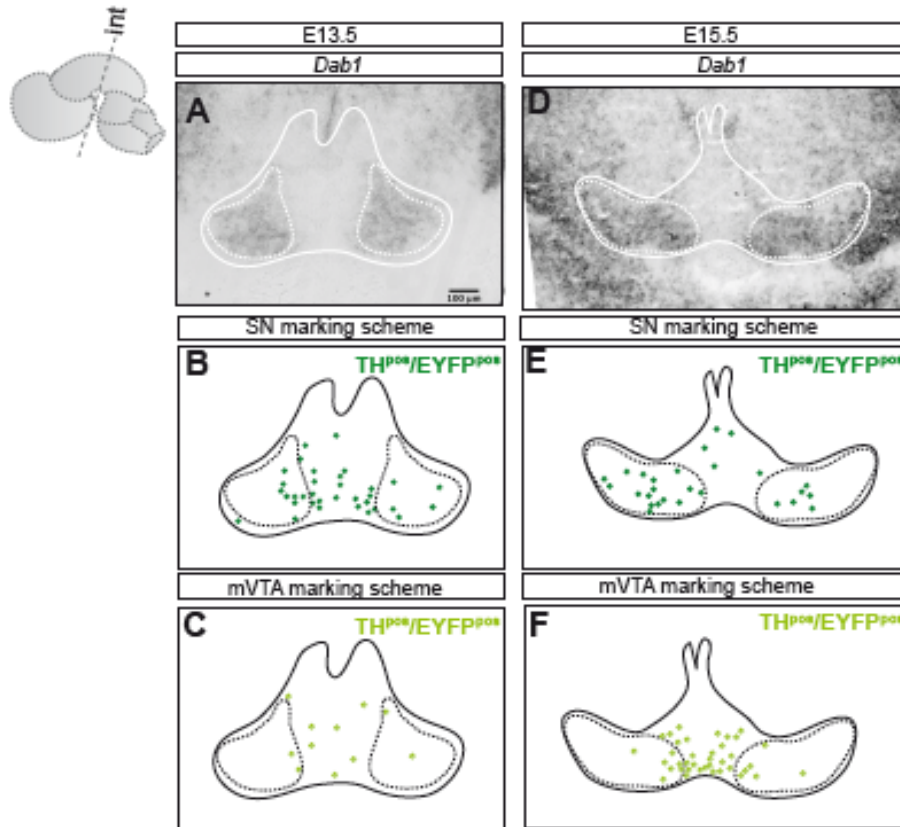
Figure 28. Dab1 is primarily expressed specifically in MbDA neurons destined for SN. (A-D) RNA *in situ* hybridization for *Dab1* at E13.5 and E15.5. (B-F) Overlay of the *Dab1*-expressing area onto representative schematics showing the distribution of MbDA neurons fate-mapped with the SN marking scheme (J, M) or the mVTA marking scheme (K, N) at intermediate section levels.

To investigate whether Reelin signaling is indeed required for the tangential migration of SN neurons, Reelin function was inhibited in slice cultures, using the function-blocking antibody CR50 (Utsunomiya-Tate et al., 2000). Function-blocking antibody, CR-50, inhibits the Reelin molecules assemble. The migratory behavior of cells fluorescently labeled with the SN marking scheme was monitored using time-lapse imaging (CR50-treated slices: N= 6; control slices: N=4) (Figure 29A-C). Inhibition of Reelin signaling led to a significant reduction in the speed of tangentially migrating cells (Figure 29B). This effect was specific, since treatment with Reelin function-blocking antibody did not alter the speed of radially migrating cells labeled with the mVTA marking scheme (CR50-treated slices: N= 6; control slices: N=4) (Figure 29C). Analysis of the trajectories of migrating EYFP^{pos} cells (Figure 29D,E) showed that Reelin inhibition resulted in a significant deviation of migrating neurons (N=46) from the tangential trajectory compared with neurons in control slices (N=33) (Figure 29E).
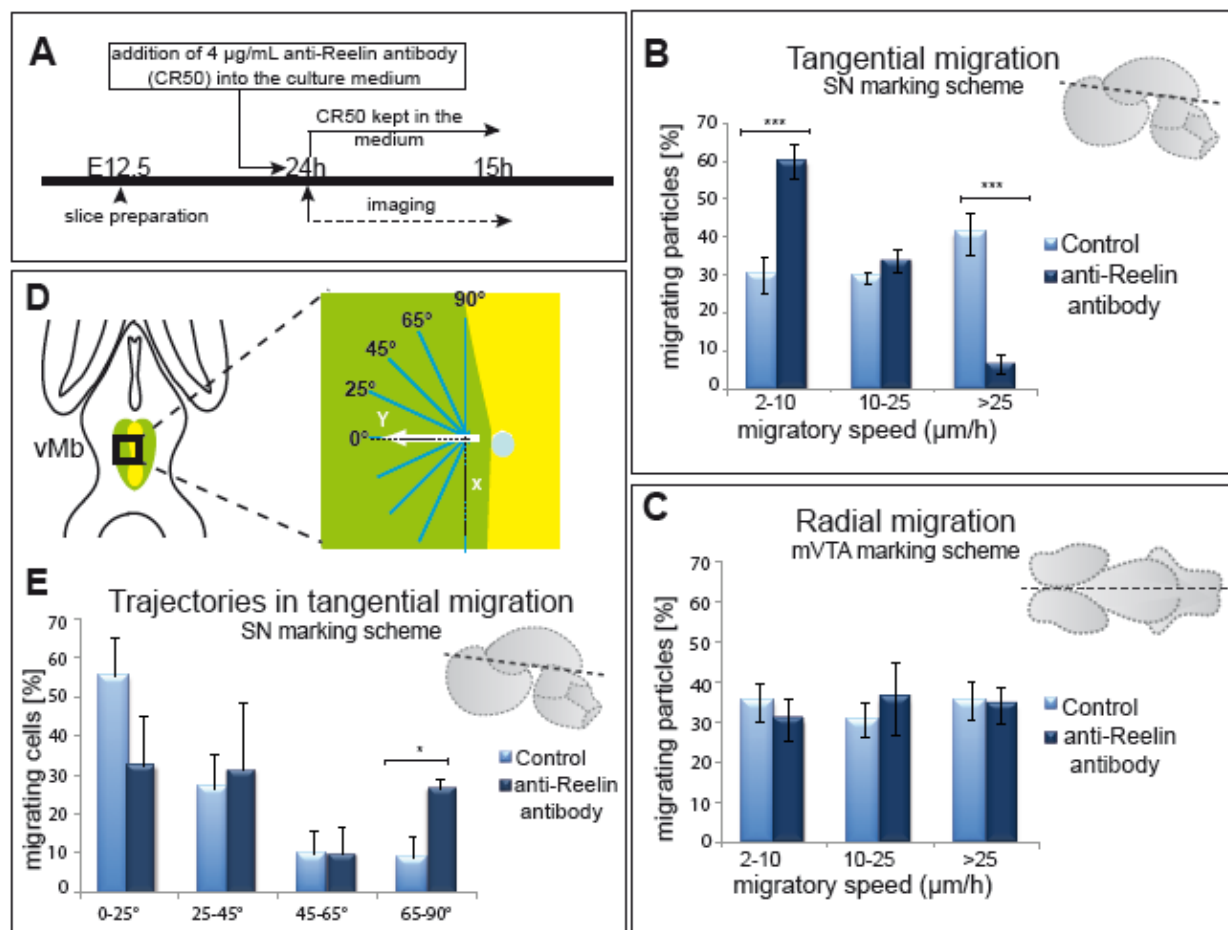
Figure 29. Tangential migration of SN MbDA neurons is mediated by Reelin signaling. (A) Experimental set-up for the inhibition of Reelin function in organotypic slice cultures. (B, C) Quantification of the accumulated migratory speed of particles in a horizontal slice labeled with the SN marking scheme (B) or in a sagittal slice labeled with the mVTA marking scheme (C) with or without the addition of Reelin function-blocking antibody. Inhibition of Reelin signaling interferes with the speed of tangentially, but not radially migrating particles. Data is presented as ±SEM, n ≥ 3 (D, E) Quantification of migrating cells trajectories in slices treated (N=46) or untreated with Reelin function-blocking antibody (N=33). (D) Schematic representation of the migratory route of a MbDA neuron on a best-fit linear trajectory and its possible deviations. In a best-fit linear trajectory the neuron migrates laterally (arrowhead) from its initial position in the ventral midline (white dot) along the y-axis (yellow dashed line). The grades of deviation (blue lines) from the y-axis to x-axis (yellow MbDAshed line) were quantified. (E) Inhibition of Reelin in a horizontal slice interferes with trajectories of tangentially migrating neurons.

Since Reelin plays a role in cell polarization in hippocampal and neocortical pyramidal neurons (Franco et al., 2011; Jossin, 2011; Matsuki et al., 2010; Matsuki et al., 2008), the morphology of TH^{pos} MbDA neurons in wildtype and *Reeler* mutant brains was analyzed at E13.5. Laterally positioned MbDA neurons in the *Reeler* mutants lacked tangentially-oriented processes, but formed processes that were perpendicular to the tangential plane (Figure 30 A, B).
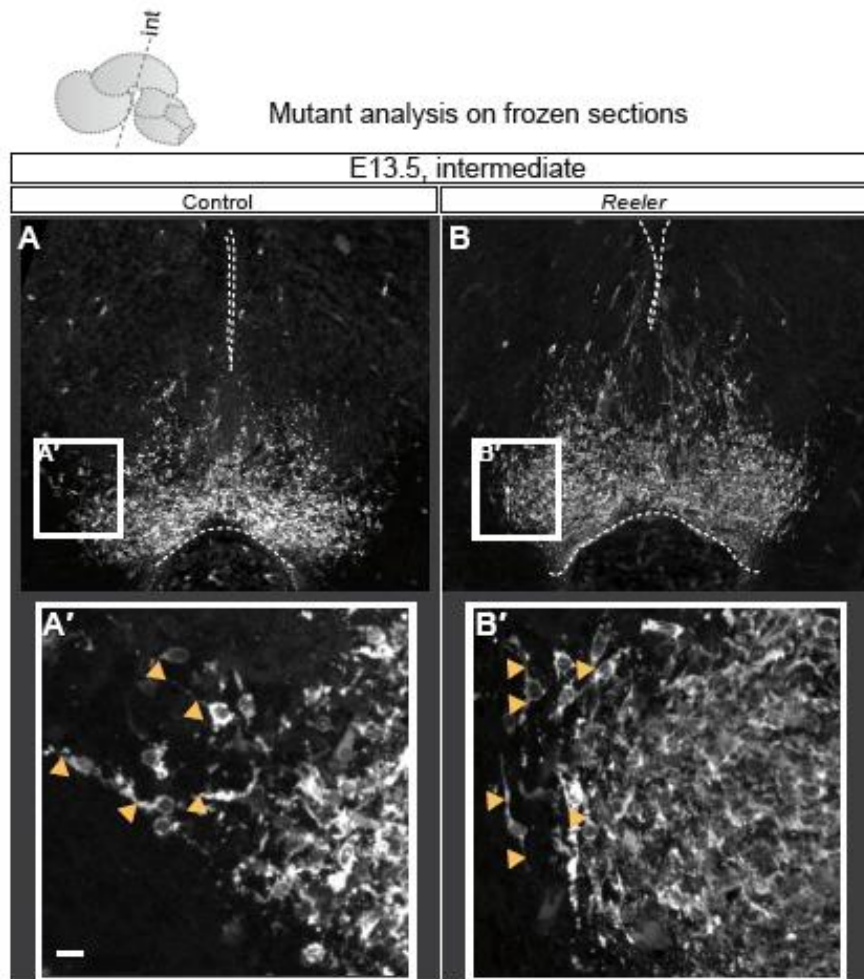
Figure 30. Reelin interferes with polarization of MbDA neurons (A, B) Immunohistochemistry for TH on E14.5 wildtype and *Reeler* mutants. Scale bar 100 µm. (A', B'). Higher magnification of the outline area in A, B. MbDA neuronal processes are indicated with orange arrowheads. Note the change in MbDA neuronal process orientation from predominantly laterally-oriented processes in wildtype to radially oriented-processes in the *Reeler* mutant. Scale bar: 10 µm

To assess whether Reelin signaling in MbDA neurons is indeed mediated by VLDLR/ApoER2 and DAB1, the midbrain phenotypes of *Reeler* mutant, *Dab1* knockout or *Vldlr/Apoer2* double KO mice at postnatal day 25 (P25) were analysed. In both, *Dab1* and *Vldlr/Apoer2* KO mice, the SN did not extend laterally and MbDA neurons appeared to accumulate within the VTA region at intermediate levels, a phenotype comparable to *Reeler* mutant mice (Figure 31 E-H). At anterior levels the SN formed, but appear disorganized (Figure 31 A-D).

These data show that Reelin regulates the speed, trajectories and polarization of tangentially migrating MbDA neurons through the VLDLR/ApoER2 and DAB1 pathway and suggest that Reelin signaling has distinct functions at anterior and intermediate levels.
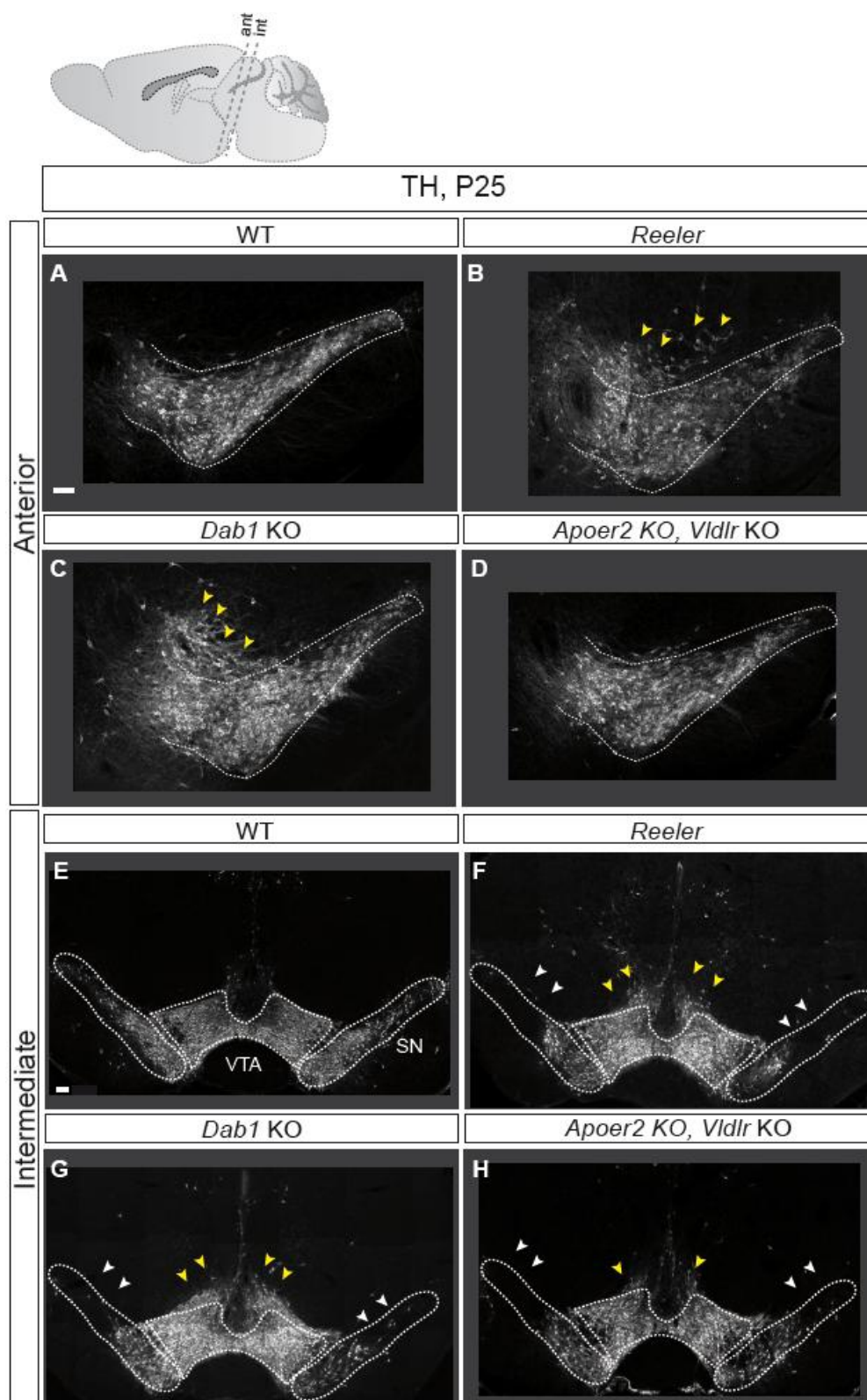
Figure 31. Reelin regulates the organization of the SN at anterior levels and the formation of SN at intermediate levels. Immunohistochemistry for TH on P25 *Reeler* mutants, *Dab1* knockout and *Vldlr/Apoer2* double knockout mutants. The lateral SN does not form in the mutants. (E-H) The anterior SN forms in mutants in which Reelin signaling is inactivated, but the neurons are disorganized. Scale bar 100 μm.

The accumulation of MbDA neurons within the VTA region and the lack of SN formation at

intermediate levels of *Reeler* mutant mice can be eventually correlated with abnormally positioned SN neurons in the VTA area. To test this hypotesis imunostainings for Calbindin (used as marker for VTA) and GIRK2 (used as marker for SN) were performed on adult sections of Reeler, *Dab1* knockout and *Vldlr/Apoer2* double KO mutants. The GIRK2^{pos} neurons are abnormally located, but still located laterally to the Calbindin[pos], VTA neurons (Figure 32 A-L). This suggests that the initial tangential migration occurs in absence of Reelin signaling and that Reelin signaling might only be required for the final stage of tangential migration. This is consistent with Dab1 expression in cells that are already positioned laterally (Figure 28 B, E).
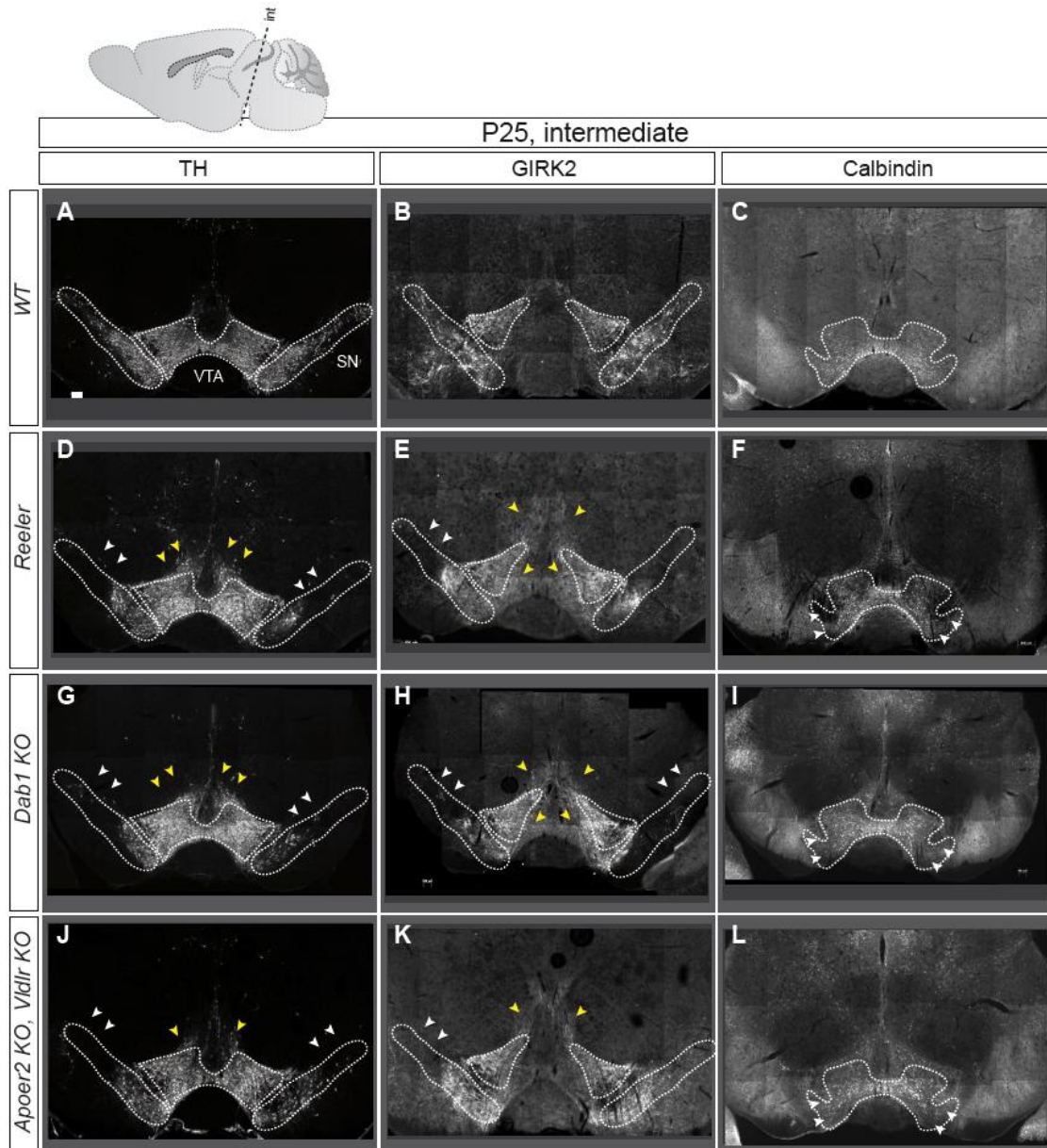

Figure 32. GIRK2^{pos} neurons are abnormally located, but still largely separated from Calbindin^{pos} VTA neurons.(A-L) Immunohistochemistry for TH on P25 *Reeler* mutants, *Dab1* knockout and *Vldlr/Apoer2* double knockout mutants. Yellow arrows highlight the areas with an apparent increase of neurons; white arrows indicate an apparent reduction of neurons. Scale bar: 100 µm

3.7 CXCR4 and its ligand CXCL12 modulate the initial migration of MbDA neurons

The mechanisms that control the initial radial migration of MbDA neurons from the VZ into the mantle layer are unknown. Given that MbDA neurons migrate towards the ventral pial surface during their radially oriented movement, it can be hypothesized that an attractant expressed by the meningeal cell layer surrounding the pial surface could be important for this process. A potential candidate is the chemokine CXCL12. CXCL12 is a potent chemoattractant during neuronal migration in the forebrain and the hindbrain, where it is secreted from meningeal cells (fore- and hindbrain) or Cajal Retzius cells (forebrain). CXCL12 signals through the CXCR4 and CXCR7 receptors (Balabanian et al., 2005; Burns et al., 2006; Sanchez-Alcaniz et al., 2011; Stumm and Hollt, 2007; Wang et al., 2010).
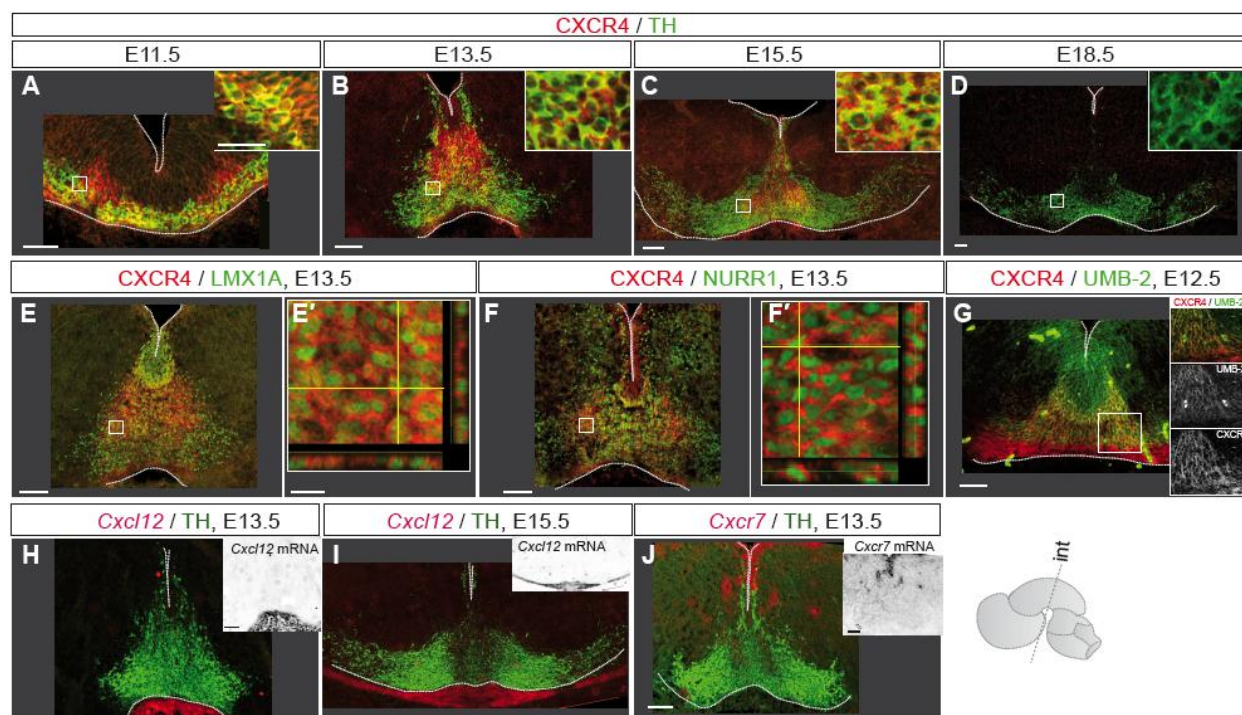

Figure 33. CXCR4 is specifically expressed in the medial MbDA neuronal population. (A-D) Immunohistochemistry for CXCR4 (red) and TH (green). CXCR4 is expressed in MbDA neurons while they migrate from the ventricular zone towards the pial surface (E11.5-E15.5). (A-C). By E18.5, CXCR4 protein is no longer detected in the vMb. Insets: High magnifications of the boxed areas (D) Immunohistochemistry for CXCR4 (red) and LMX1A (green) (E), CXCR4 (red) and Nurr1 (green) on E13.5 sections (F). High magnifications confocal z-stacks show LMX1A (E') and NURR1 (F') positive neurons surrounded by the CXCR4 protein. (G) RNA *in situ* hybridization for *Cxcr7* show no expression in the MbDA neurons. (H, I) RNA in situ hybridization for CXCL12 and immunohistochemistry for TH on E13.5 and E15.5 sections shows that CXCL12 is expressed in the meninges underlying the pial surface where MbDA neurons accumulate. (A-I) Scale bar: 100µm. (E', F') Scale bar: 10µm

To investigate if CXCL12/CXCR4 signaling plays a role in MbDA neuron migration, first the expression of *Cxcl12*, CXCR4 and *Cxcr7* was analyzed in the embryonic ventral midbrain. *Cxcl12* mRNA was expressed in the meningeal cell layer at the time of MbDA neuronal migration (Figure 33 H, I). CXCR4 was expressed in TH^{pos} MbDA neurons starting at E11.5 (Figure 33 A). At E13.5 and E15.5, CXCR4 was expressed in medially located TH^{pos} MbDA neurons, but also in TH^{neg} cells located below the VZ. (Figure 33 B, C). These TH[neg] CXCR4^{pos}

cells were positive for NURR1 (nuclear receptor related 1 protein), which is expressed in differentiating MbDA neurons before the onset of TH expression, and for LMX1A, a marker for MbDA progenitors and differentiated MbDA neurons (Figure 33 E, F). CXCR4 expression levels are slightly downregulated in cells located close to the pial surface (Figure 33 G). By E18.5, CXCR4 could no longer be detected in the ventral midbrain (Figure 33 D). In contrast, *Cxcr7* was only expressed in the ventricular zone (Figure 33 J).

The restricted spatial and temporal expression of CXCR4 in medially located MbDA neurons suggested that CXCL12/CXCR4 signaling might play a specific role in regulating the initial radial migration of MbDA neurons. To investigate this, the distribution of MbDA neurons was analyzed in mice in which *Cxcr4* (*Cxcr4* KO) or *Cxcl12* (*Cxcl12* KO) were inactivated (Ma et al., 1998; Nagasawa et al., 1996). At intermediate and posterior section levels, TH^{pos} MbDA neurons in mutant embryos accumulated in a position outside of the midline than MbDA neurons in wildtype embryos (Figure 34 A-E, 35 A-E). To quantify the change in cell distribution, ventral midbrain sections of *Cxcl12* KO and wildtype embryos were divided into several bins along the dorsoventral and mediolateral axis. The number of MbDA neurons was counted in each bin and normalized for the total number of counted MbDA neurons. This analysis confirmed the ventral to dorsal and medial to more lateral shift in the distribution of MbDA neurons in *Cxcl12* and *Cxcr4* KO embryos (Figure 34 E, F). A similar trend was observed in E16.5 *Cxcr4* KO embryos, while no obvious defect in cell distribution was observed in *Cxcl12* KO embryos at this stage (Figure 35 E, F). Interestingly, the abnormal accumulation of MbDA neurons was more severe at E14.5 than at E16.5, suggesting a partial rescue of the phenotype at later stages. These data demonstrate that CXCR4/CXCL12 modulates the initial MbDA neuronal migration.
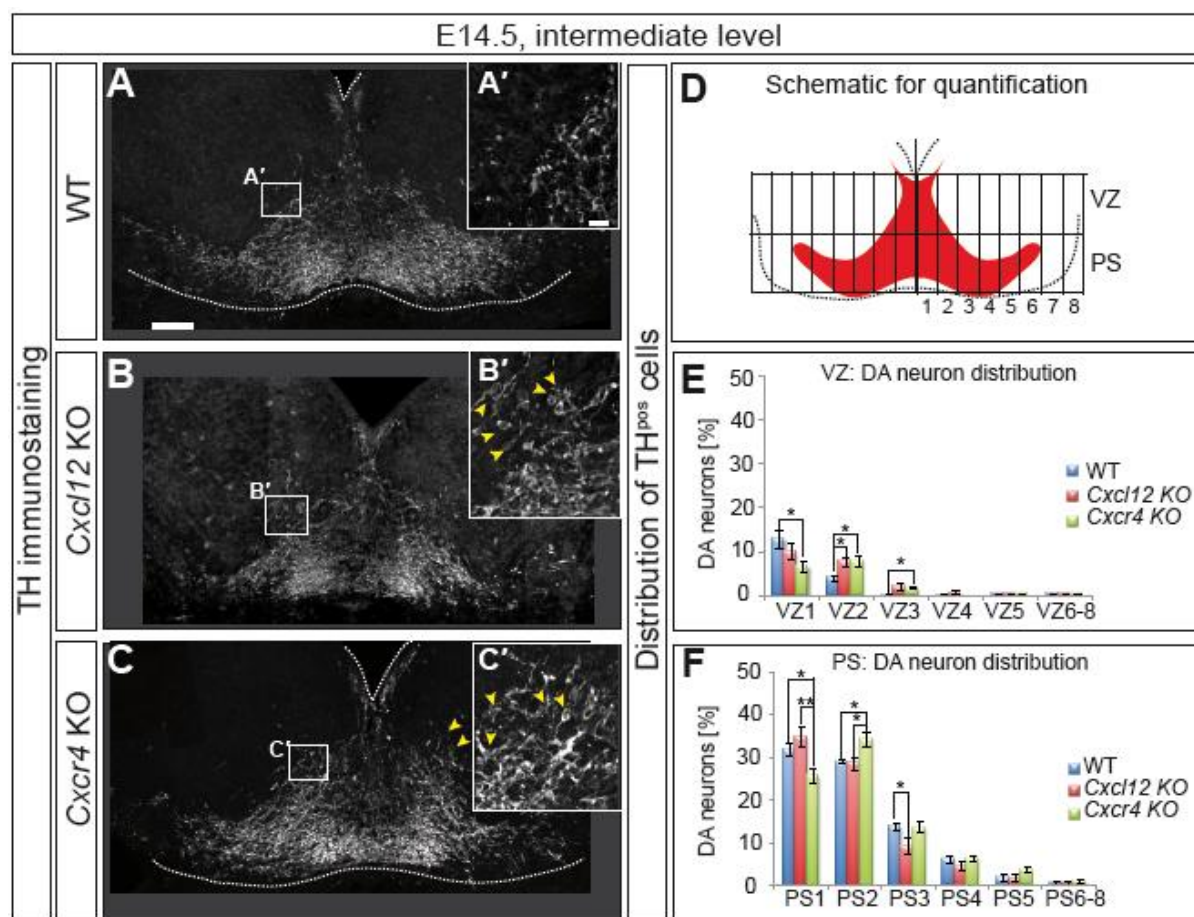
Figure 34. CXCR4 and its ligand CXCL12 modulate the migration of MbDA neurons. (A-F) Immunohistochemistry for TH shows the abnormal distribution of MbDA neurons in *CXCL12* and *CXCR4* knockout brains at E14.5 at intermediate levels (A-C). Yellow arrowheads indicate ectopically localized MbDA neurons. (A'-C') High magnifications of the boxed areas. (D-F) The ventral midbrain was divided into 2 bins along the dorsoventral axis and into 8 bins along the mediolateral axis in wildtype, *Cxcl12 and Cxcr4* KO brains at E14.5. TH^pos cells were counted in each bin and presented as a % of TH^pos cells from the total number of TH^pos cells counted. (E, F) MbDA neurons show an altered dorsoventral and mediolateral distribution. Data are presented as ±SEM, N=4. Statistical significance determined by ANOVA and post-hoc LSD analysis, *$p<0.05$, **$p<0.01$. Scale bar: 20 µm (A'-C'), 100 µm (A-C). PS: pial surface.
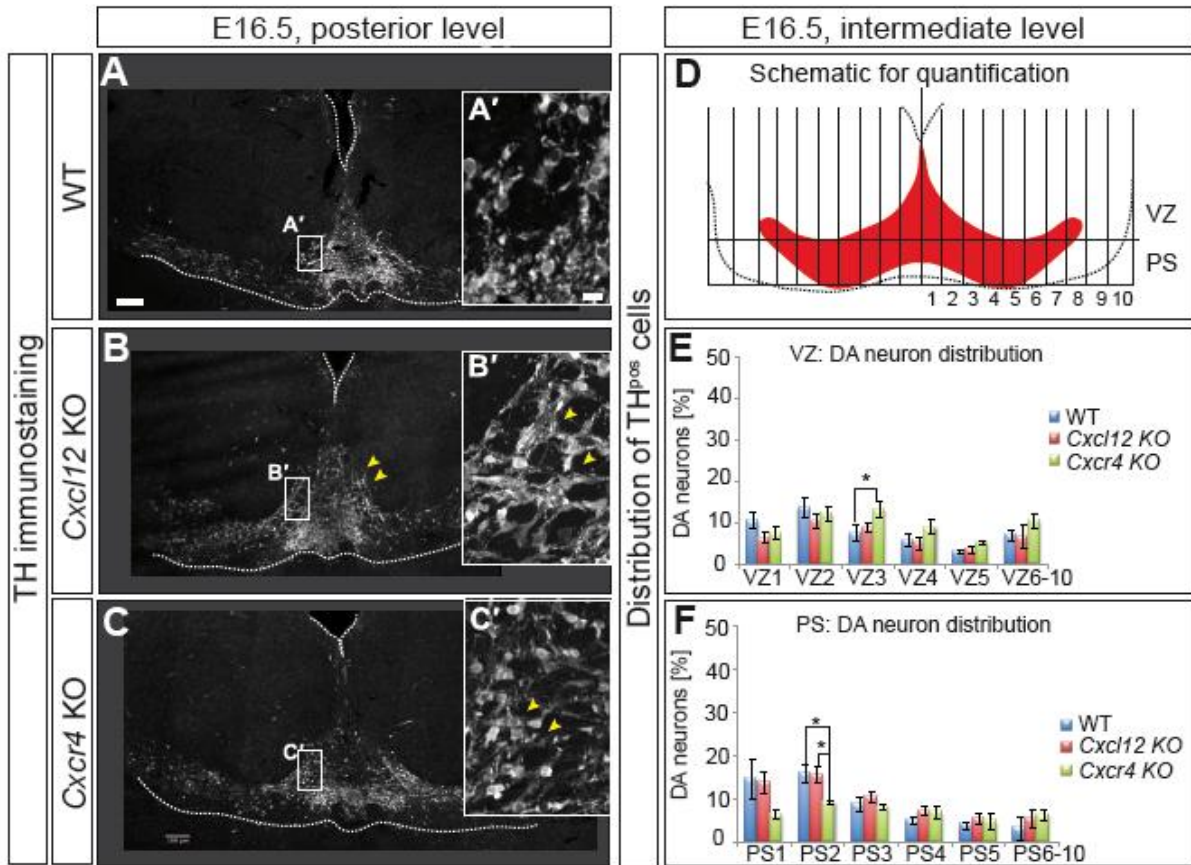
Figure 35. CXCR4 and its ligand CXCL12 have a transient effect on migration of MbDA neurons. (A-F) Immunohistochemistry for TH shows the abnormal distribution of MbDA neurons in *CXCL12* and *CXCR4* knockout brains at E16.5 at posterior levels (A-C). Yellow arrowheads indicate ectopically localized MbDA neurons. (A'-C') High magnifications of the boxed areas. (D-F) The ventral midbrain was divided into 2 bins along the dorsoventral axis and into 10 bins along the mediolateral axis in wildtype, *Cxcl12 and Cxcr4* KO brains at E16.5. TH^{pos} cells were counted in each bin and presented as a % of TH^{pos} cells from the total number of TH^{pos} cells counted. (E, F) At E16.5 MbDA neurons show a milder alteration in dorsoventral distribution than at E14.5 in *Cxcl12 and Cxcr4* KO brain. Data are presented as ±SEM, N=4. Statistical significance determined by ANOVA and post-hoc LSD analysis, *p<0.05, **p< 0.01. Scale bar: 20 µm (A'-C'), 100 µm (A-C).

To examine whether perturbation of CXCR4/CXCL12 signaling influences MbDA migration by regulating the speed or trajectories of migrating MbDA neurons, CXCR4 signaling was inhibited in slice cultures with the CXCR4 antagonist AMD3100. The migration of cells labeled with the SN or mVTA marking scheme was monitored (treated slices: N= 4; untreated slices: N=5) (Figure 36 A). However, neither the speed nor the trajectories of migrating cells was changed in cultures treated with the CXCR4 antagonist (Figure 36 B, C).
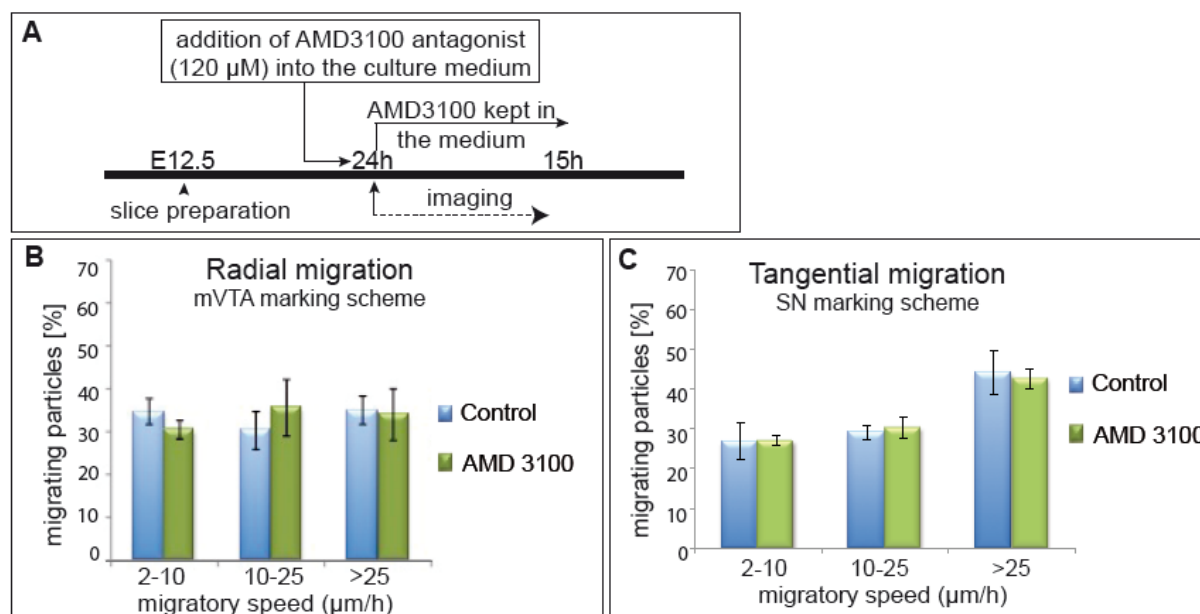
Figure 36. (A) Experimental set-up for the inhibition of CXCR4 function in organotypic slice cultures. AMD3100 inhibitor was added to organotypic slice cultures. (B, C) Quantification of the accumulated migratory speed of particles in a sagittal slice labeled with the mVTA marking scheme (A) or a horizontal slice labeled with the SN marking scheme (B) with or without the addition of AMD3100. Inhibition of CXCR4 interferes with the speed of tangentially, but not radially migrating particles. Data is presented as ±SEM, n ≥ 3. Scale bar: 100 μm.

4. DISCUSSION

Understanding how migrating neurons navigate within the increasing complexity of the developing brain is a fundamental question in developmental neuroscience. Neurons navigate from ventricular zones along either radial or tangential paths and often settle in regions distinct from their origin. Neuronal migration mechanisms have been studied in great detail in dorsal brain areas, such as the cortex or the cerebellum, where neurons arrange themselves into distinct cell layers. However, much less is known about neuronal migratory behavior in ventral brain areas, such as the midbrain, where neurons assemble into cell clusters.

This study provides a detailed molecular and functional characterization of the migratory paths that are taken by MbDA neurons in the ventral midbrain. The results presented in this thesis demonstrate that MbDA neurons destined for the SN have to undergo an active tangential migration process to reach their final position in the ventral midbrain, whereas MbDA neurons destined for the VTA primarily undergo radial migration. The tangential migratory process is mediated by Reelin signaling, which controls the rate of migration, migration trajectories and leading process polarization of MbDA neurons destined for the SN. The initial radial migration of MbDA neurons from their progenitor zone toward the mantle layer is modulated by CXCR4/CXCL12 signaling.

4.1 Migratory paths of MbDA neurons

TH positive MbDA neurons are generated in the VZ of the ventral midbrain (Mb) starting at E10.5 (Bayer et al., 1995; Kawano et al., 1995). Subsequently, MbDA neurons migrate towards the mantle layer to form the SN and the VTA. Despite their distinct location in the ventral midbrain, the SN and VTA form a continuous structure, making it difficult to define the exact boundaries between the two cell clusters (Bjorklund and Dunnett, 2007). Nevertheless, MbDA neurons that populate the lateral ventral midbrain and form the SN have to take a different migratory route than MbDA neurons that cluster in the medial ventral midbrain and form the VTA.

The results of the present study propose the following model for MbDA neuronal migration. Neurons destined to form the SN undergo a three-step migration: 1) they migrate radially from the VZ towards the pial surface, 2) they switch to tangential migration in order to move away from the midline and segregate from VTA neurons, 3) they undergo a long distance tangential migration to reach their final position in the ventral-lateral Mb. In contrast, neurons that form the VTA primarily undergo a one step migration, i.e. radial migration from the VZ towards the pial surface. This model is supported by results obtained from analysis of the distribution of MbDA

neurons destined for the SN and mVTA at different stages during development, 3D morphological analysis of the entire MbDA area and time-lapse imaging in organotypic slice cultures. Two pieces of evidence demonstrate that the lateral movement of future SN neurons is an active migration process and not just a lateral displacement caused by newly generated medial cells or by the overall growth of the tissue: 1) MbDA neurons destined for the SN and VTA are initially located in the medial ventral Mb (E12.5-E13.5), but only neurons destined for the SN are found at significantly more lateral positions at later developmental stages (>E14.5). 2) Time-lapse imaging shows that neurons destined for the SN migrate tangentially away from the midline (E12.5-E14.5). These observations suggest that there is an initial lateral migration of SN neurons from the medial-ventral towards the lateral ventral Mb (E12.5-E14.5) resulting in the segregation of SN destined neurons from the VTA destined neurons by E14.5. Analysis of the distribution of SN destined MbDA neurons after E14.5 demonstrate that these neurons continue to move laterally at subsequent stages.

Previous attempts to characterize the migratory routes of MbDA neurons using birthdating of ventral midbrain progenitors, sometimes in combination with TH immunostaining, have led to contradictory conclusions (Hanaway et al., 1971; Marchand and Poirier, 1983; Kawano et al., 1995, Shults et al., 1990). Thus, several potential migratory paths have been proposed for neurons that form the SN. The first study (Hanaway et al., 1971) analyzed the location and birthdates of radioactively labeled midbrain neurons at different stages between E12.5 and E16.5 and proposed a different model than the one indicated in this thesis. The authors suggested that SN destined neurons migrate radially from the VZ towards the lateral ventral Mb. Further, the authors indicate that VTA destined neurons migrate radially towards the medial ventral Mb and that subsequently, a subset of these cells migrate tangentially towards more lateral positions. Other birthdating studies, using BrdU labeling combined with TH immunostaining, suggested a model similar to the one proposed in this thesis (Kawano et al., 1995; Shults et al. 1990). These studies suggest that the cells contributing to the SN and VTA initially follow a radial route (E11.5-E13.5) along radial glia processes that extend from the ventricular zone to the mantle layer. Then, the cells move laterally, presumably on a tangential migratory route (>E12.5), from the ventral midline towards the lateral Mb along tangentially arranged nerve fibers. However, MbDA neurons destined for the SN and the VTA could only be distinguished from each other upon reaching their final positions rather than during their actual migratory phase. It must also be taken into consideration, that in all these studies, the migratory behavior of the neurons could not be monitored directly and was only inferred from the analysis of the distribution of labeled cells in sections.

The current study overcomes this problem by using novel systems of labeling and observing SN and VTA destined neurons. The MbDA precursor cells that give rise to SN and VTA clusters have been specifically labeled using the genetic inducible fate mapping method. This genetic

labeling method makes use of the differential expression of SHH in MbDA progenitors at different developmental stages (E8.5 versus E11.5). Thus, only the MbDA precursor cells that give rise predominantly to the SN or the mVTA could be labeled. Since the labeling is heritable, the descendents of MbDA precursor cells that give rise to one or the other MbDA neuron subpopulation could be tracked at any time point during development. Moreover, this fluorescent labeling also allowed monitoring of the behavior of the cells in organotypic slice cultures. Thus by specifically monitoring the migratory behavior of MbDA neurons that form SN or mVTA, this analysis could dissect for the first time the paths of MbDA contributing to either SN or mVTA.

As discussed previously, MbDA neurons most likely migrate radially along radial fibers, however the molecular profile of these fibers is unclear. Kawano and colleagues (1995) suggested that MbDA neurons migrate along radial fibers expressing tenascin, an extracellular matrix protein between E10.5 and E13.5. However, in the present study it was found that tenascin is not expressed in the radial fibers in the medial ventral Mb, where MbDA migrate radially, but only in the lateral Mb at E13.5. Radial fibers in the medial ventral Mb were found to express the intermediate filament protein and radial fiber marker Nestin between E11.5 and E14.5 (Allen Developing Mouse Brain Atlas, 2012 and this study). Additionally, another intermediate filament, vimentin, is expressd at E12.5 in the medial ventral midbrain as shown by (Shults et al., 1990).

The tangential migration of MbDA neurons is presumably supported by tangential axonal fibers that function as a scaffold (Kawano et al., 1995). These fibers originate from cell bodies in the lateral mesencephalon, but they could not be assigned to any of the known mesencephalic fiber tracts. These tangentially oriented fibers transiently express NCAM-H (highly polysialylated neuronal cell adeshion molecule) and L1 (immunoglobulin superfamily molecules) between E11.5 and E15.5 coinciding with the time period of MbDA migration (Ohyama et al., 1998).

At anterior levels, only the SN, but not the VTA is present in the adult brain. Hence the three-step migration paradigm for SN neurons proposed in the current study is most obvious at intermediate anteroposterior levels of the developing MbDA neuronal field, where both SN and VTA are formed. MbDA neurons destined for the anterior SN assume relatively lateral positions immediately after their radial migration. However, the present analysis of the mediolateral distribution of anterior SN neurons suggests that tangential migration also contributes to their final lateral position. At posterior levels, only a few labeled MbDA neurons are observed in lateral positions with the SN marking scheme. The lack of a specific labeling for MbDA neurons that give rise to RRF MbDA neurons made it impossible to assess the migratory behavior of this MbDA neuronal subpopulation.

The potential difference in the migratory behavior of anterior and posterior SN neurons correlates with a proposed difference in their origin: anterior SN neurons are thought to be of posterior diencephalic origin, while more posterior MbDA neurons are mesencephalic. These di-

and mesencephalic populations are different in their molecular profile during their progenitor and early differentiation phase. It remains unclear whether these differences persist at later stages of development, but if they do, they could possibly explain the distinct migratory behavior of the two populations (Lahti et al., 2012; Smits et al., 2006)

4.2 Reelin-mediated signaling pathway plays a role in SN formation by regulating the tangential migration of MbDA neurons destined to the SN

Reelin, a large extracellular glycoprotein, regulates migration in several other areas of the brain and signals via the transmembrane receptors ApoER2 and VLDLR. Upon binding of Reelin to its receptors, the cytoplasmic adaptor protein DAB1 is phosphorylated and mediates downstream Reelin signaling (Ballif et al., 2004; D'Arcangelo et al., 1999).

It has been previously shown that the SN does not form in the *Reeler* mutants, which have a spontaneous mutation in the *Reelin* gene that results in Reelin loss-of-function (Kang et al., 2010, Nishikawa et al., 2003). Though these studies analyzed the intermediate levels of the developing MbDA neuronal field in *Reeler* mutants, where both SN and VTA are formed, they did not assess the underlying cellular mechanisms by which Reelin regulates SN formation. In the current study, the *Reeler* mice and the mutant mice in which other components of the Reelin signaling pathway were inactivated, were analyzed at different anteroposterior levels. Moreover, the present results show that Reelin and its downstream pathway components are expressed in ventral midbrain during the time period that corresponds to MbDA migration and seem to regulate multiple aspects of the tangential migration of MbDA neurons destined to SN.

4.2.1 Expression of Reelin and its downstream signaling components in the embryonic ventral midbrain

It was unclear from which source Reelin is secreted during MbDA migration. One study (Nishikawa et al., 2003) that used the anti-Reelin antibody CR-50 showed that Reelin protein is present in the MbDA area of the ventral Mb, as well as in the striatum at E15.5. The authors proposed that Reelin is supplied to the ventral Mb, by incoming projections from the striatal patch neurons, via axonal transport. A number of studies have shown that Reelin is present in axons, suggesting that it may be transported along axons over long distances (Derer et al., 2001; Martinez-Cerdeno et al., 2002; Pappas et al., 2001; Roberts et al., 2005). As demonstrated in the current study, by E15.5, many MbDA neurons have already migrated and the MbDA that give rise to SN are already segregated laterally. This means that Reelin should be present in ventral Mb before E15.5 if it plays indeed a role in regulating MbDA neuronal migration.

This study shows that the *Reelin* mRNA is present in Mb already at E13.5, a time point when MbDA neuronal migration occurs. Furthermore, the *Reelin* mRNA colocalizes with BRN3A, a marker for red nucleus neurons. These findings indicate that the red nucleus might be the

source of Reelin in the ventral Mb at the time of MbDA migration. It is interesting that red nucleus neurons, which are derived from a ventral progenitor domain that is laterally adjacent to the MbDA neuron progenitor domain, appear to be an early source of Reelin. MbDA and red nucleus progenitors share several molecular markers such as SHH and the transcription factor FOXA2 (Blaess et al., 2011; Prakash et al., 2009; Prakash and Wurst, 2006). Red nucleus neurons are born between E10.25 and E10.75 and subsequently migrate radially to their final position in the ventral midbrain (Prakash et al., 2009). The first SN neurons are born around E10.5, suggesting that SN and red nucleus neurons could undergo radial migration during the same time period. It is intriguing that there appears to be a coordinated migration between two ventral neuronal populations with similar birth dates and adjacent progenitor domains. It remains to be investigated whether mutants that lack the red nucleus also have defects in the formation of the SN. Mutants in which the number of red nucleus neurons is merely reduced do not show an obvious phenotype in SN formation (Prakash et al., 2009). In addition, Vasudevan and colleagues show that MbDA neurons location plays a role in modulating the migration of GABAergic neurons (Vasudevan et al., 2012). Altogether these results suggest a migratory regulation network of different neuronal subpopulations in the ventral midbrain.

Apoer2 and *Vldlr mRNA* are present throughout the ventral midbrain starting at E13.5. However, *Dab1*, the key regulator of Reelin signaling is specifically expressed in the most laterally located MbDA neurons. These lateral MbDA neurons are positioned ventral to cells in the red nucleus that express *Reelin* mRNA and they overlap with cells marked with the SN marking scheme. In light of this data, it seems that only the MbDA neuronal population destined for the SN is able to respond to Reelin signaling.

4.2.2 Defects in MbDA positioning when the Reelin signaling pathway is inactivated

Kang and colleagues (2010) showed an abnormal positioning of MbDA neurons in *Reeler* mice at the intermediate level, where SN and VTA are located. They demonstrated that the number of MbDA neurons in P0 *Reeler* mutants is significantly reduced in the SN area, whereas the total number of MbDA neurons is not reduced. The reduction in MbDA neuron number in SN seems to correlate with an accumulation of MbDA located more medially, at the lateral border of the VTA.

The data presented here complete the analysis of MbDA in the *Reeler* mutant at all anteroposterior levels and shows that the SN forms at anterior levels, but appears disorganized. At posterior levels, MbDA neurons in the RRF also appear to be disorganized in the mutant mice. These findings suggest that the lack of SN formation and the ectopic cluster present at the lateral border of VTA at the intermediate level is not due to a change in fate of the SN neurons towards VTA neurons. This hypothesis is further sustained by data showing that the cluster of cells at the lateral border of VTA expresses GIRK2, a marker of SN neurons (this

study). GIRK2 is normally expressed laterally in the SN MbDA population and its presence at the lateral border of VTA indicates that these cells fail to migrate laterally and form the SN. Interestingly, despite the migratory defect in *Reeler* mutant mice, the projections towards their striatal targets are normal (Nishikawa et al., 2003).

The effect of Reelin on SN neurons is mediated through the canonical VLDLR/ApoER2 and DAB1 signaling pathway. Data presented here show that *Dab1* KO mice phenocopy the phenotype observed in the *Reeler* mutants. This is consistent with previous studies (Kang et al, 2010), which showed that *Yotari* mice, that have a spontaneous loss-of-function mutation in *Dab1*, have the same phenotype as *Reeler* mice. The thesis data also show that *Vldlr KO* and *Apoer2 KO* mice have no obvious defect in MbDA positioning. However, the *Vldlr/Apoer2* double KO mice show a phenotype that is slightly milder than that of the *Reeler* and *Dab1* KO mice. In contrast, the recent study of Sharaf and colleagues (2013), which quantified MbDA neurons in *Vldlr* and *Apoer2* single KO mice shows that MbDA neurons are mispositioned in these mice, even though the phenotype is milder than that of *Reeler* and *Dab1* KO mice. Moreover, the authors show that the phenotype is more pronounced in *Vldlr* KO mice than in *ApoER2* KO mice and they also suggest that *Vldlr/Apoer2* double KO mice have the same phenotype as the *Reeler* muntant and *Dab1* KO mice. However, a quantified comparison of the *Vldlr* KO and *Apoer2* KO mice was not provided. To clarify these discrepancies between the two studies the MbDA phenotype of the *Vldlr/Apoer2* double KO should be further quantified. The milder *Vldlr/Apoer2* phenotype observed in this study suggests that there might be other coreceptors for Reelin involved in MbDA migration. In the cortex, inactivation of EphBs (Ephrin receptor tyrosine kinases) results in defects in migration that recapitulate the *Reeler* phenotype (Bouche et al., 2013; Senturk et al., 2011). However, in the present study EphBs were not found to be expressed in the ventral midbrain. In addition to EphB, Protocadherin and integrins have also been proposed to function as co-receptors for Reelin in the cortex (Anton et al., 1999; Senturk et al., 2011; Senzaki et al., 1999). It remains unexplored whether they might play a role in MbDA neuronal migration.

4.2.3 Mechanisms of Reelin function in MbDA neuronal migration

The mechanism of Reelin function has been studied in great detail in the radial migration of cortical projection neurons and several models have been proposed to explain how Reelin controls cortical migration. Reelin has been shown to act on fiber scaffold differentiation (Forster et al., 2002) or on polarization of migrating neurons (Jossin and Cooper, 2011). Moreover, it has been suggested that Reelin functions as a chemoattractant, a chemorepellent, a stop signal, a signal for neurons to detach from radial glia, or a signal stabilizing the leading process (Dulabon et al., 2000; Franco et al., 2011; Gilmore and Herrup, 2000; Jossin, 2011; Ogawa et al., 1995; Sanada et al., 2004; Schiffmann et al., 1997; Sheppard and Pearlman, 1997). The Reelin signal

is believed to function either as a permissive or as an instructive factor (Jossin, 2004; Magdaleno and Curran, 2001)

This thesis is the first study to investigate the detailed mechanism of Reelin function in the Mb. Data presented here shows that Reelin regulates the tangential migration of MbDA neurons destined for the SN by modulating their trajectory and speed. Furthermore, Reelin plays a role in the polarization of MbDA neurons. However, it still remains unclear how Reelin regulates the polarization of MbDA neurons and whether Reelin is an instructive or a permissive factor for MbDA migration. The mechanisms of Reelin function in MbDA neuronal migration are discussed in detail in the following sections.

4.2.3.1 Reelin signaling regulates tangential migration of SN destined MbDA neurons

The time-lapse imaging in organotypic slice cultures presented here demonstrates that inhibition of Reelin signaling interferes specifically with the speed and trajectories of tangentially migrating neurons destined for the SN. Similar results, but in radially migrating cortical neurons in the ventricular and subventricular zone, where the first transition of bipolar to multipolar migration occurs, have been shown by Britto and colleagues (Britto et al., 2011; Britto et al., 2013). The authors show that cortical neurons displayed defective radial trajectories and migratory speeds in *Reeler* mutants. However, in contrast to the studies performed on cortical and cerebellar neurons (Sanada et al., 2004; Kuo et al. 2005; Myiata et al., 2010), radial migration of MbDA neurons is not affected by the inhibition of Reelin signaling.

The specific effect of Reelin on tangentially migrating neurons is consistent with data showing that *Dab1* is only expressed in laterally positioned MbDA neurons at E13.5. Since GIRK2 expressing SN neurons are clustered at the lateral border of the VTA and not intermingled with Calbindin expressing VTA neurons, Reelin signaling does not seem to play a role in the tangential migration that results in segregation of the SN and VTA neurons. These observations indicate that Reelin is involved only in the last step of tangential migration, which results in the formation of the laterally positioned SN cluster. The mechanisms that regulate the switch from radial to tangential migration and the segregation of SN and VTA neurons in the medial zone remain to be identified.

4.2.3.2 Reelin signaling plays a role in MbDA neuronal polarization

Analysis of *Reeler* mice at E13.5 shows a misorientation of the cellular processes (radial orientation instead of tangential) of the laterally positioned MbDA neurons. Moreover, in slice cultures, the tangential migrating MbDA neurons destined for the SN change their trajectory when Reelin is inhibited. The change in trajectory could be caused by the misorientation of the leading process, which gives the migrating cell its directionality. These data suggest that Reelin plays a role in the polarization of the SN destined MbDA neurons that migrate tangentially. However, a role of Reelin in establishing the polarization of MbDA neurons is unlikely, since

already at E11.5 and E12.5 the MbDA neurons destined for the SN have tangentially oriented processes before they start to express *Dab1*. This indicates that at the time when MbDA neurons start to respond to Reelin, they already present a bipolar, tangential morphology. Moreover, *Reeler* mice do not show a misorientation of the cellular processes at E12.5. These findings suggest that Reelin might play a role in the maintenance of tangential orientation of cellular processes of SN destined MbDA neurons.

One mechanism by which Reelin can play a role in the maintenance of neuronal polarity is by stabilizing the cytoskeleton (Witte and Bradke, 2008). Reelin is involved in regulation of the cytoskeleton as it interacts with intracellular signals that modulate Actin dynamics, such as Rho GTPases and Cofilin (Leemhuis and Boch, 2011; Krüger et al., 2010, Chai et al., 2009). In bipolar, radially migrating cortical neurons, Reelin stabilizes the actin cytoskeleton in the leading processes by inducing phosphorilation of cofilin. Cofilin depolymerizes F-actin, thereby supplying actin monomers for the formation of new actin filaments. The phosphorylation of cofilin renders cofilin unable to depolymerize F-actin in the leading processes of migrating neurons. This reduces actin dynamics and stabilizes the cytoskeleton (Chai et al., 2009b; Leemhuis et al., 2010). Furthermore, in multipolar, radially migrating cortical neurons, Reelin is involved in the formation of the proper polarization via Rap1 (Ras related protein, GTPase) and NCad (N-cadherin) (Jossin and Cooper, 2011; Franco et al., 2011). In *Reeler* mutants, NCad is reduced and the multipolar neurons migrate in a disorganized manner, which leads to a defective cortical lamination. Reelin triggers polarization when neurons start to migrate by activating Rap1 and stabilizing NCad. This model, called 'polarity model' is however only valid for multipolar, immature neurons, and it is unclear whether it could be applied for MbDA migration.

4.2.3.3 Reelin is not likely to regulate the formation of guidance fibers for MbDA neuronal migration

It has been previously proposed that MbDA neurons giving rise to SN and VTA migrate radially along glia fibers and subsequently, tangentially arranged fibers serve as a support for the tangential migration of SN destined neurons. Studies that unraveled Reelin function in the neuronal migration in other brain areas have proposed that Reelin can also play a role in establishing of radial fibers. For example, Förster and colleagues (2002) showed that Reelin signaling through Dab1 is important for the formation of the radial glia scaffold in the dentate gyrus of the hippocampus. In *Reeler* mutants and mice lacking *Dab1,* radial glia fibers expressing Nestin do not form and consequently the granule cells fail to migrate and accumulate in the hilar region.

In the ventral Mb, radial glia fibers extend from the VZ, where the cell bodies are, towards the pial surface. However, *Dab1* mRNA is neither expressed in the VZ nor in the medial ventral midbrain, and function blocking experiments in slice cultures show no effect on MbDA radial

93

migration. Furthermore, it has been previously shown that the ventral midbrain radial fibers expressing BLBP (brain lipid binding protein), RC2 (radial glia) and vimentin (intermediate filaments) are not affected at E14.5 - E15.5 in *Reeler* mutants (Kang et al., 2010; Nishikawa et al, 2003). These observations suggest that Reelin is not involved in radial glia formation and hence, does not seem to affect MbDA radial migration indirectly.

Another possibility is that Reelin plays a role in the formation of tangential fibers. However, tangential fibers expressing the polysialylated neural cell adhesion molecule (N-CAM), at intermediate levels of the MbDA neuron field between E11.5 and E15.5 (Ohyama et al., 1998) were not affected in *Reeler* or *Yotari* mutant mice (Kang et al., 2010; Nishikawa et al., 2003). This evidence suggests that Reelin does not play a role in the tangential fiber formation.

4.2.3.4 Does Reelin act as an instructive or a permissive signal for MbDA neuronal migration?

In the cortex, it has been previously shown that Reelin can be cleaved into smaller fragments that could potentially diffuse and build a chemoattractive gradient (Jossin et al., 2004; Lambert de Rouvroit et al., 1999). Moreover, Reelin can function as attractant in the cortex. Sanada and colleagues (2004) showed that if *Dab1* is inactivated in a mosaic manner in migrating cortical neurons, wild-type cells migrate towards the Reelin-expressing layer, while *Dab1* null neurons stay beneath the wild-type cells. This data indicate that wild-type neurons are attracted by the Reelin source and that this attraction is mediated through Dab1. Whether Reelin is similarly processed and has an attractive effect on MbDA neurons in the ventral Mb remains to be examined.

Since Reelin regulates the tangentially migration of MbDA neurons, it could play a role in attracting the SN neurons laterally. To attract MbDA neurons, Reelin should be expressed in a region lateral to these neurons, in the direction of their migration. However, the thesis results show that the *Reelin* mRNA expression domain, which overlaps with the red nucleus, is located dorsally rather than laterally to tangentially migrating, *Dab1*-expressing MbDA neurons at E13.5. In addition and as discussed previously, Reelin protein could also be detected throughout the SN, supposedly secreted by incoming projections from striatal neurons at E15.5 (Nishikawa et al., 2003). Whether Reelin protein is expressed in a similar position at an earlier stage has not been yet investigated due to the lack of an efficient antibody staining. The expression data would suggest that Reelin is unlikely to be an attractant for MbDA neurons due to its location.

4.3 CXCL12/CXCR4 signaling modulates the initial migration step of MbDA neurons

CXCL12 has been previously described as a potent chemoattractant during neuronal migration in the forebrain and the hindbrain, where it is secreted from meningeal cells (fore- and hindbrain or Cajal Retzius cells (forebrain). CXCL12 signals through the CXCR4 and CXCR7 receptors

(Balabanian et al., 2005; Burns et al., 2006; Sanchez-Alcaniz et al., 2011; Stumm and Hollt, 2007; Wang et al., 2010).

This study demonstrates that CXCL12 and its receptor CXCR4 are expressed in ventral midbrain during the time period of MbDA migration, and this CXCL12/CXCR4 signaling modulates the radial migration of MbDA neurons, from the ventricular zone to the mantle layer.

4.3.1 CXCR4 is expressed in MbDA neurons during their migration phase

CXCR4 is expressed in the medial ventral Mb, in the area between the VZ and the pial surface, between E11.5 to E17.5, during a time when MbDA neurons undergo radial migration. CXCR4 expression overlaps with the MbDA neuronal markers, TH and LMX1A. The chemokine CXCL12, a CXCR4 specific ligand, is expressed in the meninges of the underlying pial surface.

CXCL12 can attach to extracellular matrix molecules such as proteoglycans or heparin, and a potential candidate for CXCL12 attachment in the ventral midbrain is 6B4 PG (6B4 proteoglycan-phosphacan), a chondroitin sulfate proteoglycan previously shown to be expressed in MbDA neurons (Ohyama et al., 1998).

The concentration of CXCL12 can be not only modulated by proteolytic cleavage through metalloproteinase (Bussilo and Benovic, 2007), but also by CXCR7 receptor, which can act as a scavenger by binding and removing the extracellular CXCL12 in the cortex (Cubedo et al., 2009; Wang et al., 2011). However, it is shown here that *Cxcr7* is not expressed in the MbDA neurons area. Therefore, in the midbrain CXCL12 activity is likely mediated by proteolytic degradation. However, whether metalloproteinase that mediate proteolytic degradation of CXCR4 are expressed in the ventral Mb remains to be explored.

4.3.2 CXCR4 and CXCL12 mutants might regulate the radial migration of MbDA neurons

CXCL12/CXCR4 signaling has been previously shown to play a role in regulating the tangential migration of neurons in different brain areas such as GABAergic interneurons and Cajal-Retzius cells in the cortex and precerebellar neurons (Borrell and Marin, 2006; Lysco et al., 2011; Zhu et al., 2009, Stumm et al., 2003; Tanaka et al., 2010; Liapi et al., 2008). CXCL12/CXCR4 signaling also regulates radial migration of cortical projection neurons, hippocampal granule neurons and sympathetic neural precursor cells (Bagri et al., 2002; Dziembowska et al., 2005; Kasemeier-Kulesa et al., 2010; Liapi et al., 2008). The current study shows a significant accumulation of MbDA neurons in a dorsal position just lateral of the midline area in E14.5 *Cxcr4* and *Cxcl12* KO mice. This change in the dorsal ventral midbrain area is accompanyed by a reduction in ventrally positioned MbDA neurons in *Cxcl12* mutants. These findings as well as the lack of expression of CXCR4 in laterally positioned DA neurons suggest a role for CXCR4/CXCL12 signaling in radial migration.

However, the distribution of cells in the *Cxcr4* KO mice indicates a potential more complicated

effect of CXCR4 signaling on DA neuronal migration, since less DA neurons are observed along the ventral midline of *Cxcr4* mutants. Moreover, the phenotype in both KO mice appears to be transient, since the MbDA mispositioning was more severe at E14.5 than at E16.5.This observation suggest that CXCL12/CXCR4 signaling is not essential for radial migration, but rather regulates the efficiency of early MbDA neuronal migration. Since CXCL12 is the only known ligand for CXCR4, it is unexpected that the *Cxcr4* KO phenotype is partially different from the *Cxcl12* KO phenotype. CXCL12-independent functions of CXCR4 have not been demonstrated, but it was recently shown that the neurotransmitter GABA can directly bind CXCR4 and act as an allosteric modulator (Guyon et al., 2013). Whether GABA or other potential modulators could influence CXCR4 function in absence of CXCL12 in the ventral midbrain remains to be explored.

Upon the inhibition of CXCL12/CXCR4 signaling in organotypic slice cultures, neither the speed nor the trajectory of radially migrating cells was significantly changed. MbDA neurons in which CXCR4 is inactivated might therefore simply stop their radial-oriented migration too early and consequently, accumulate closer to their progenitor domain, as compared to the wildtype MbDA neurons. Premature cessation of migration, upon CXCR4 inactivation, has been reported for migrating sympathetic precursor cells in the chick (Kasemeier-Kulesa et al., 2010). Alternatively, loss of CXCL12/CXCR4 signaling might lead to a delay in the onset of radial migration, a mechanism that would be consistent with the amelioration of the observed phenotype between E14.5 and E16.5.

A delay in migration has been previously reported for other molecules thought to be essential for migration. Lissencephaly-1 (LIS1, also known as Pafah1b1) is a central component of a protein complex that regulates nuclear migration. Reducing LIS1 activity in mice leads to severe defects in multiple types of radially migrating neurons, including cortical projection neurons (Wynshaw-Boris et al., 2010). However, a relatively recent study has shown that *LIS1* deficient neurons do not show a complete migratory arrest, and eventually reach the proper cortical layers, albeit with a significant delay (Hippenmeyer et al., 2010).

4.3.3 CXCL12 can act as a chemoattractant signal

Previous findings from other brain areas such as the hippocampus, cortex and cerebellum have shown that CXCL12 can act as a paracrine or long-range attractant signal for migrating neurons.

4.3.3.1 CXCL12 can act as a paracrine chemoattractant signal

Many studies have proposed that CXCL12 is expressed along the migratory pathways of migrating neurons expressing CXCR4, where it acts as a paracrine signal (Stumm and Hollt, 2007; Stumm et al., 2003). For example, Cajal-Retzius cells expressing CXCR4 migrate

tangentially from the cortical hem towards the cortical surface, along the marginal zone, which is covered by meninges secreting CXCL12. The CXCL12 secreted by the meningeal membranes is necessary and sufficient to guide the tangential migration of Cajal-Retzius cells, by stimulating cell movement and ensuring that the Cajal-Retzius cells localize and disperse at the marginal zone. The treatment of cortical slices, or *in utero* electroporation with the antagonist of CXCR4, AMD3100, results in the dispersion of some Cajal-Retzius cells from the marginal zone into deep layers of the developing cortex, while other Cajal-Retzius cells fail to migrate (Borrell and Marin, 2006).

Another example is the case of precerebellar neurons, which migrate tangentially beneath the pial surface from the lower rombic lip to specific locations in the hindbrain. CXCL12 secreted from meningeal tissue regulates this migration, by acting as a short-range chemoattractant for precerebellar neurons and keeping the migratory stream close to the pial surface. In *Cxcl12* deficient mutants, marginal migration of precerebellar neurons is disrupted, and ectopic clusters are formed (Zhu et al., 2009). An example in which CXCL12 is not expressed in meninges and is involved in radial migration by acting as a chemoattractant paracrine signal, are the gonadotropin-releasing hormone (GnRH) neurons, which migrate from the vomeronasal organ, along the nasal mesenchyme towards the hypothalamus. CXCL12 is expressed in a concentration gradient by different cells of the nasal mesenchyme. CXCR4 expressing GnRH neurons migrate along the mesenchyme expressing CXCL12, towards the increasing level of CXCL12 expression (Schwarting et al., 2007).

However, a paracrine action of CXCL12 in migrating MbDA neurons seems unlikely. Even though *Cxcl12* is expressed in the meninges, most CXCR4-expressing MbDA neurons are located within some distance of the pial surface. Moreover, in the *CXCR4* deficient mice, many MbDA neurons reach the proper level, close to the pial surface, and appear to be properly distributed along the medial lateral extension of the ventralMb

4.3.3.2 CXCL12 can act as a long-range chemoattractant signal

Cxcl12 and *Cxcr4* KO mice show an ectopic clustering of MbDA neurons in the dorsal aspect of the MbDA neuronal field. CXCL12 is expressed near the pial surface and CXCR4 expressing MbDA neurons are located between the VZ and the pial surface. Therefore, the ectopic clustering of MbDA neurons in *Cxcl12* and *Cxcr4* KO mice seems to suggest that CXCL12 functions as a long-range chemoattractive signal for MbDA neurons.

Evidence that CXCL12 can act as a long-range chemoattractant has been shown in other brain areas such as the hippocampus, where granule cells migrate radially, from the neuroepithelium towards the dendate anlage. CXCL12 is expressed in the anlage of the dendate gyrus, and CXCR4 is expressed within the granule cells migrating domain. When CXCL12 is expressed ectopically in hippocampal slices, the migratory stream of granule cells is disrupted, and they

migrate towards the ectopic CXCL12 source. This data suggests that CXCL12 acts as a long-range attractant for radially migrating dentate gyrus granule cells (Bagri et al., 2002; Hesselgesser et al., 1997; Klein et al., 2001).

In this study, the *in situ* hybridization used for detecting CXCL12 mRNA, does not allow for visualization of a concentration gradient of CXCL12 in the ventral midbrain.

4.3.4 Possible mechanism of CXCL12 function

The downstream mechanisms of CXCL12/CXCR 4 pathway are largely unknown. However, Lysco et al. (2011) found that CXCL12 controls the migration of interneurons by increasing their speed and reducing their branching frequency. Experiments performed by inhibiting CXCL12 signaling in slice cultures showed that inducing branching is sufficient to cause cells to prematurely exit from the migratory stream. The suppression of branching by CXCL12 allows the neurons to maintain a simpler morphology that facilitates rapid migration in a defined stream. The authors suggest that the CXCL12 acts through a G_i coupled signal transduction pathway (Lazarini et al., 2000). By inhibiting adenyl cyclase, G_i protein subunit lowers cAMP levels and protein kinase A (PKA) activity. The branching and speed of migrating neurons can be regulated by cAMP, as it has been shown that exogenous cAMP added to neuronal cultures increases branching and decreases speed of laminin-induced neurites (Weeks et al., 1991).

However in this study, the speed of radially migrating MbDA neurons was not found to be altered. Further analysis of branching should be performed in order to clarify if CXCL12 function in the ventral Mb through cAMP.

5. CONCLUSIONS

This study demonstrates that MbDA neurons destined for the SN first migrate radially and then switch to tangential migration, while neurons destined for the VTA almost exclusively undergo radial migration. The tangential, but not the radial migration is Reelin mediated. Reelin signaling is mediated through Dab1 and regulates the polarity of MbDA neurons, their migration trajectories and speed of migration. CXCR4/CXCL12 signaling is likely important for radially migrating neurons, as the dorsoventral distribution of MbDA neurons is changed when this signaling pathway is inactivated. The current study provides the first direct monitoring of distinct migratory pathways of different MbDA neuronal populations and investigates two of the underlying molecular mechanisms (Figure 37). Insight into MbDA neuronal migration is important for enriching our knowledge of MbDA development and could also serve as a model for migration of other neuronal cell types in ventral brain areas, where the processes of migration are not well understood.

Generation of MbDA neurons from pluripotent stem cells might become an important tool for cell-replacement therapy to substitute lost MbDA neurons in Parkinson's disease, as well as for modeling of Parkinson's disease *in vitro*. Molecules identified here, such as Dab1 that are particularly expressed in the SN subpopulation, can serve as markers to identify SN MbDA neurons during their generation from induced pluripotent stem cells.
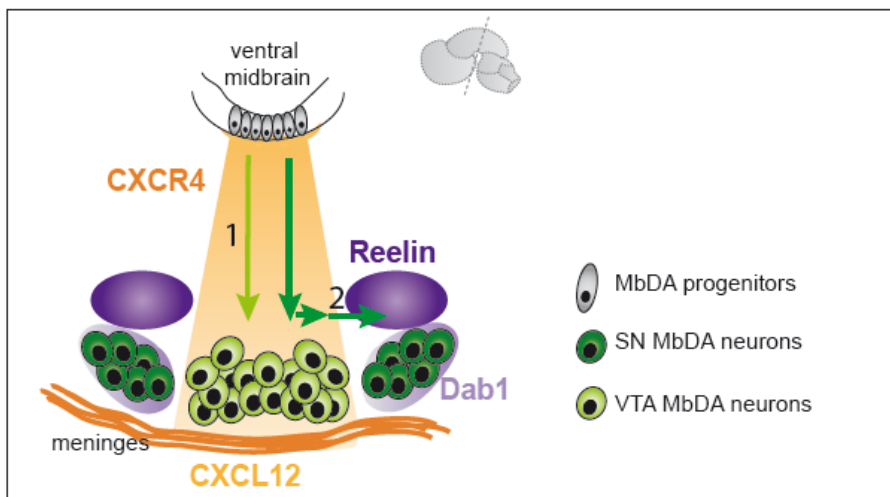

Figure 37. Reelin and CXCL12/CXCR4 signaling modulate distinct migratory behaviors of MbDA neurons. CXCL12 is expressed in meninges (yellow) and its receptor CXCR4 is expressed in differentiating MbDA neurons in the medial ventral midbrain (light yellow). CXCL12/CXCR4 signaling modulates the initial radial migration of all MbDA neurons. Reelin (purple) is expressed just above Dab1-expressing (light purple) MbDA neurons that migrate laterally. Reelin regulates the last step of tangential migration of MbDA neurons.

6. FUTURE DIRECTIONS

This thesis presents a detailed analysis of the routes and mechanisms involved in the migration of MbDA neurons that form the SN and medial VTA. The results presented here provide the basis and are a prerequisite for further investigation of MbDA neuronal migration. The here presented analysis of the migratory behavior of MbDA neurons used a GIFM method to label MbDA progenitors that preferentially give rise to SN or medial VTA and to track their descendants during the period of migration. One caveat of this method is that the labeled precursors do not exclusively develop into MbDA neurons, but also give rise to other cells types (Blaess et al 2011). A more precise analysis could be performed by using GIFM in combination with a reporter line in which the reporter gene is under the control of regulatory elements of a MbDA neuron-specific gene, such as TH or Pitx3. Such a reporter construct could be used to specifically label differentiating (TH or Pitx3 expressing) MbDA neurons that are destined to contribute either to the VTA or SN. The *TH* and *Pitx3* promoter constructs have been well characterized and previously used to generate transgenic or knock-in mice that express reporter genes in MbDA neurons (Matsushita et al., 2002; Sawamoto et al., 2001; Vives et al., 2008; Zhao et al., 2004).

In the current study, MbDA migratory behavior was observed in real time, in organotypic slice cultures. This approach allowed for analysis of migratory trajectories and speed of migrating fate mapped MbDA neurons. To assess the radial versus tangential migration of MbDA neurons either sagittal or horizontal organotypic slices were prepared, respectively. However, the widefield microscope used for imaging only allowed visualization of migrating MbDA neurons in a 2D plane and a potential migration within the slice (Z direction) was not possible. Moreover, the poor resolution of imaged cells made it impossible to properly assess their morphology. Since migration is a process involving complex cytoskeleton dynamics, it will be interesting to further explore the mode of MbDA neuron migration by gaining more insights into their morphology, which allow to speculate about the underlying cytoskeleton dynamics during migration. To be able to properly visualize detailed morphological changes, a more sophisticated imaging set-up is required, such as 2-photon microscopy. This microscopy technique provides a long range tissue penetration with relatively low photo bleaching and a very good resolution, which would ensure an improved visualization of cellular processes in 3D time-lapse imaging of migrating MbDA neurons. Moreover, using this approach, further experiments could be conducted to shed light on the molecular mechanism involved in morphological changes linked to cytoskeleton dynamics during MbDA migration. Thus, Reeler mice and mice in which *Dab1* was inactivated can be combined with SHH GIFM and migrating fate mapped MbDA neurons can be imaged

in organotypic slice cultures using 2-photon microscopy. Alternatively, the direct effect of Reelin overexpression or inhibition can be assessed by adding Reelin protein at ectopic locations or by using the CR50 function-blocking antibody in organotypic slice cultures. Such an approach could provide important information whether Reelin can directly or indirectly interfere with morphological changes linked to cytoskeleton dynamics. Additionally, other molecules potentially involved in MbDA polarization by interacting with Reelin can be tested. For example, it has been previously described that Reelin stabilizes the actin cytoskeleton of neuronal leading processes by inducing Cofilin phosphorylation (Chai et al., 2009a). Cofilin it is located at the leading edge of migrating neurons and binds to actin filaments (F-actin), promoting their disassembly. Thus Cofilin acts as an actin depolymerizing protein and by providing actin monomers, promotes lamellipodia formation (Jovceva et al., 2007; Kiuchi et al., 2007). It will be interesting to assess if Cofilin is involved in tangential migration of MbDA neurons by inactivating Cofilin in organotypic slice cultures and analysis of mutant mice.

CDK5 (cyclin dependent kinase 5) is another potential molecule involved in MbDA neuronal migration. CDK5 has been showed to interact with the Reelin pathway and to play a role in migration of cortical and cerebellar neurons (Ayala et al., 2007; Kawauchi et al., 2006b; Kawauchi and Hoshino, 2008; Nishimura et al., 2009; Umeshima and Kengaku, 2013). CDK5 is a serine/threonine cyclin-dependent kinase known to modulate the extension of the leading process through phosphorylation of important actin regulators (Dhavan and Tsai, 2001; Kawauchi et al., 2006a; Nikolic et al., 1998). In the cortex, *Cdk5* null mice have defects similar defects to Reeler mutants: newly generated neurons fail to migrate past their predecessors, and accumulate progressively in deeper layers, resulting in an inverted "outside-in" cortex (Gilmore et al., 1998; Ohshima et al., 1996). Also, studies in cortex have shown that Cdk5 can phosphorylate Dab1. However, it is unclear if Cdk5 can modulate Reelin signaling through Dab1 phosphorylation (Beffert et al., 2004; Ohshima et al., 2007b). It is tempting to investigate whether Cdk5 also plays a role in MbDA neuronal migration. Inhibitors for Cdk5, such as olomoucine and roscovitine have been previously used to suppress CDK5 activity in slice culture (Nishimura (Nishimura et al., 2009; Umeshima and Kengaku, 2013) and could be easily tested in organotypic slices of MbDA neurons.

This thesis has shown for the first time that CXCR4 is specifically expressed in medially located MbDA neurons at the time of their migration and when CXCR4/CXCL12 signaling is inactivated some MbDA neurons accumulate more dorsally. These results suggest an involvement of in CXCR4/CXCL12 signaling in MbDA radial migration, but further experiments need to be performed in order to prove this hypothesis, especially since in cultures treated with the CXCR4 antagonist migrating MbDA neurons showed no change in their speed or trajectories. To assess whether other aspects of migration such as the timing of migration onset or cessation are affected, it would be interesting to analyze the migration

of MbDA neurons labeled with SN or VTA marking scheme on the background of the *Cxcr4* or *Cxcl12* KO strains. Further analysis should be performed in slice cultures to assess how CXCR4/CXCL12 regulates MbDA migration.

Furthermore, it will of interest to examine the effects of mis- or overexpression of Reelin and CXCL12 in slice cultures. A possible experiment is using hanging drops of cell lines expressing Reelin or CXCL12, embedded in agarose and sectioned and then placed as an overlay onto organotypic slices. Such an experiment provided important insights into the effect of Reelin on the polarity of different cortical neurons (Britto et al., 2013).

Many aspects of the guidance of migrating neurons are shared with axonal guidance, such as chemotactic cues and substrate. These two processes occur in the same time frame during MbDA development and both require neuronal polarization. Leading processes of migrating neurons are morphological similar with the growth cones of migrating axons. It is unclear how migrating neurons polarized in their direction of migration at the same time start to form axonal projections. Therefore, it will be interesting to find out how the formation of axonal projections and migration are spatially and temporally integrated during migration of MbDA neurons. The fluorescence labeling method used in this study does not allow for a good visualization of cellular processes, because the expression of the reporter protein is not strong enough to label the entire axon. To improve the labeling a useful approach will be to use a reporter construct, which in conjunction with GIFM can result in a strong labeling of the processes of migrating MbDA neurons. (Madisen et al., 2009) previously described such a reporter construct. In this construct an exogenous strong CAG promotor is inserted in ubiquitously expressed *Rosa26* locus to drive higher expression. A fluorescent marker gene (such as EYFP, dtTomato) is placed downstream of the CAG promotor and a floxed *Stop* cassette controls it. To image migration and axonal formation of MbDA neurons ultramicroscopy can be used. The advantage of using such a method is that ultramicrospy combines optical sectioning with fast multidimensional imaging of entire tissues with minimal photo bleaching and good optical resolution (Erturk et al., 2010; Niedworok et al., 2012). Imaging and 3D reconstructions of axons in fixed, cleared brains at different stages can provide information about MbDA axonal morphology at different stages. Additionally, time-lapse imaging using ultramicroscopy in organotypic slice culture can provide a useful insight into how axonal development and migration are spatially and simultaneously coordinated. In principle, an organotypic slice can be imaged at any plane by being positioned relative to the stationary light sheet that uses a precise motorized translation and rotation stage. 3D time-lapse of the migrating MbDA neurons can be generated and used to track the MbDA cellular processes during their migration and axonal formation (Ahrens et al., 2013).

Altogether these experiments will help further address the molecular mechanism of MbDA neuronal migration during embryonic development.

7. REFERENCES

Ahrens, M. B., Orger, M. B., Robson, D. N., Li, J. M. and Keller, P. J. (2013). Whole-brain functional imaging at cellular resolution using light-sheet microscopy. *Nat Methods* **10**, 413-20.

Alfahel-Kakunda, A. and Silverman, W. F. (1997). Calcium-binding proteins in the substantia nigra and ventral tegmental area during development: correlation with dopaminergic compartmentalization. *Brain Res Dev Brain Res* **103**, 9-20.

Andersson, E., Tryggvason, U., Deng, Q., Friling, S., Alekseenko, Z., Robert, B., Perlmann, T. and Ericson, J. (2006). Identification of intrinsic determinants of midbrain dopamine neurons. *Cell* **124**, 393-405.

Andersson, E. R., Salto, C., Villaescusa, J. C., Cajanek, L., Yang, S., Bryjova, L., Nagy, II, Vainio, S. J., Ramirez, C., Bryja, V. et al. (2013). Wnt5a cooperates with canonical Wnts to generate midbrain dopaminergic neurons in vivo and in stem cells. *Proc Natl Acad Sci U S A* **110**, E602-10.

Ang, E. S., Jr., Haydar, T. F., Gluncic, V. and Rakic, P. (2003). Four-dimensional migratory coordinates of GABAergic interneurons in the developing mouse cortex. *J Neurosci* **23**, 5805-15.

Ang, S. L. (2006). Transcriptional control of midbrain dopaminergic neuron development. *Development* **133**, 3499-506.

Ang, S. L. (2009). Foxa1 and Foxa2 transcription factors regulate differentiation of midbrain dopaminergic neurons. *Adv Exp Med Biol* **651**, 58-65.

Anton, E. S., Kreidberg, J. A. and Rakic, P. (1999). Distinct functions of alpha3 and alpha(v) integrin receptors in neuronal migration and laminar organization of the cerebral cortex. *Neuron* **22**, 277-89.

Ayala, R., Shu, T. and Tsai, L. H. (2007). Trekking across the brain: the journey of neuronal migration. *Cell* **128**, 29-43.

Bagri, A., Gurney, T., He, X., Zou, Y. R., Littman, D. R., Tessier-Lavigne, M. and Pleasure, S. J. (2002). The chemokine SDF1 regulates migration of dentate granule cells. *Development* **129**, 4249-60.

Ballif, B. A., Arnaud, L., Arthur, W. T., Guris, D., Imamoto, A. and Cooper, J. A. (2004). Activation of a Dab1/CrkL/C3G/Rap1 pathway in Reelin-stimulated neurons. *Curr Biol* **14**, 606-10.

Ballmaier, M., Zoli, M., Leo, G., Agnati, L. F. and Spano, P. (2002). Preferential alterations in the mesolimbic dopamine pathway of heterozygous reeler mice: an emerging animal-based model of schizophrenia. *Eur J Neurosci* **15**, 1197-205.

Bar, I., Lambert De Rouvroit, C., Royaux, I., Krizman, D. B., Dernoncourt, C., Ruelle, D., Beckers, M. C. and Goffinet, A. M. (1995). A YAC contig containing the reeler locus with preliminary characterization of candidate gene fragments. *Genomics* **26**, 543-9.

Barnes, A. P., Lilley, B. N., Pan, Y. A., Plummer, L. J., Powell, A. W., Raines, A. N., Sanes, J. R. and Polleux, F. (2007). LKB1 and SAD kinases define a pathway required for the polarization of cortical neurons. *Cell* **129**, 549-63.

Barrett, T., Xie, T., Piao, Y., Dillon-Carter, O., Kargul, G. J., Lim, M. K., Chrest, F. J., Wersto, R., Rowley, D. L., Juhaszova, M. et al. (2001). A murine dopamine neuron-specific cDNA library and microarray: increased COX1 expression during methamphetamine neurotoxicity. *Neurobiol Dis* **8**, 822-33.

Bayer, S. A., Wills, K. V., Triarhou, L. C. and Ghetti, B. (1995). Time of neuron origin and gradients of neurogenesis in midbrain dopaminergic neurons in the mouse. *Exp Brain Res* **105**, 191-9.

Beffert, U., Weeber, E. J., Morfini, G., Ko, J., Brady, S. T., Tsai, L. H., Sweatt, J. D. and Herz, J. (2004). Reelin and cyclin-dependent kinase 5-dependent signals cooperate in regulating neuronal migration and synaptic transmission. *J Neurosci* **24**, 1897-906.

Bellion, A., Baudoin, J. P., Alvarez, C., Bornens, M. and Metin, C. (2005). Nucleokinesis in tangentially migrating neurons comprises two alternating phases: forward migration of the Golgi/centrosome associated with centrosome splitting and myosin contraction at the rear. *J Neurosci* **25**, 5691-9.

Bentivoglio, M. and Morelli, M. (2005). The organization and circuits of mesencephalic dopaminergic neurons and the distribution of dopamine receptors in the brain. *Handbook of chemical neuroanatomy* **Vol XXI**, 1–106.

Bjorklund, A. and Dunnett, S. B. (2007). Fifty years of dopamine research. *Trends Neurosci* **30**, 185-7.

Blaess, S., Bodea, G. O., Kabanova, A., Chanet, S., Mugniery, E., Derouiche, A., Stephen, D. and Joyner, A. L. (2011). Temporal-spatial changes in Sonic Hedgehog expression and signaling

reveal different potentials of ventral mesencephalic progenitors to populate distinct ventral midbrain nuclei. *Neural Dev* **6**, 29.

Bock, H. H. and Herz, J. (2003). Reelin activates SRC family tyrosine kinases in neurons. *Curr Biol* **13**, 18-26.

Bock, H. H., Jossin, Y., Liu, P., Forster, E., May, P., Goffinet, A. M. and Herz, J. (2003). Phosphatidylinositol 3-kinase interacts with the adaptor protein Dab1 in response to Reelin signaling and is required for normal cortical lamination. *J Biol Chem* **278**, 38772-9.

Borrell, V. and Marin, O. (2006). Meninges control tangential migration of hem-derived Cajal-Retzius cells via CXCL12/CXCR4 signaling. *Nat Neurosci* **9**, 1284-93.

Bouche, E., Romero-Ortega, M. I., Henkemeyer, M., Catchpole, T., Leemhuis, J., Frotscher, M., May, P., Herz, J. and Bock, H. H. (2013). Reelin induces EphB activation. *Cell Res* **23**, 473-90.

Britto, J. M., Tait, K. J., Lee, E. P., Gamble, R. S., Hattori, M. and Tan, S. S. (2013). Exogenous Reelin Modifies the Migratory Behavior of Neurons Depending on Cortical Location. *Cereb Cortex*.

Brodski, C., Weisenhorn, D. M., Signore, M., Sillaber, I., Oesterheld, M., Broccoli, V., Acampora, D., Simeone, A. and Wurst, W. (2003). Location and size of dopaminergic and serotonergic cell populations are controlled by the position of the midbrain-hindbrain organizer. *J Neurosci* **23**, 4199-207.

Brose, K. and Tessier-Lavigne, M. (2000). Slit proteins: key regulators of axon guidance, axonal branching, and cell migration. *Curr Opin Neurobiol* **10**, 95-102.

Busillo, J. M. and Benovic, J. L. (2007). Regulation of CXCR4 signaling. *Biochim Biophys Acta* **1768**, 952-63.

Cariboni, A., Hickok, J., Rakic, S., Andrews, W., Maggi, R., Tischkau, S. and Parnavelas, J. G. (2007). Neuropilins and their ligands are important in the migration of gonadotropin-releasing hormone neurons. *J Neurosci* **27**, 2387-95.

Castelo-Branco, G., Rawal, N. and Arenas, E. (2004). GSK-3beta inhibition/beta-catenin stabilization in ventral midbrain precursors increases differentiation into dopamine neurons. *J Cell Sci* **117**, 5731-7.

Castelo-Branco, G., Wagner, J., Rodriguez, F. J., Kele, J., Sousa, K., Rawal, N., Pasolli, H. A., Fuchs, E., Kitajewski, J. and Arenas, E. (2003). Differential regulation of midbrain dopaminergic neuron development by Wnt-1, Wnt-3a, and Wnt-5a. *Proc Natl Acad Sci U S A* **100**, 12747-52.

Chai, X., Forster, E., Zhao, S., Bock, H. H. and Frotscher, M. (2009a). Reelin acts as a stop signal for radially migrating neurons by inducing phosphorylation of n-cofilin at the leading edge. *Commun Integr Biol* **2**, 375-7.

Chai, X., Forster, E., Zhao, S., Bock, H. H. and Frotscher, M. (2009b). Reelin stabilizes the actin cytoskeleton of neuronal processes by inducing n-cofilin phosphorylation at serine3. *J Neurosci* **29**, 288-99.

Chen, M. L., Chen, S. Y., Huang, C. H. and Chen, C. H. (2002). Identification of a single nucleotide polymorphism at the 5' promoter region of human reelin gene and association study with schizophrenia. *Mol Psychiatry* **7**, 447-8.

Chen, W. S., Antic, D., Matis, M., Logan, C. Y., Povelones, M., Anderson, G. A., Nusse, R. and Axelrod, J. D. (2008). Asymmetric homotypic interactions of the atypical cadherin flamingo mediate intercellular polarity signaling. *Cell* **133**, 1093-105.

Chenu, F., El Mansari, M. and Blier, P. (2009). Long-term administration of monoamine oxidase inhibitors alters the firing rate and pattern of dopamine neurons in the ventral tegmental area. *Int J Neuropsychopharmacol* **12**, 475-85.

Chi, C. L., Martinez, S., Wurst, W. and Martin, G. R. (2003). The isthmic organizer signal FGF8 is required for cell survival in the prospective midbrain and cerebellum. *Development* **130**, 2633-44.

Chung, S., Leung, A., Han, B. S., Chang, M. Y., Moon, J. I., Kim, C. H., Hong, S., Pruszak, J., Isacson, O. and Kim, K. S. (2009). Wnt1-lmx1a forms a novel autoregulatory loop and controls midbrain dopaminergic differentiation synergistically with the SHH-FoxA2 pathway. *Cell Stem Cell* **5**, 646-58.

Cubedo, N., Cerdan, E., Sapede, D. and Rossel, M. (2009). CXCR4 and CXCR7 cooperate during tangential migration of facial motoneurons. *Mol Cell Neurosci* **40**, 474-84.

D'Arcangelo, G., Homayouni, R., Keshvara, L., Rice, D. S., Sheldon, M. and Curran, T. (1999). Reelin is a ligand for lipoprotein receptors. *Neuron* **24**, 471-9.

Dahlstrom, A. and Fuxe, K. (1964). Localization of monoamines in the lower brain stem. *Experientia* **20**, 398-9.

Dailly, E., Chenu, F., Renard, C. E. and Bourin, M. (2004). Dopamine, depression and antidepressants. *Fundam Clin Pharmacol* **18**, 601-7.

Danielian, P. S. and McMahon, A. P. (1996). Engrailed-1 as a target of the Wnt-1 signalling pathway in vertebrate midbrain development. *Nature* **383**, 332-4.

Demyanenko, G. P., Shibata, Y. and Maness, P. F. (2001). Altered distribution of dopaminergic neurons in the brain of L1 null mice. *Brain Res Dev Brain Res* **126**, 21-30.

Derer, P., Derer, M. and Goffinet, A. (2001). Axonal secretion of Reelin by Cajal-Retzius cells: evidence from comparison of normal and Reln(Orl) mutant mice. *J Comp Neurol* **440**, 136-43.

Deutch, A. Y., Goldstein, M., Baldino, F., Jr. and Roth, R. H. (1988). Telencephalic projections of the A8 dopamine cell group. *Ann N Y Acad Sci* **537**, 27-50.

Dhavan, R. and Tsai, L. H. (2001). A decade of CDK5. *Nat Rev Mol Cell Biol* **2**, 749-59.

Dodt, H. U., Leischner, U., Schierloh, A., Jahrling, N., Mauch, C. P., Deininger, K., Deussing, J. M., Eder, M., Zieglgansberger, W. and Becker, K. (2007). Ultramicroscopy: three-dimensional visualization of neuronal networks in the whole mouse brain. *Nat Methods* **4**, 331-6.

Dziembowska, M., Tham, T. N., Lau, P., Vitry, S., Lazarini, F. and Dubois-Dalcq, M. (2005). A role for CXCR4 signaling in survival and migration of neural and oligodendrocyte precursors. *Glia* **50**, 258-69.

Edmondson, J. C. and Hatten, M. E. (1987). Glial-guided granule neuron migration in vitro: a high-resolution time-lapse video microscopic study. *J Neurosci* **7**, 1928-34.

Elias, L. A., Turmaine, M., Parnavelas, J. G. and Kriegstein, A. R. (2010). Connexin 43 mediates the tangential to radial migratory switch in ventrally derived cortical interneurons. *J Neurosci* **30**, 7072-7.

Erturk, A., Becker, K., Jahrling, N., Mauch, C. P., Hojer, C. D., Egen, J. G., Hellal, F., Bradke, F., Sheng, M. and Dodt, H. U. (2010). Three-dimensional imaging of solvent-cleared organs using 3DISCO. *Nat Protoc* **7**, 1983-95.

Fatemi, S. H. (2005). Reelin glycoprotein in autism and schizophrenia. *Int Rev Neurobiol* **71**, 179-87.

Fedtsova, N. and Turner, E. E. (2001). Signals from the ventral midline and isthmus regulate the development of Brn3.0-expressing neurons in the midbrain. *Mech Dev* **105**, 129-44.

Ferri, A. L., Lin, W., Mavromatakis, Y. E., Wang, J. C., Sasaki, H., Whitsett, J. A. and Ang, S. L. (2007). Foxa1 and Foxa2 regulate multiple phases of midbrain dopaminergic neuron development in a dosage-dependent manner. *Development* **134**, 2761-9.

Forster, E., Jossin, Y., Zhao, S., Chai, X., Frotscher, M. and Goffinet, A. M. (2006). Recent progress in understanding the role of Reelin in radial neuronal migration, with specific emphasis on the dentate gyrus. *Eur J Neurosci* **23**, 901-9.

Forster, E., Tielsch, A., Saum, B., Weiss, K. H., Johanssen, C., Graus-Porta, D., Muller, U. and Frotscher, M. (2002). Reelin, Disabled 1, and beta 1 integrins are required for the formation of the radial glial scaffold in the hippocampus. *Proc Natl Acad Sci U S A* **99**, 13178-83.

Franco, S. J., Martinez-Garay, I., Gil-Sanz, C., Harkins-Perry, S. R. and Muller, U. (2011). Reelin regulates cadherin function via Dab1/Rap1 to control neuronal migration and lamination in the neocortex. *Neuron* **69**, 482-97.

Frykman, P. K., Brown, M. S., Yamamoto, T., Goldstein, J. L. and Herz, J. (1995). Normal plasma lipoproteins and fertility in gene-targeted mice homozygous for a disruption in the gene encoding very low density lipoprotein receptor. *Proc Natl Acad Sci U S A* **92**, 8453-7.

Fuchigami, T., Sato, Y., Tomita, Y., Takano, T., Miyauchi, S. Y., Tsuchiya, Y., Saito, T., Kubo, K., Nakajima, K., Fukuda, M. et al. (2013). Dab1-mediated colocalization of multi-adaptor protein CIN85 with Reelin receptors, ApoER2 and VLDLR, in neurons. *Genes Cells* **18**, 410-24.

Gadisseux, J. F., Evrard, P., Misson, J. P. and Caviness, V. S. (1989). Dynamic structure of the radial glial fiber system of the developing murine cerebral wall. An immunocytochemical analysis. *Brain Res Dev Brain Res* **50**, 55-67.

Gasser, U. E. and Hatten, M. E. (1990). Neuron-glia interactions of rat hippocampal cells in vitro: glial-guided neuronal migration and neuronal regulation of glial differentiation. *J Neurosci* **10**, 1276-85.

Gleeson, J. G. and Walsh, C. A. (2000). Neuronal migration disorders: from genetic diseases to developmental mechanisms. *Trends Neurosci* **23**, 352-9.

Goffinet, A. M. (1984). Events governing organization of postmigratory neurons: studies on brain development in normal and reeler mice. *Brain Res* **319**, 261-96.

Greene, J. G., Dingledine, R. and Greenamyre, J. T. (2005). Gene expression profiling of rat midbrain dopamine neurons: implications for selective vulnerability in parkinsonism. *Neurobiol Dis* **18**, 19-31.

Gupta, A., Sanada, K., Miyamoto, D. T., Rovelstad, S., Nadarajah, B., Pearlman, A. L., Brunstrom, J. and Tsai, L. H. (2003). Layering defect in p35 deficiency is linked to improper neuronal-glial interaction in radial migration. *Nat Neurosci* **6**, 1284-91.

Hanaway, J., McConnell, J. A. and Netsky, M. G. (1971). Histogenesis of the substantia nigra, ventral tegmental area of Tsai and interpeduncular nucleus: an autoradiographic study of the mesencephalon in the rat. *J Comp Neurol* **142**, 59-73.

Harfe, B. D., Scherz, P. J., Nissim, S., Tian, H., McMahon, A. P. and Tabin, C. J. (2004). Evidence for an expansion-based temporal Shh gradient in specifying vertebrate digit identities. *Cell* **118**, 517-28.

Hawthorne, A. L., Wylie, C. J., Landmesser, L. T., Deneris, E. S. and Silver, J. (2010). Serotonergic neurons migrate radially through the neuroepithelium by dynamin-mediated somal translocation. *J Neurosci* **30**, 420-30.

Hayashi, S. and McMahon, A. P. (2002). Efficient recombination in diverse tissues by a tamoxifen-inducible form of Cre: a tool for temporally regulated gene activation/inactivation in the mouse. *Dev Biol* **244**, 305-18.

Hayes, L., Zhang, Z., Albert, P., Zervas, M. and Ahn, S. (2011). Timing of Sonic hedgehog and Gli1 expression segregates midbrain dopamine neurons. *J Comp Neurol* **519**, 3001-18.

Heins, N., Malatesta, P., Cecconi, F., Nakafuku, M., Tucker, K. L., Hack, M. A., Chapouton, P., Barde, Y. A. and Gotz, M. (2002). Glial cells generate neurons: the role of the transcription factor Pax6. *Nat Neurosci* **5**, 308-15.

Higginbotham, H. R. and Gleeson, J. G. (2007). The centrosome in neuronal development. *Trends Neurosci* **30**, 276-83.

Howell, B. W., Hawkes, R., Soriano, P. and Cooper, J. A. (1997). Neuronal position in the developing brain is regulated by mouse disabled-1. *Nature* **389**, 733-7.

Hynes, M., Stone, D. M., Dowd, M., Pitts-Meek, S., Goddard, A., Gurney, A. and Rosenthal, A. (1997). Control of cell pattern in the neural tube by the zinc finger transcription factor and oncogene Gli-1. *Neuron* **19**, 15-26.

Ikemoto, S. (2007). Dopamine reward circuitry: two projection systems from the ventral midbrain to the nucleus accumbens-olfactory tubercle complex. *Brain Res Rev* **56**, 27-78.

Joksimovic, M., Anderegg, A., Roy, A., Campochiaro, L., Yun, B., Kittappa, R., McKay, R. and Awatramani, R. (2009). Spatiotemporally separable Shh domains in the midbrain define distinct dopaminergic progenitor pools. *Proc Natl Acad Sci U S A* **106**, 19185-90.

Jossin, Y. (2004). Neuronal migration and the role of reelin during early development of the cerebral cortex. *Mol Neurobiol* **30**, 225-51.

Jovceva, E., Larsen, M. R., Waterfield, M. D., Baum, B. and Timms, J. F. (2007). Dynamic cofilin phosphorylation in the control of lamellipodial actin homeostasis. *J Cell Sci* **120**, 1888-97.

Joyner, A. L. and Zervas, M. (2006). Genetic inducible fate mapping in mouse: establishing genetic lineages and defining genetic neuroanatomy in the nervous system. *Dev Dyn* **235**, 2376-85.

Kang, W. Y., Kim, S. S., Cho, S. K., Kim, S., Suh-Kim, H. and Lee, Y. D. (2010). Migratory defect of mesencephalic dopaminergic neurons in developing reeler mice. *Anat Cell Biol* **43**, 241-51.

Kasemeier-Kulesa, J. C., McLennan, R., Romine, M. H., Kulesa, P. M. and Lefcort, F. (2010). CXCR4 controls ventral migration of sympathetic precursor cells. *J Neurosci* **30**, 13078-88.

Kato, A., Kurita, S., Hayashi, A., Kaji, N., Ohashi, K. and Mizuno, K. (2008). Critical roles of actin-interacting protein 1 in cytokinesis and chemotactic migration of mammalian cells. *Biochem J* **414**, 261-70.

Kawano, H., Ohyama, K., Kawamura, K. and Nagatsu, I. (1995). Migration of dopaminergic neurons in the embryonic mesencephalon of mice. *Brain Res Dev Brain Res* **86**, 101-13.

Kawauchi, D., Taniguchi, H., Watanabe, H., Saito, T. and Murakami, F. (2006a). Direct visualization of nucleogenesis by precerebellar neurons: involvement of ventricle-directed, radial fibre-associated migration. *Development* **133**, 1113-23.

Kawauchi, T., Chihama, K., Nabeshima, Y. and Hoshino, M. (2006b). Cdk5 phosphorylates and stabilizes p27kip1 contributing to actin organization and cortical neuronal migration. *Nat Cell Biol* **8**, 17-26.

Kawauchi, T. and Hoshino, M. (2008). Molecular pathways regulating cytoskeletal organization and morphological changes in migrating neurons. *Dev Neurosci* **30**, 36-46.

Kele, J., Simplicio, N., Ferri, A. L., Mira, H., Guillemot, F., Arenas, E. and Ang, S. L. (2006). Neurogenin 2 is required for the development of ventral midbrain dopaminergic neurons. *Development* **133**, 495-505.

Kittappa, R., Chang, W. W., Awatramani, R. B. and McKay, R. D. (2007). The foxa2 gene controls the birth and spontaneous degeneration of dopamine neurons in old age. *PLoS Biol* **5**, e325.

Kiuchi, T., Ohashi, K., Kurita, S. and Mizuno, K. (2007). Cofilin promotes stimulus-induced lamellipodium formation by generating an abundant supply of actin monomers. *J Cell Biol* **177**, 465-76.

Kruger, M. T., Zhao, S., Chai, X., Brunne, B., Bouche, E., Bock, H. H. and Frotscher, M. (2010). Role for Reelin-induced cofilin phosphorylation in the assembly of sympathetic preganglionic neurons in the murine intermediolateral column. *Eur J Neurosci* **32**, 1611-7.

Kwiatkowski, A. V., Rubinson, D. A., Dent, E. W., Edward van Veen, J., Leslie, J. D., Zhang, J., Mebane, L. M., Philippar, U., Pinheiro, E. M., Burds, A. A. et al. (2007). Ena/VASP Is Required for neuritogenesis in the developing cortex. *Neuron* **56**, 441-55.

Lammel, S., Hetzel, A., Hackel, O., Jones, I., Liss, B. and Roeper, J. (2008). Unique properties of mesoprefrontal neurons within a dual mesocorticolimbic dopamine system. *Neuron* **57**, 760-73.

Lammel, S., Ion, D. I., Roeper, J. and Malenka, R. C. (2011). Projection-specific modulation of dopamine neuron synapses by aversive and rewarding stimuli. *Neuron* **70**, 855-62.

Lammel, S., Lim, B. K., Ran, C., Huang, K. W., Betley, M. J., Tye, K. M., Deisseroth, K. and Malenka, R. C. (2012). Input-specific control of reward and aversion in the ventral tegmental area. *Nature* **491**, 212-7.

Lazarini, F., Casanova, P., Tham, T. N., De Clercq, E., Arenzana-Seisdedos, F., Baleux, F. and Dubois-Dalcq, M. (2000). Differential signalling of the chemokine receptor CXCR4 by stromal cell-derived factor 1 and the HIV glycoprotein in rat neurons and astrocytes. *Eur J Neurosci* **12**, 117-25.

Leemhuis, J., Bouche, E., Frotscher, M., Henle, F., Hein, L., Herz, J., Meyer, D. K., Pichler, M., Roth, G., Schwan, C. et al. (2010). Reelin signals through apolipoprotein E receptor 2 and Cdc42 to increase growth cone motility and filopodia formation. *J Neurosci* **30**, 14759-72.

Li, J. Y. and Joyner, A. L. (2001). Otx2 and Gbx2 are required for refinement and not induction of mid-hindbrain gene expression. *Development* **128**, 4979-91.

Liapi, A., Pritchett, J., Jones, O., Fujii, N., Parnavelas, J. G. and Nadarajah, B. (2008). Stromal-derived factor 1 signalling regulates radial and tangential migration in the developing cerebral cortex. *Dev Neurosci* **30**, 117-31.

Lin, W., Metzakopian, E., Mavromatakis, Y. E., Gao, N., Balaskas, N., Sasaki, H., Briscoe, J., Whitsett, J. A., Goulding, M., Kaestner, K. H. et al. (2009). Foxa1 and Foxa2 function both upstream of and cooperatively with Lmx1a and Lmx1b in a feedforward loop promoting mesodiencephalic dopaminergic neuron development. *Dev Biol* **333**, 386-96.

Liu, A. and Joyner, A. L. (2001). EN and GBX2 play essential roles downstream of FGF8 in patterning the mouse mid/hindbrain region. *Development* **128**, 181-91.

Lopez-Bendito, G., Cautinat, A., Sanchez, J. A., Bielle, F., Flames, N., Garratt, A. N., Talmage, D. A., Role, L. W., Charnay, P., Marin, O. et al. (2006). Tangential neuronal migration controls axon guidance: a role for neuregulin-1 in thalamocortical axon navigation. *Cell* **125**, 127-42.

Ma, Q., Jones, D., Borghesani, P. R., Segal, R. A., Nagasawa, T., Kishimoto, T., Bronson, R. T. and Springer, T. A. (1998). Impaired B-lymphopoiesis, myelopoiesis, and derailed cerebellar neuron migration in CXCR4- and SDF-1-deficient mice. *Proc Natl Acad Sci U S A* **95**, 9448-53.

Madisen, L., Zwingman, T. A., Sunkin, S. M., Oh, S. W., Zariwala, H. A., Gu, H., Ng, L. L., Palmiter, R. D., Hawrylycz, M. J., Jones, A. R. et al. (2009). A robust and high-throughput Cre reporting and characterization system for the whole mouse brain. *Nat Neurosci* **13**, 133-40.

Magdaleno, S., Keshvara, L. and Curran, T. (2002). Rescue of ataxia and preplate splitting by ectopic expression of Reelin in reeler mice. *Neuron* **33**, 573-86.

Magdaleno, S. M. and Curran, T. (2001). Brain development: integrins and the Reelin pathway. *Curr Biol* **11**, R1032-5.

Malatesta, P., Hartfuss, E. and Gotz, M. (2000). Isolation of radial glial cells by fluorescent-activated cell sorting reveals a neuronal lineage. *Development* **127**, 5253-63.

Manitt, C. and Kennedy, T. E. (2002). Where the rubber meets the road: netrin expression and function in developing and adult nervous systems. *Prog Brain Res* **137**, 425-42.

Marchand, R. and Poirier, L. J. (1983). Isthmic origin of neurons of the rat substantia nigra. *Neuroscience* **9**, 373-81.

Marin, O. and Rubenstein, J. L. (2001). A long, remarkable journey: tangential migration in the telencephalon. *Nat Rev Neurosci* **2**, 780-90.

Martinez, S., Crossley, P. H., Cobos, I., Rubenstein, J. L. and Martin, G. R. (1999). FGF8 induces formation of an ectopic isthmic organizer and isthmocerebellar development via a repressive effect on Otx2 expression. *Development* **126**, 1189-200.

Martinez-Cerdeno, V., Galazo, M. J., Cavada, C. and Clasca, F. (2002). Reelin immunoreactivity in the adult primate brain: intracellular localization in projecting and local circuit neurons of the cerebral cortex, hippocampus and subcortical regions. *Cereb Cortex* **12**, 1298-311.

Martini, F. J., Valiente, M., Lopez Bendito, G., Szabo, G., Moya, F., Valdeolmillos, M. and Marin, O. (2009). Biased selection of leading process branches mediates chemotaxis during tangential neuronal migration. *Development* **136**, 41-50.

Matise, M. P., Epstein, D. J., Park, H. L., Platt, K. A. and Joyner, A. L. (1998). Gli2 is required for induction of floor plate and adjacent cells, but not most ventral neurons in the mouse central nervous system. *Development* **125**, 2759-70.

Matsushita, N., Okada, H., Yasoshima, Y., Takahashi, K., Kiuchi, K. and Kobayashi, K. (2002). Dynamics of tyrosine hydroxylase promoter activity during midbrain dopaminergic neuron development. *J Neurochem* **82**, 295-304.

Mavromatakis, Y. E., Lin, W., Metzakopian, E., Ferri, A. L., Yan, C. H., Sasaki, H., Whisett, J. and Ang, S. L. (2011). Foxa1 and Foxa2 positively and negatively regulate Shh signalling to specify ventral midbrain progenitor identity. *Mech Dev* **128**, 90-103.

Maxwell, S. L., Ho, H. Y., Kuehner, E., Zhao, S. and Li, M. (2005). Pitx3 regulates tyrosine hydroxylase expression in the substantia nigra and identifies a subgroup of mesencephalic dopaminergic progenitor neurons during mouse development. *Dev Biol* **282**, 467-79.

Mertz, J. and Kim, J. (2010). Scanning light-sheet microscopy in the whole mouse brain with HiLo background rejection. *J Biomed Opt* **15**, 016027.

Miyata, T., Kawaguchi, A., Okano, H. and Ogawa, M. (2001). Asymmetric inheritance of radial glial fibers by cortical neurons. *Neuron* **31**, 727-41.

Nadarajah, B., Brunstrom, J. E., Grutzendler, J., Wong, R. O. and Pearlman, A. L. (2001). Two modes of radial migration in early development of the cerebral cortex. *Nat Neurosci* **4**, 143-50.

Nakatani, T., Kumai, M., Mizuhara, E., Minaki, Y. and Ono, Y. (2010). Lmx1a and Lmx1b cooperate with Foxa2 to coordinate the specification of dopaminergic neurons and control of floor plate cell differentiation in the developing mesencephalon. *Dev Biol* **339**, 101-13.

Neil, M. A., Juskaitis, R. and Wilson, T. (1997). Method of obtaining optical sectioning by using structured light in a conventional microscope. *Opt Lett* **22**, 1905-7.

Niedworok, C. J., Schwarz, I., Ledderose, J., Giese, G., Conzelmann, K. K. and Schwarz, M. K. (2012). Charting monosynaptic connectivity maps by two-color light-sheet fluorescence microscopy. *Cell Rep* **2**, 1375-86.

Nikolic, M., Chou, M. M., Lu, W., Mayer, B. J. and Tsai, L. H. (1998). The p35/Cdk5 kinase is a neuron-specific Rac effector that inhibits Pak1 activity. *Nature* **395**, 194-8.

Nishikawa, S., Goto, S., Yamada, K., Hamasaki, T. and Ushio, Y. (2003). Lack of Reelin causes malpositioning of nigral dopaminergic neurons: evidence from comparison of normal and Reln(rl) mutant mice. *J Comp Neurol* **461**, 166-73.

Nishimura, Y. V., Sekine, K., Chihama, K., Nakajima, K., Hoshino, M., Nabeshima, Y. and Kawauchi, T. (2009). Dissecting the factors involved in the locomotion mode of neuronal migration in the developing cerebral cortex. *J Biol Chem* **285**, 5878-87.

Noctor, S. C., Flint, A. C., Weissman, T. A., Dammerman, R. S. and Kriegstein, A. R. (2001). Neurons derived from radial glial cells establish radial units in neocortex. *Nature* **409**, 714-20.

Noctor, S. C., Flint, A. C., Weissman, T. A., Wong, W. S., Clinton, B. K. and Kriegstein, A. R. (2002). Dividing precursor cells of the embryonic cortical ventricular zone have morphological and molecular characteristics of radial glia. *J Neurosci* **22**, 3161-73.

Nunes, I., Tovmasian, L. T., Silva, R. M., Burke, R. E. and Goff, S. P. (2003). Pitx3 is required for development of substantia nigra dopaminergic neurons. *Proc Natl Acad Sci U S A* **100**, 4245-50.

O'Rourke, N. A., Dailey, M. E., Smith, S. J. and McConnell, S. K. (1992). Diverse migratory pathways in the developing cerebral cortex. *Science* **258**, 299-302.

Ohshima, T., Hirasawa, M., Tabata, H., Mutoh, T., Adachi, T., Suzuki, H., Saruta, K., Iwasato, T., Itohara, S., Hashimoto, M. et al. (2007a). Cdk5 is required for multipolar-to-bipolar transition during radial neuronal migration and proper dendrite development of pyramidal neurons in the cerebral cortex. *Development* **134**, 2273-82.

Ohshima, T., Suzuki, H., Morimura, T., Ogawa, M. and Mikoshiba, K. (2007b). Modulation of Reelin signaling by Cyclin-dependent kinase 5. *Brain Res* **1140**, 84-95.

Ohyama, K., Kawano, H., Asou, H., Fukuda, T., Oohira, A., Uyemura, K. and Kawamura, K. (1998). Coordinate expression of L1 and 6B4 proteoglycan/phosphacan is correlated with the migration of mesencephalic dopaminergic neurons in mice. *Brain Res Dev Brain Res* **107**, 219-26.

Ono, Y., Nakatani, T., Sakamoto, Y., Mizuhara, E., Minaki, Y., Kumai, M., Hamaguchi, A., Nishimura, M., Inoue, Y., Hayashi, H. et al. (2007). Differences in neurogenic potential in floor plate cells along an anteroposterior location: midbrain dopaminergic neurons originate from mesencephalic floor plate cells. *Development* **134**, 3213-25.

Pan, P. Y. and Ryan, T. A. (2012). Calbindin controls release probability in ventral tegmental area dopamine neurons. *Nat Neurosci* **15**, 813-5.

Pappas, G. D., Kriho, V. and Pesold, C. (2001). Reelin in the extracellular matrix and dendritic spines of the cortex and hippocampus: a comparison between wild type and heterozygous reeler mice by immunoelectron microscopy. *J Neurocytol* **30**, 413-25.

Perlmann, T. and Wallen-Mackenzie, A. (2004). Nurr1, an orphan nuclear receptor with essential functions in developing dopamine cells. *Cell Tissue Res* **318**, 45-52.

Prakash, N., Brodski, C., Naserke, T., Puelles, E., Gogoi, R., Hall, A., Panhuysen, M., Echevarria, D., Sussel, L., Weisenhorn, D. M. et al. (2006). A Wnt1-regulated genetic network controls the identity and fate of midbrain-dopaminergic progenitors in vivo. *Development* **133**, 89-98.

Prakash, N. and Wurst, W. (2006). Genetic networks controlling the development of midbrain dopaminergic neurons. *J Physiol* **575**, 403-10.

Quattrocchi, C. C., Wannenes, F., Persico, A. M., Ciafre, S. A., D'Arcangelo, G., Farace, M. G. and Keller, F. (2002). Reelin is a serine protease of the extracellular matrix. *J Biol Chem* **277**, 303-9.

Rakic, P. (1990). Principles of neural cell migration. *Experientia* **46**, 882-91.

Rakic, P. (2000a). Molecular and cellular mechanisms of neuronal migration: relevance to cortical epilepsies. *Adv Neurol* **84**, 1-14.

Rakic, P. (2000b). Radial unit hypothesis of neocortical expansion. *Novartis Found Symp* **228**, 30-42; discussion 42-52.

Reyes, S., Fu, Y., Double, K., Thompson, L., Kirik, D., Paxinos, G. and Halliday, G. M. (2012). GIRK2 expression in dopamine neurons of the substantia nigra and ventral tegmental area. *J Comp Neurol* **520**, 2591-607.

Rice, D. S., Sheldon, M., D'Arcangelo, G., Nakajima, K., Goldowitz, D. and Curran, T. (1998). Disabled-1 acts downstream of Reelin in a signaling pathway that controls laminar organization in the mammalian brain. *Development* **125**, 3719-29.

Ritter, J. G., Spille, J. H., Kaminski, T. and Kubitscheck, U. (2010). A cylindrical zoom lens unit for adjustable optical sectioning in light sheet microscopy. *Biomed Opt Express* **2**, 185-93.

Roberts, R. C., Xu, L., Roche, J. K. and Kirkpatrick, B. (2005). Ultrastructural localization of reelin in the cortex in post-mortem human brain. *J Comp Neurol* **482**, 294-308.

Rogers, J. H. (1992). Immunohistochemical markers in rat brain: colocalization of calretinin and calbindin-D28k with tyrosine hydroxylase. *Brain Res* **587**, 203-10.

Ross, M. E. and Walsh, C. A. (2001). Human brain malformations and their lessons for neuronal migration. *Annu Rev Neurosci* **24**, 1041-70.

Sambrook, J. and Russell, W. D. (2001). Molecular Cloning. *Cold Spring Harbor Laboratory Press*.

Saucedo-Cardenas, O., Quintana-Hau, J. D., Le, W. D., Smidt, M. P., Cox, J. J., De Mayo, F., Burbach, J. P. and Conneely, O. M. (1998). Nurr1 is essential for the induction of the dopaminergic phenotype and the survival of ventral mesencephalic late dopaminergic precursor neurons. *Proc Natl Acad Sci U S A* **95**, 4013-8.

Sawamoto, K., Nakao, N., Kobayashi, K., Matsushita, N., Takahashi, H., Kakishita, K., Yamamoto, A., Yoshizaki, T., Terashima, T., Murakami, F. et al. (2001). Visualization, direct isolation, and transplantation of midbrain dopaminergic neurons. *Proc Natl Acad Sci U S A* **98**, 6423-8.

Schaar, B. T. and McConnell, S. K. (2005). Cytoskeletal coordination during neuronal migration. *Proc Natl Acad Sci U S A* **102**, 13652-7.

Schacht, P., Johnson, S. B. and Santi, P. A. (2011). Implementation of a continuous scanning procedure and a line scan camera for thin-sheet laser imaging microscopy. *Biomed Opt Express* **1**, 598-609.

Schein, J. C., Hunter, D. D. and Roffler-Tarlov, S. (1998). Girk2 expression in the ventral midbrain, cerebellum, and olfactory bulb and its relationship to the murine mutation weaver. *Dev Biol* **204**, 432-50.

Schwenk, F., Kuhn, R., Angrand, P. O., Rajewsky, K. and Stewart, A. F. (1998). Temporally and spatially regulated somatic mutagenesis in mice. *Nucleic Acids Res* **26**, 1427-32.

Senturk, A., Pfennig, S., Weiss, A., Burk, K. and Acker-Palmer, A. (2011). Ephrin Bs are essential components of the Reelin pathway to regulate neuronal migration. *Nature* **472**, 356-60.

Shults, C. W., Hashimoto, R., Brady, R. M. and Gage, F. H. (1990). Dopaminergic cells align along radial glia in the developing mesencephalon of the rat. *Neuroscience* **38**, 427-36.

Sillitoe, R. V. and Vogel, M. W. (2008). Desire, disease, and the origins of the dopaminergic system. *Schizophr Bull* **34**, 212-9.

Simon, H. H., Saueressig, H., Wurst, W., Goulding, M. D. and O'Leary, D. D. (2001). Fate of midbrain dopaminergic neurons controlled by the engrailed genes. *J Neurosci* **21**, 3126-34.

Simon, H. H., Thuret, S. and Alberi, L. (2004). Midbrain dopaminergic neurons: control of their cell fate by the engrailed transcription factors. *Cell Tissue Res* **318**, 53-61.

Simunovic, F., Yi, M., Wang, Y., Stephens, R. and Sonntag, K. C. (2008). Evidence for gender-specific transcriptional profiles of nigral dopamine neurons in Parkinson disease. *PLoS One* **5**, e8856.

Smidt, M. P., Asbreuk, C. H., Cox, J. J., Chen, H., Johnson, R. L. and Burbach, J. P. (2000). A second independent pathway for development of mesencephalic dopaminergic neurons requires Lmx1b. *Nat Neurosci* **3**, 337-41.

Smidt, M. P., Smits, S. M., Bouwmeester, H., Hamers, F. P., van der Linden, A. J., Hellemons, A. J., Graw, J. and Burbach, J. P. (2004). Early developmental failure of substantia nigra dopamine neurons in mice lacking the homeodomain gene Pitx3. *Development* **131**, 1145-55.

Smidt, M. P., Smits, S. M. and Burbach, J. P. (2003). Molecular mechanisms underlying midbrain dopamine neuron development and function. *Eur J Pharmacol* **480**, 75-88.

Solecki, D. J., Trivedi, N., Govek, E. E., Kerekes, R. A., Gleason, S. S. and Hatten, M. E. (2009). Myosin II motors and F-actin dynamics drive the coordinated movement of the centrosome and soma during CNS glial-guided neuronal migration. *Neuron* **63**, 63-80.

Spille, J. H., Kaminski, T., Konigshoven, H. P. and Kubitscheck, U. (2012). Dynamic three-dimensional tracking of single fluorescent nanoparticles deep inside living tissue. *Opt Express* **20**, 19697-707.

Srinivas, S., Watanabe, T., Lin, C. S., William, C. M., Tanabe, Y., Jessell, T. M. and Costantini, F. (2001). Cre reporter strains produced by targeted insertion of EYFP and ECFP into the ROSA26 locus. *BMC Dev Biol* **1**, 4.

Sulzer, D. (2007). Multiple hit hypotheses for dopamine neuron loss in Parkinson's disease. *Trends Neurosci* **30**, 244-50.

Takeuchi, A. and O'Leary, D. D. (2006). Radial migration of superficial layer cortical neurons controlled by novel Ig cell adhesion molecule MDGA1. *J Neurosci* **26**, 4460-4.

Tanaka, T., Serneo, F. F., Tseng, H. C., Kulkarni, A. B., Tsai, L. H. and Gleeson, J. G. (2004). Cdk5 phosphorylation of doublecortin ser297 regulates its effect on neuronal migration. *Neuron* **41**, 215-27.

Terashima, T., Kishimoto, Y. and Ochiishi, T. (1994). Musculotopic organization in the motor trigeminal nucleus of the reeler mutant mouse. *Brain Res* **666**, 31-42.

Tessier-Lavigne, M. and Goodman, C. S. (1996). The molecular biology of axon guidance. *Science* **274**, 1123-33.

Tissir, F. and Goffinet, A. M. (2003). Reelin and brain development. *Nat Rev Neurosci* **4**, 496-505.

Tissir, F., Wang, C. E. and Goffinet, A. M. (2004). Expression of the chemokine receptor Cxcr4 mRNA during mouse brain development. *Brain Res Dev Brain Res* **149**, 63-71.

Umeshima, H. and Kengaku, M. (2013). Differential roles of cyclin-dependent kinase 5 in tangential and radial migration of cerebellar granule cells. *Mol Cell Neurosci* **52**, 62-72.

Van den Heuvel, D. M. and Pasterkamp, R. J. (2008). Getting connected in the dopamine system. *Prog Neurobiol* **85**, 75-93.

Vasudevan, A., Won, C., Li, S., Erdelyi, F., Szabo, G. and Kim, K. S. (2012). Dopaminergic neurons modulate GABA neuron migration in the embryonic midbrain. *Development* **139**, 3136-41.

Veenvliet, J. V., Dos Santos, M. T., Kouwenhoven, W. M., von Oerthel, L., Lim, J. L., van der Linden, A. J., Koerkamp, M. J., Holstege, F. C. and Smidt, M. P. (2013). Specification of dopaminergic subsets involves interplay of En1 and Pitx3. *Development* **140**, 3373-84.

Vitalis, T., Cases, O., Engelkamp, D., Verney, C. and Price, D. J. (2000). Defect of tyrosine hydroxylase-immunoreactive neurons in the brains of mice lacking the transcription factor Pax6. *J Neurosci* **20**, 6501-16.

Vives, J., Sasajala, P., Chang, K. H., Zhao, S. and Li, M. (2008). A mouse model for tracking nigrostriatal dopamine neuron axon growth. *Genesis* **46**, 125-31.

Wang, Y., Li, G., Stanco, A., Long, J. E., Crawford, D., Potter, G. B., Pleasure, S. J., Behrens, T. and Rubenstein, J. L. (2011). CXCR4 and CXCR7 have distinct functions in regulating interneuron migration. *Neuron* **69**, 61-76.

Weeks, B. S., Papadopoulos, V., Dym, M. and Kleinman, H. K. (1991). cAMP promotes branching of laminin-induced neuronal processes. *J Cell Physiol* **147**, 62-7.

Winterer, G. and Weinberger, D. R. (2004). Genes, dopamine and cortical signal-to-noise ratio in schizophrenia. *Trends Neurosci* **27**, 683-90.

Wise, R. A. (2009). Roles for nigrostriatal--not just mesocorticolimbic--dopamine in reward and addiction. *Trends Neurosci* **32**, 517-24.

Yan, C. H., Levesque, M., Claxton, S., Johnson, R. L. and Ang, S. L. (2011). Lmx1a and lmx1b function cooperatively to regulate proliferation, specification, and differentiation of midbrain dopaminergic progenitors. *J Neurosci* **31**, 12413-25.

Ye, W., Shimamura, K., Rubenstein, J. L., Hynes, M. A. and Rosenthal, A. (1998). FGF and Shh signals control dopaminergic and serotonergic cell fate in the anterior neural plate. *Cell* **93**, 755-66.

Yip, Y. P., Thomas, T., Voss, A. K. and Yip, J. W. (2012). Migration of sympathetic preganglionic neurons in the spinal cord of a C3G-deficient mouse suggests that C3G acts in the reelin signaling pathway. *J Comp Neurol* **520**, 3194-202.

Yoshida, K., Tobet, S. A., Crandall, J. E., Jimenez, T. P. and Schwarting, G. A. (1995). The migration of luteinizing hormone-releasing hormone neurons in the developing rat is associated with a transient, caudal projection of the vomeronasal nerve. *J Neurosci* **15**, 7769-77.

Zhao, S., Maxwell, S., Jimenez-Beristain, A., Vives, J., Kuehner, E., Zhao, J., O'Brien, C., de Felipe, C., Semina, E. and Li, M. (2004). Generation of embryonic stem cells and transgenic mice expressing green fluorescence protein in midbrain dopaminergic neurons. *Eur J Neurosci* **19**, 1133-40.

Zhou, Q., Li, J., Wang, H., Yin, Y. and Zhou, J. (2011). Identification of nigral dopaminergic neuron-enriched genes in adult rats. *Neurobiol Aging* **32**, 313-26.

Allen Institute for Brain Science. Allen Developing Mouse Brain Atlas. 2012. Available from: http://developingmouse.brain-map.org.

8. ACKNOWLEDGEMENT

CURRICULUM VITAE
Gabriela Oana Bodea

Address	Institute of Reconstructive Neurobiology,
	University of Bonn, Life and Brain Center
	Sigmund-Freud-Str. 25, 53127 Bonn, Germany
	Office phone +49(0)228 6885 575
	E-mail: gbodea@uni-bonn.de

Education

2008 – Present	**PhD candidate**, University of Bonn, Germany
	Member of the international graduate school of Theoretical and Experimental Medicine (THEME), focus: medical neuroscience
2006 – 2008	**MSc in Biochemistry and Molecular Biology** University of Bucharest, Romania
2002 – 2006	**BSc in Biochemistry**, University of Bucharest, Romania

Academic honours and fellowships
- Award for an excellent presentation, 15th EURON PhD Student Meeting, Bad Honnef, Germany, September 2011
- Erasmus fellowship for Master thesis preparation at University of Bonn, 2008

Selected courses
- Company of Biologists Workshop "Imaging in Cell Biology: Where Next", Windsor (UK) 2012.
- EMBO Practical Course on 3D Developmental Imaging, Oeiras (PT) 2010

Publications
- **Bodea, G. O**., Spille, J-.H., Abe P., Senturk Andersson, A., Acker-Palmer, A., Stumm, R., Kubitscheck, U., Blaess, S. (2013). Reelin and CXCL12 regulate distinct migratory behaviors during the development of the dopaminergic system. *In revision, Development*, October 2013
- Barry, D., Roque, H., Dumoux, M., Kriston-Vizi, J., **Bodea, G.O**., Harper, C. (2013). Meeting report - imaging in cell biology: where next? J Cell Sci, 2013 Jan 1; 126 (Pt 1): 43-4
- **Bodea, G. O.,** Blaess, S. (2012). Organotypic slice cultures of embryonic ventral midbrain: a system to study dopaminergic neuronal development *in vitro*. J Vis Exp, 2012 Jan 31; (59): e3350.
- Blaess, S., **Bodea, G. O**., Kabanova, A., Chanet, S., Mugniery, E., Derouiche, A., et al., (2011). Temporal-spatial changes in Sonic Hedgehog expression and signaling reveal different potentials of ventral mesencephalic progenitors to populate distinct ventral midbrain nuclei. Neural Dev, 2011 Jun 20; 6:29.
- Dinu, D., **Bodea, G. O**., Ceapa, C. D., Munteanu, M. C., Roming, F. I., Serban, A. I., et al., (2011). Adapted response of the antioxidant defense system to oxidative stress induced by deoxynivalenol in Hek-293 cells. Toxicon, 2011 Jun; 57 (7-8): 1023-1032

Talks
- "Unraveling the migratory behavior of dopaminergic neuronal subpopulations in the murine ventral midbrain" – 15th EURON PhD Student Meeting, Bad Honnef, Germany, September 2011

International conferences contribution

- **Bodea, G. O**., Spille, J-.H., Abe P., Senturk Andersson, A., Acker-Palmer, A., Stumm, R., Kubitscheck, U., Blaess, S. (2013). Molecular mechanisms regulating neuronal migration during the development of the dopaminergic system, 43rd Annual Meeting of the Society for Neuroscience, San Diego, California, November 2013

- **Bodea, G. O**., Spille, J-.H., Kubitscheck, U., Blaess, S. (2012). Unraveling the molecular mechanisms regulating dopaminergic neuron migration in the developing midbrain, FENS 8th Annual Meeting, Barcelona, Spain, July 2012

- **Bodea, G. O**. and Blaess, S. (2012). Deciphering the molecular mechanisms of the dopaminergic neurons migration in the developing murine mesencephalon. 4th International Symposium Crossroads in Biology, Cologne, Germany, February 2012

- **Bodea, G. O**. and Blaess, S. (2011). Unraveling the migratory pathways of dopaminergic neuron subpopulations in the developing murine ventral mesencephalon. Joint Meeting of German and Japanese Societies of Developmental Biologists, Dresden, Germany, March 2011

- **Bodea, G. O**. and Blaess, S. (2010). Characterizing migration patterns of dopaminergic neuron subpopulations in the murine ventral midbrain, FENS 7th Annual Meeting, Amsterdam, The Netherlands, July 2010

I dedicate this thesis to my mother and my husband for

their constant support and unconditional love

DECLARATION / ERKLÄRUNG

I, Gabriela Oana Bodea, hereby declare that the work submitted here is the result of my own investigation, except where otherwise stated. This work has not been submitted to any other university or institute and I have not applied for a doctorate procedure so far.

Hiermit versichere ich, dass diese Dissertation von mir persönlich, selbständig und ohne jede unerlaubte Hilfe angefertigt wurde. Die vorliegende Arbeit wurde an keiner anderen Hochschule als Dissertation eingereicht. Ich habe früher noch keinen Promotionsversuch unternommen.

Gabriela Oana Bodea; Author   October 17th, 2013